Multivariable Stability Robustness for Control of Flexible Beams and Trusses

by

Leonard Lublin

S.B. State University of New York at Buffalo (1989)

SUBMITTED TO THE DEPARTMENT OF
AERONAUTICS AND ASTRONAUTICS
IN PARTIAL FULFILLMENT OF THE REQUIREMENTS
FOR THE DEGREE OF
Master of Science
at the
Massachusetts Institute of Technology
June 1992

Signature of Author _____
Department of Aeronautics and Astronautics
May 12, 1992

Certified by _____
Professor Michael Athans
Thesis Supervisor, Department of Electrical Engineering and Computer Science

Certified by _____
Professor Edward F. Crawley
Thesis Co-Supervisor, Department of Aeronautics and Astronautics

Accepted by _____
Professor Harold Y. Wachman
Chairman, Department Graduate Committee

Multivariable Stability Robustness for Control of Flexible Beams and Trusses

by

Leonard Lublin

SUBMITTED TO THE DEPARTMENT OF AERONAUTICS AND ASTRONAUTICS
ON MAY 12, 1992, IN PARTIAL FULFILLMENT OF THE
REQUIREMENTS FOR THE DEGREE OF
MASTER OF SCIENCE

A holistic and fundamental understanding of several critical issues involved in the design of robust, high authority, multivariable controllers for lightly damped structural systems is presented. The work is carried out in the framework of a simple, two dimensional sample problem within which a mathematical model of the actual system to be controlled is available and used to verify insights into the nature of the problem at hand. Using the sample problem as an example, it is shown how realistic modeling errors for lightly damped structural systems manifest themselves in the standard tools used in control system design. The extent to which it is possible to deal with these modeling uncertainties to ensure stability robustness is also discussed. Clear visualizations of why it is possible to guarantee stability robustness for the high frequency unmodeled dynamics and why no simple and useful ways of guaranteeing robustness for the more structured mismodeled dynamics are also provided. A few frequency weighted $\mathcal{H}_2$ designs for the sample problem are developed to show to what extent existing controller synthesis and stability robustness results can be used to design robust, high authority, multivariable controllers. The outcome of the designs show that it is possible to achieve a decent level of performance where the model is well known while guaranteeing robustness to the unmodeled dynamics. Even though no guarantees on the robustness to the mismodeled dynamics are available, a Nyquist domain-visualization is used to show that slight mismodeled dynamics in the nominal model may not be that detrimental to the closed loop stability of multivariable controllers.

Thesis Supervisor: Dr. Michael Athans, Ph. D.,
Title: Professor of Systems Science and Engineering
Thesis Co-Supervisor: Dr. Edward F. Crawley, Sc.D.,
Title: Professor of Aeronautics and Astronautics

Acknowledgments

In the three long years that it took to arrive at this thesis, I have had the pleasure of interacting with a diverse group of individuals who deserve some credit for this work. First off, I would like to thank my loving parents for their support and encouragement throughout all of my educational experiences. I would also like to express my appreciation to Professor Michael Athans for his guidance, encouragement, and criticism during this research endeavor. I hope he can forgive me for making this the longest running Master's Thesis he has ever supervised. My thesis co-supervisor, Professor Edward F. Crawley, also deserves thanks for contributing his expertise to the structural aspects of this control theoretic work. I hope Ed will forgive me for destroying his one and only trailer hitch that fine day in Vermont. It goes without saying that all of my colleagues in SERC also deserve recognition. In particular, I am especially grateful to Doug MacMartin for helping me understand some of the deep concepts buried in the robust control literature, to Etienne Balmes for lending his vast insight of vector spaces to my multivariable phase analysis, and to Joel Douglas and Professor Nesbitt Hagood for helping me understand the state of the art in parametric error robustness methods. Even though they did not contribute to the technical aspects of this work, I want to express my gratitude to my office mates in the Romper Room for putting up with me whilst I struggled with the writing of this thesis. Last but not least, I would like to thank all of my wonderful friends [1] and xXXXXXXXXX-Night [2] for helping me maintain my sanity during my last three

[1] K.M., M.L, J.G., E.K., C.C., M.G., K.B., G.L., E.N., N.T., B.B., L.L., J.P., R.P., R.N.J., and P.R..

[2] Don't just say it, scream it.

years at the Institute.

This work was sponsored by the M.I.T. Space Engineering Research Center under NASA grant NAGW-1335 with Dr. Robert Hayduk serving as technical monitor.

Contents

1 Introduction **13**

1.1 Motivation 13

1.2 Background 15

1.3 Contributions of Thesis 18

1.4 Outline 20

2 Robustness Sample Problem **22**

2.1 System Description and Philosophy 22

2.2 Modeling 28

2.2.1 State Space Models Using Finite Element Data 28

2.2.2 Full Order Finite Element Models for the Beam and Truss . . 31

2.2.3 Scaling the Signals 38

2.2.4 Model Order Reduction 44

3 Assessing the Uncertainty **52**

3.1 Individual SISO Transfer Functions 56

3.2 Multivariable Magnitude Information 61

3.3 Multivariable Phase Information 62

3.3.1 The Singular Value Decomposition and Multivariable Phase Information 64

3.3.2 Multivariable Phase for the Sample Problem 70

3.4 Parametric Uncertainties 74

4 Dealing With the Uncertainty **77**

4.1 Robustness for Unmodeled Dynamics 80

4.1.1 Additive Error in Scalar Systems 80

4.1.2 Relative Error in Multivariable Systems 83

4.1.3 Unstructured Uncertainty Models for the Sample Problem . . 88

4.2 Robustness for Mismodeled Dynamics 98

4.2.1 Visualizing Mismodeled Dynamics in the Nyquist Domain . . 99

4.2.2 The Structured Singular Value and Mismodeled Dynamics . . 107

4.2.3 Structured Uncertainty Models for the Sample Problem 112

5 $\mathcal{H}_2$ Control Designs **123**

5.1 Design Specifications 124

5.2 Frequency Weighted $\mathcal{H}_2$ Synthesis 128

5.3 Frequency Weight Selection 137

5.4 Sample Problem Designs 140

5.4.1 Design # 1: Standard LQG 140

5.4.2 Design # 2: Typical frequency Weighted $\mathcal{H}_2$ 143

6 Conclusions and Suggestions for Future Work **162**

6.1 Conclusions 162

6.2 Future Work 164

A Sample Problem Data **166**

B A Matlab Function to Evaluate Singular Value Phase Information **172**

C Specific $\mathcal{H}_2$ Design Models for the Sample Problem **176**

C.1 Standard LQG Design 177

C.2 Frequency Weighted $\mathcal{H}_2$ Design 178

List of Figures

1.1 The SERC Interferometer testbed. 14

2.1 Actual truss system with sensors y_i, actuators u_i, and disturbances, d_i. Positive convention showing. 23

2.2 Equivalent beam approximation of the truss with sensors y_i, actuators u_i and disturbances, d_i. Positive convention showing. 24

2.3 Block diagram depicting the framework of the sample problem. 25

2.4 Truss Substructure. Static test used to evaluate equivalent cross–sectional area. 32

2.5 Comparsion of the undamped structural modes of the sample problem. Similar mode shape scale factors were used to depict all the modes. . 35

2.6 Statically equivalent loading situation for the truss and beam inputs. 36

2.7 Geometric compatibility of the truss and beam outputs. The top figures show an exaggerated deformation from the undeformed configurations shown in the bottom figures. Here "N.A." denotes the neutral axis of the respective structures. 37

2.8 Unscaled Truss Outputs. 41

2.9 Scaled Truss Outputs. 41

2.10 Comparison of the scaled and unscaled beam input to output loop singular values. 43

2.11 Comparison of the beam open loop input to output singular values for the full order model and the reduced order model without the static correction term. 48

2.12 Comparison of the beam open loop input to output singular values for the full order model and the reduced order model with the static correction term. 49

3.1 Comparison of Nyquist plots with typical structural damping and typical servo damping near the critical point. Only the map of $g(j\omega)$ for $\omega \in (0, \infty)$ is shown to maintain clarity. 53

3.2 Comparison of scalar, control loop transfer functions for the beam and truss. 59

3.3 Comparison of scalar, control loop transfer functions for the beam and truss. 60

3.4 Comparison of the open loop singular values of $G_2(s)$ for the beam and truss. 62

3.5 Comparison of the output phases for the beam, $\psi_{i1}(\omega)$, and truss, $\alpha_{i1}(\omega)$, given an input along the direction of the maximum right singular vector of the beam. 72

3.6 Comparison of the output phases for the beam, $\psi_{i2}(\omega)$, and truss, $\alpha_{i2}(\omega)$, given an input along the direction of the minimum right singular vector of the beam. 73

4.1 Standard feedback control system. 78

4.2 The Nyquist contour, D_r. 78

4.3 Portion of the Nyquist plot for a scalar nominal system, $t(s)$ and a typical actual system, $\tilde{t}(s)$, with a representation of the additive error and unstructured uncertainty disk at ω_o. 81

4.4 Nominal system with a multiplicative perturbation, $\Delta_m(s)$ at the plant output. 83

4.5 *Top:* Comparison of error models for a multiplicative perturbation at the output of the beam model: Hands on error bound is $|w_m(j\omega)|$ from (4.25), H-infinity motivated bound is $|w_m(j\omega)|$ from (4.28), and exact multiplicative error is $\overline{\sigma}\Delta_m(j\omega)$ from (4.29). *Bottom:* Comparison of the open loop singular values of $G_2(s)$ for the beam and truss. 95

4.6 Blow up of the Nyquist plot of $g(\hat{\alpha}, s)$ near the critical point. The dark region indicates the possible locations of the actual plant, $\tilde{g}(j\omega_o)$ at $\omega_o = 50\ rad/sec$. The shaded disk represents the multiplicative error, with radius $|l(\omega_o)|$ given by (4.39), between the nominal model and an actual model, assumed to be $g(\underline{\alpha}, s)$. 103

4.7 P–Δ : The general feedback system description. 107

4.8 The Closed loop general feedback system description. 107

5.1 Open loop performance metric for the sample problem: $\overline{\sigma}G_1(j\omega)$ and the open loop RMS values of $y(t)$. 127

5.2 The general feedback system description. 128

5.3 Block diagram of the beam model with frequency weights. 129

5.4 Nominal performance of the standard LQG design shown by a comparison of the magnitude of the open loop and closed loop output to disturbance transfer function matrices of the beam system: $\overline{\sigma}G_1(j\omega)$ .vs. $\overline{\sigma}G_{cl}(j\omega)$. 141

5.5 The robustness of the standard LQG design to the unmodeled dynamics evaluated by (5.42) for the closed loop gain, $\overline{\sigma}C_{sr}(j\omega)$, and hands on error bound, $|w_m(j\omega)|$, from (4.25). 142

5.6 - Nominal performance of the frequency weighted $\mathcal{H}_2$ design shown by a comparison of the magnitude of the open loop and closed loop output to disturbance transfer function matrices of the beam system: $\overline{\sigma}G_1(j\omega)$ .vs. $\overline{\sigma}G_{cl}(j\omega)$. 145

5.7 The Magnitude of the weights (5.49, 5.50, 5.51) used in the frequency weighted $\mathcal{H}_2$ design. 145

5.8 The robustness of the frequency weighted $\mathcal{H}_2$ design to the unmodeled dynamics evaluated by (5.42) for the closed loop gain, $\overline{\sigma}C_{sr}(j\omega)$, and hands on error bound, $|w_m(j\omega)|$, from (4.25). 146

5.9 Bode type plots of $|\mathcal{N}_{sr}(j\omega)|$ and the $\angle\mathcal{N}_{sr}(j\omega)$ for $\mathcal{N}_{sr}(j\omega)$ from (5.54). Note the linear frequency scale. 151

5.10 A graphical comparison of stability robustness Condition *2* from Theorem 4.3 for the frequency weighted $\mathcal{H}_2$ design: $\overline{\sigma}C_{sr}(j\omega)$ .vs. $1/\overline{\sigma}\left[\Delta_m(j\omega)\right]$. Here $\Delta_m(s)$ is the exact multiplicative error between the beam and truss from (4.29). 152

5.11 Nyquist plot of the frequency weighted $\mathcal{H}_2$ control system, $\mathcal{N}_{sr}(j\omega)$ from (5.54). Only the map of $\mathcal{N}_{sr}(j\omega)$ for $\omega \in (0, \infty)$ is shown to maintain clarity. 154

5.12 Blow up of the Nyquist plot of the frequency weighted $\mathcal{H}_2$ control system, $\mathcal{N}_{sr}(j\omega)$ from (5.54), near the critical point. Only the map of $\mathcal{N}_{sr}(j\omega)$ for $\omega \in (0, \infty)$ is shown to maintain clarity. 154

5.13 Blow up of the Nyquist plot of the frequency weighted $\mathcal{H}_2$ design, $\mathcal{N}_{sr}(j\omega)$, near the critical point. The shaded regions indicate the possible locations of the actual plant, $\tilde{\mathcal{N}}_{sr}(j\omega)$, based on the mismodeled dynamics description of (5.56) at the frequencies in (5.57). 155

5.14 Blow up of the Nyquist plot of the frequency weighted $\mathcal{H}_2$ design, $\mathcal{N}_{sr}(j\omega)$, near the critical point. The shaded region indicates the possible locations of the actual plant, $\tilde{\mathcal{N}}_{sr}(j\omega)$, based on the mismodeled dynamics description of (5.56) at $\omega = 47.5\, rad/sec.$ 156

5.15 Blow up of the Nyquist plot of the frequency weighted $\mathcal{H}_2$ design, $\mathcal{N}_{sr}(j\omega)$, near the critical point. The shaded region indicates the possible locations of the actual plant, $\tilde{\mathcal{N}}_{sr}(j\omega)$, based on the mismodeled dynamics description of (5.56) at $\omega = 87\, rad/sec.$ 157

5.16 Blow up of the Nyquist plot of the frequency weighted $\mathcal{H}_2$ design, $\mathcal{N}_{sr}(j\omega)$, near the critical point. The shaded region indicates the possible locations of the actual plant, $\tilde{\mathcal{N}}_{sr}(j\omega)$, based on the mismodeled dynamics description of (5.56) at $\omega = 284\, rad/sec$. 158

C.1 The general feedback system description. 176

C.2 Block diagram of the beam model with frequency weights. 177

List of Tables

2.1 Comparison of the DC gain and multivariable transmission zeros for various models of the beam. Frequencies are in *rad/sec.* 47

3.1 Comparison of frequencies for the mismodeled poles and zeros, in *rad/sec*, for the sample problem. 75

4.1 Mismodeled uncertainty description of the nominal system (4.32). Frequencies are in *rad/sec.* 102

4.2 Realistic mismodeled uncertainty description of the beam model. Frequencies are in *rad/sec.* 114

4.3 Parametric uncertainty description for a linear representation of the errors in the beam model. Frequencies are in *rad/sec.* 120

B.1 Legend between the notation of the singular value phase information developed in Chapter 3 and the variables used in the function to evaluate the phase information. 172

Chapter 1

Introduction

In this chapter the motivation, background, contributions, and outline of this work will be presented.

1.1 Motivation

In recent years, the concept of using controlled structures technology to improve the nominal performance and or allow for vastly improved performance in spacecraft has been widely researched [1,2]. Among the many diverse technologies being explored to achieve these goals are passive damping, disturbance isolation, low authority control, and high authority control. The M.I.T. Space Engineering Research Center's Interferometer testbed, shown in Figure 1.1, is a laboratory experiment that allows these various approaches to controlled structures technology to be validated in a realistic setting. As discussed in detail in [3], the testbed is a scaled version of a proposed, spaced based, imaging interferometer. The primary performance requirement for the testbed is to maintain the internal pathlength errors between multiple points on the tetrahedron to within stringent tolerances in the presence of an internal disturbance source that causes the structure to vibrate. While such an objective lends itself to all the areas of controlled structures technology research, the work in this thesis falls strictly under the category of high authority control techniques.

Given the desired performance specification of the Interferometer testbed, one can

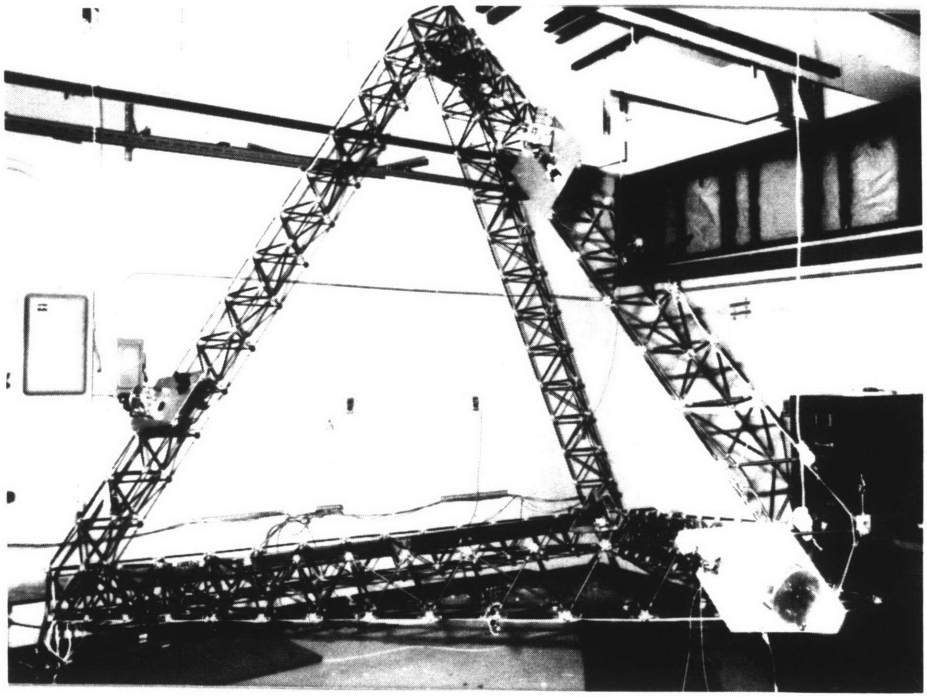

Figure 1.1: The Interferometer testbed.

envision the desire to minimize certain pathlength errors between various points on the structure as the desire to control the shape of the tetrahedron. With the recent advances in piezoelectric materials and their use in active strut actuators [4], it is entirely possible to pursue a multivariable control strategy that seeks to regulate the shape of the Interferometer structure to achieve the desired performance. While numerous multivariable design methods can be used to synthesize such controllers for the interferometer, they all require accurate mathematical models of the actual system. Unfortunately, the Interferometer testbed is a complex and lightly damped structure that is not at all easy to model. This inherent characteristic of the Interferometer introduces added complexity to the desire to use a multivariable shape control strategy to achieve the desired performance specifications.

In essence, the Interferometer system is open loop stable, and any feedback controller for it would be designed with the intention of meeting the pathlength error specifications. However, any model of the Interferometer will contain errors, and the control system designer must ensure that a controller which is designed based on a

mathematical model of it will not cause a closed loop instability when applied to the Interferometer. This issue of stability robustness is of primary concern for multivariable controllers because there is no way to measure phase and gain margins to quantify a control system's robustness to modeling errors as there is for scalar systems. Add to this the lightly damped and complex nature of the Interferometer and the motivation for this thesis becomes clear.

Basically, the motivation for this thesis comes from the desire to understand how to deal with the realistic types of modeling uncertainty that will be present in a model of the Interferometer system so that it is possible to design high authority, multivariable, robustly stable control systems for the Interferometer to meet the stringent pathlength error specifications. Even though the motivation comes specifically from the Interferometer testbed, it is important to realize that the same issues that drive the research on the testbed are inherent to almost any structural control problem. Hence, results based on research for the Interferometer are applicable to any lightly damped and complex structural system. Analogously, the research to date in the field of controlled structures technology is also applicable to the problems of the Interferometer.

1.2 Background

As we noted, a number of crucial issues in multivariable control system design are brought to the surface by the motivation to understand how to implement robustly stable, high authority shape controllers on the Interferometer testbed. The primary issues include how to accurately model lightly damped structural systems, how to classify the uncertainty in these models, how to deal with the types of uncertainty that arise, and how to synthesize robustly stable controllers based on an uncertain models that meet the desired performance specifications. Each one of these topics has been researched extensively individually and less so as an entire entity.

Traditionally, dynamical models of complex structural systems like the Interferometer are derived from standard finite element techniques [5, 6]. However, recent

experimental investigations in the controlled structures community have brought to light the limitations of finite element techniques to produce accurate, high bandwidth models of realistic, complex structures [7,8]. As a result, a variety of system identification approaches are currently being investigated to provide more accurate structural models [9–12]. Unfortunately no matter which modeling approach is used, the resulting model will inevitably contain errors.

For structural systems, the types of modeling errors one can expect typically fall into two categories: Low frequency structured or parametric errors and high frequency unstructured errors [13,14]. A typical approach to classifying these errors has been to blend the a priori knowledge of the fidelity of an analytical modeling approach, such as finite elements, with an experimental verification procedure, such as frequency response analysis [13]. Once the modeling errors are identified, the designer must decide how to deal with the inevitable uncertainties.

Since any modeling method can not produce an exact model of a structural system and high authority multivariable controllers depend on accurate models, the primary focus in high authority structural control research centers on finding simple and useful tests that guarantee robustness to the inevitable modeling errors. Fortunately, simple and useful stability robustness tests exist for the class of unstructured errors. Specifically, the relative error stability robustness results, like the multiplicative error stability robustness criterion [15, 16], can be used to verify the robustness of a given controller to an unstructured uncertainty at a specific point in the feedback loop of a system. Unfortunately, the unstructured error stability robustness results are too conservative when applied to the class of structured uncertainties that arise in the modeling process. In an effort to reduce this conservatism, Doyle introduced the structured singular value framework within which stability and performance robustness can be guaranteed for both structured and unstructured uncertainty [17,18]. While the framework provides the answer, in theory, to the stability robustness problem, it is still not a useful means of guaranteeing stability robustness since it requires the minimization of a highly non–linear and non–convex function to test the robustness of a control system [18]. To date work continues on making the structured

singular value framework viable for guaranteeing robustness [19].

The structured singular value framework is not the only methodology available for dealing with structured modeling errors. There is also a large body of research that considers other approaches to dealing with structured modeling errors that can be applied to guarantee stability robustness for a structural system. Hagood provides a thorough overview of these in [20]. As is the case with the structured singular value framework, almost all of the other results in the field that consider how to deal with structured modeling errors have limited applicability for realistic systems due to the restrictive nature of the assumptions used to arrive at the various results and due to the computational complexities involved in the resulting methods. As a consequence, to date there is still no simple, useful, unconservative, and widely accepted way of guaranteeing stability robustness for structured modeling errors, as there is for guaranteeing robustness for unstructured modeling errors. Clearly, the situation becomes worse when we consider the real situation in which we have *both* types of modeling errors.

It is important to realize that most of the stability robustness results come in the form of a test that a control system, that is a nominal model, an uncertainty description, and a compensator, must satisfy. Such tests fall into the category of analysis methods that merely provide a way of judging the robustness of a given design. Once the modeling errors are analyzed and the appropriate stability robustness constraints are formalized, it is the job of the controller synthesis to provide a compensator that meets the performance specifications and the stability constraints provided by the robustness analysis. The $\mathcal{H}_2$ (LQG) and $\mathcal{H}_\infty$ controller synthesis methodologies both allow the use of frequency dependent weights that can be used to design compensators that meet the performance and robustness specifications for realistic structural control problems [21, 22].

While each of the above disciplines are typically researched as individual entities, the ability to design high authority, stably robust control systems relies on all these disciplines as a holistic entity. The bridge between these distinct research fields and the development of high authority control systems for structural testbeds has been

carried out by a few research groups [23–25]. At the Jet Propulsion Laboratory, researchers working on a cantilevered truss structure tried to implement robustly stable high authority shape controllers and were forced to resolve all of the complex issues outlined above [24]. Even though they were able to implement some $\mathcal{H}_\infty$ controllers on the actual structure, none of them satisfied the necessary robustness specifications for the unstructured uncertainties they defined, nor was there any consideration of the more structured modeling errors in their model that were classified in [13]. This situation is typical of the difficulties involved in bringing together the diverse fields of research needed to design robust, high authority controllers. Further, this difficulty coupled with a lack of a fundamental understanding of how the different pieces of research should be fit together to meet the desired design specifications was another strong motivational factor for this work.

1.3 Contributions of Thesis

The primary contribution of this thesis is an exposition of the critical issues involved in designing robustly stable, multivariable, high authority controllers for complex structural systems like the Interferometer testbed. Recall that the critical issues encompass structural modeling, assessing the uncertainty in the resulting model, understanding how to design robust controllers based on the uncertain model, and actually synthesizing high authority robust controllers based on the uncertain models.

In an effort to avoid the complexity involved in working with the actual Interferometer, a simple two dimensional truss and beam sample problem that captures the primary attributes of the Interferometer in a realistic way and provides a complete mathematical framework in which to carry out the investigation is utilized to discuss and exemplify the critical issues. Since many different disciplines are involved in the design of a robust, high authority controller and since the behavior of the actual system can only be approximated, it is difficult to figure out what contributes to the unpredictable results, poor performance, or lack of robustness of a control system designed based on an uncertain model when it is applied to a real system. The use

of the sample problem directly avoids this issue by providing a realistic problem that both captures the complex issues involved in designing robust controllers and furnishes an exact model of the actual system which can be used to verify exactly what is contributing to the poor performance or lack of robustness of a control system. In this way, the development and use of the sample problem to study the interrelation amongst the various pieces of technology needed to design robust, multivariable, high authority controllers is in itself a contribution of the work.

While no new theoretical results will be presented, the actual process of going from system description to high authority controllers will be explored in a somewhat tutorial manner to provide a fundamental understanding of how the diverse disciplines interrelate and can be used to design high authority, robust, multivariable controllers for complex structural systems. In going through the complete controller synthesis cycle, a clear visualization and overview of many issues involved in the stability robustness aspects of the problem will be presented.

In the process of assessing the uncertainty in a model of the sample problem, a new method for analyzing the fidelity of a multivariable model using phase information extracted from the singular value decomposition of the model will be examined. While the role this phase information plays in analyzing stability robustness is not clear, it will be shown that it provides a viable way of assessing the phase fidelity of a multivariable model. Since there are a limited number of phase results for multivariable systems, this method of analyzing the fidelity of a multivariable model is clearly one of the contributions of this thesis.

As far as the critical issue of how to deal with the inevitable errors in a model of a complex structural system are concerned, this work contributes a clear visualization of how to deal with unstructured uncertainties, why unstructured error descriptions are too conservative for dealing with structured modeling errors, and why no useful and nonconservative techniques for guaranteeing robustness for structured modeling errors exists to date. The visualization is carried out using a Nyquist domain interpretation of stability robustness in the scalar setting to make the interpretations of the existing theory clear and then in the multivariable case using the sample problem to extend

the visualizations to a realistic problem.

On the issue of synthesizing controllers based on inaccurate models, a frequency weighted $\mathcal{H}_2$ controller synthesis for the sample problem will be presented. Using this design methodology to synthesize controllers, it will be shown that it is possible to design high authority, multivariable controllers for structural systems that deliver useful performance and satisfy an unstructured error robustness test. Further even though there was no way in the synthesis to account for the structured modeling errors, a Nyquist domain visualization of the structured uncertainties in the model will be presented to verify that the $\mathcal{H}_2$ controllers are robust to the structured modeling errors as well as the unstructured modeling errors.

1.4 Outline

Given the motivation to understand the fundamental aspects of the complete controller synthesis process for structural systems, this work was organized in the logical progression from system description all the way through useful controller results. In Chapter 2 the actual sample problem and the philosophy behind it that will be used to describe and exemplify various stability robustness issues will be presented. Once the setup of the sample problem is at hand, the finite element modeling process, the means as well as the necessity of scaling the vector valued signals, and the model order reduction procedure that were used for the sample problem model will be described.

Having described the system and modeling process of the sample problem in Chapter 2, the assessment of the uncertainty in the model will be presented in Chapter 3. The chapter will present both a realistic way of assessing the uncertainty in a typical structural model and a verification of these approaches using the exact mathematical framework of the sample problem. The verification will be carried out by studying the ways in which the realistic modeling errors manifest themselves in the common tools of multivariable control design. By the completion of Chapter 3, a thorough understanding of the fidelity of typical structural models as well as some insights into how to obtain quantifiable descriptions of the modeling errors will be at hand.

Since the modeling errors throughout Chapter 3 will be classified as either unmodeled or mismodeled dynamics, that is unstructured or structured uncertainties, Chapter 4 will provide an in depth discussion of how to deal with such errors in a model of a complex structural system to ensure robustly stable compensators. The chapter will rely heavily on a Nyquist domain interpretation of stability robustness to compare, contrast, and describe the various approaches to dealing with the modeling uncertainty. Specifically, visualizations of structured and unstructured uncertainty regions for scalar systems in the Nyquist domain will be used to explain the applicability of relative error robustness tests for unstructured uncertainties, the conservatism of relative error robustness tests for structured uncertainties, and the difficulty of deriving non–conservative robustness conditions for structured uncertainties. Using the in depth understanding of the various robustness techniques based on the scalar visualizations, useful and appropriate models of the uncertainty in the sample problem model that could be used to synthesize stably robust, multivariable controllers will be presented in Chapter 4 and used in Chapter 5.

The final step in the holistic approach to the design of robust, high authority controllers given a model, knowledge of the modeling errors, and understanding of how to handle the modeling errors is the actual synthesis of the control system. In Chapter 5, frequency weighted $\mathcal{H}_2$ designs for the sample problem will be presented to verify that it is indeed possible to design robustly stable, high authority, multivariable controllers for complex structural systems that do achieve a decent level of performance. In doing so, the process of including frequency weights in the synthesis along with a discussion on how to choose the weights to meet the stringent design specifications will be presented.

Finally, in Chapter 6 the conclusions of the process of going from a model description to the desired high authority controllers will be presented with some suggestions for further research directions.

Chapter 2

Robustness Sample Problem

Sample problems are useful tools for providing worthwhile insight into the nuances of the complex systems they mimic [26–28]. In this chapter, a sample problem that captures the critical issues involved in implementing multivariable shape control on the Interferometer testbed is described. The sample problem consists of a truss and beam which are intended to be the actual system and the design model of that system. Since the majority of the work in this thesis is based on mathematical experiments of the sample problem, the philosophy behind the choice of the sample problem as well as the modeling process of the sample problem are described in detail.

2.1 System Description and Philosophy

In order to understand the predominant issues in applying multivariable shape control to the Interferometer in a simple and concise manner, a two dimensional cantilevered truss, shown in Figure 2.1, along with a beam approximation of the truss, shown in Figure 2.2, were chosen as the sample problem to study. A long, slender, beam like truss was selected so that the system would have low frequency global vibration dynamics, where the whole truss moves in unison, and high frequency local vibration characteristics, where individual elements of the truss vibrate. Such dynamics are typical for the class of structural systems that have been targeted for active feedback control. The type of the disturbance sources, which unavoidably excite the afore-

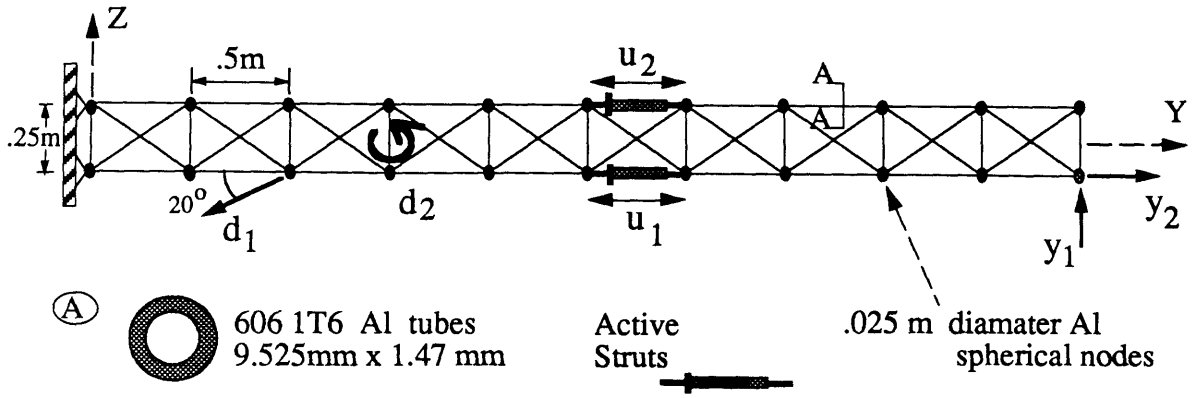

Figure 2.1: Actual truss system with sensors y_i, actuators u_i, and disturbances, d_i. Positive convention showing.

mentioned dynamics, included in the truss system are indicative of typical spacecraft disturbance sources, as outlined in [29]. Specifically, the point load disturbance, d_1, mimics undesirable forces transmitted to the structure from vibrating machinery while the torque disturbance, d_2, accounts for disruptive moments applied to the structure from torque wheel imbalances. Both disturbances produce vibrations in the truss that in turn cause vertical and axial displacements of the lower right node of the truss that are measured by the two sensors, y_1 and y_2, located there. The location of the sensors off the neutral axis, which is the Y axis when the truss is undeformed, was intended to add dynamic coupling to the control problem; since axial and bending modes of a cantilevered truss are uncoupled when observed from the neutral axis. While the the disturbances unavoidably corrupt the desired behavior of the truss, the active struts are used to regulate the undesirable dynamics of the truss. Active struts are high bandwidth, high precision, structural load carrying elements that effectively apply an axial force, u_1 and u_2 in the truss system, at the nodes of the structure to which they are connected [4, 30]. To get a feel for the influence the active struts have in the truss, realize that simultaneously commanding a compressive force to active strut 1, $-u_1$, and a tensile force to active strut 2, $+u_2$, will cause the tip of the truss to bend downward. This type of control authority is well suited to regulate the position of the truss' tip. The location of the active strut actuators, tip sensors, and system

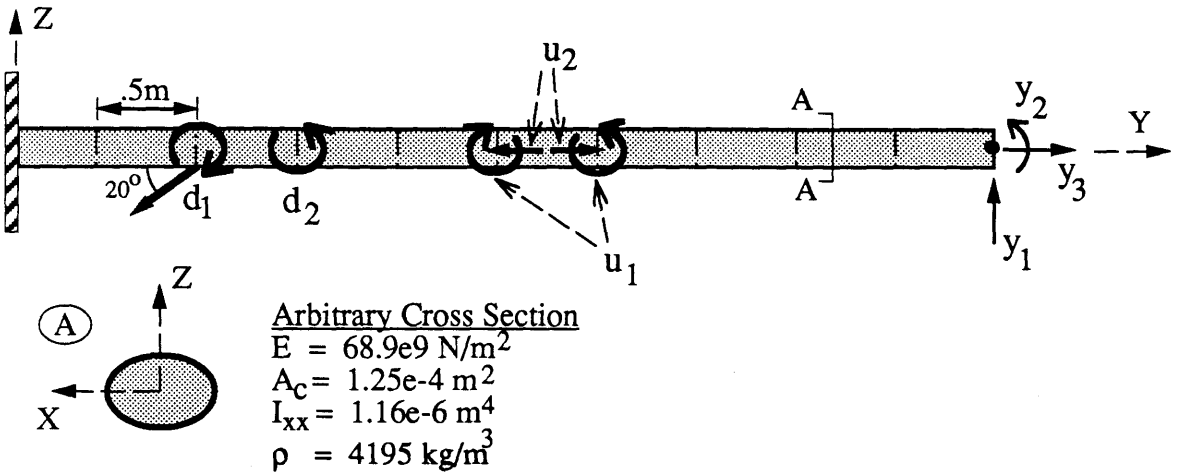

Figure 2.2: Equivalent beam approximation of the truss with sensors y_i, actuators u_i and disturbances, d_i. Positive convention showing.

disturbances, as well as the clamped–free boundary conditions, were chosen so that the control loops of the sample problem were analogous to those of the Interferometer testbed. It should be intuitively obvious that it is much simpler to model and work with the truss sample problem than the true Interferometer system.

Less obvious is the fact that the sample problem, while simpler than the Interferometer, captures many of the difficulties that would be encountered in designing multivariable controllers for the Interferometer. Consider the objective of minimizing the motion, caused by the disturbances, of the truss' tip using the active struts. This objective is completely analogous to the multiple point alignment specification for the Interferometer. The control loop topology of both systems is non–collocated, which introduces the possibility of low frequency non–minimum phase zeros that limit achievable performance [31]. Furthermore, the performance of a control system is intimately tied to the accuracy of the models upon which it is based [14]. As is the case with both the Interferometer testbed and the two dimensional truss systems, an accurate model of these structural systems requires a large order state space representation. Practical issues of compensator implementation thus necessitate model and or compensator order reduction. Unfortunately no matter what the order of the models are, they will contain uncertainties. To mimic the fact that an exact model of the

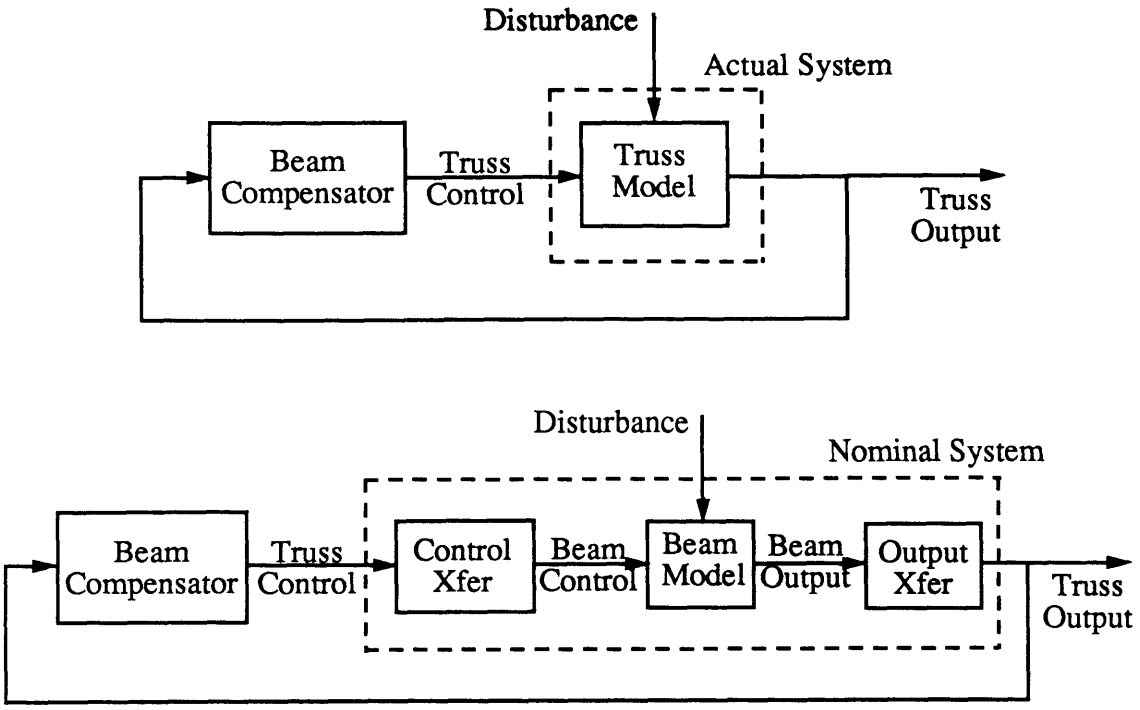

Figure 2.3: Block diagram depicting the framework of the sample problem.

Interferometer can not be formulated in reality, a beam–column approximation of the truss, shown in Figure 2.2, is used as the system upon which controllers intended for the truss are based. In these ways, the sample problem captures some of the inherent difficulties of designing multivariable control systems for complex structural systems like the Interferometer testbed.

The aforementioned issue of modeling uncertainty is of primary concern in lightly damped multivariable systems like the Interferometer. Since models of such systems are plagued by uncertainty, the designer must ensure that controllers based upon mathematical models do not destabilize the actual system. That is the control designs must exhibit stability robustness. Adopting a philosophy where the truss is the actual system to control and the beam a model of that system allows for a mathematical framework in which to study these issues.

A block diagram that clearly depicts the philosophy of the sample problem that will be exploited in this work is shown in Figure 2.3. Essentially, the beam system will provide a realistic model of the actual truss system that can be used to synthesize com-

pensators. In the robust control literature, such models are referred to as the nominal or design model. Notice that the nominal, or beam, model includes transformations so that any compensator based on the beam, referred to as the "Beam Compensator" in Figure 2.3, produces truss inputs based on truss measurements. In this way, beam compensators can be directly applied to a model of the truss system, which is known as an evaluation or actual model in the robust control literature, to evaluate their performance and stability characteristics. It is this mathematically complete setup that provides a simple yet realistic framework within which to understand how to deal with the complex issue of multivariable stability robustness.

Since the philosophy of using a model of the beam to control the actual truss system will be the cornerstone of many of the illustrations and results in this work, it is vital to understand that the beam model is a justifiable approximation of the actual truss system. Without a doubt, the beam will capture the low frequency dynamics of the truss, since the truss acts like a cantilevered beam at low frequencies. At the same time, the inability of the beam to capture the higher frequency, local strut, vibration modes of the truss mimics the difficulty of modeling the high frequency dynamics in structural systems. Notice also from Figures 2.1 and 2.2 that the beam does contain a similar input, output, and disturbance topology to the truss; though it is important to understand that there is not a one to one correspondence between the u_i, y_i, and d_i variables of the beam and truss shown in these Figures [1]. In fact since the behavior of the beam is completely characterized in terms of its neutral axis, the disturbances, control forces, and output measurements in the beam system have been defined so that they are the static equivalent of the corresponding quantities in the truss system reflected to its neutral axis. Physically speaking, the beam disturbances excite the dynamics of the beam in the same way that the truss disturbances excite the dynamics of the truss by applying moments and point loads to the beam near its base. The three outputs located on the neutral axis at the beam tip that measure the motion caused by the disturbances are needed to mimic the measurements in

[1]The subscript indexing of these quantities simply references their location in the vectors of inputs, outputs, and disturbances that arise in the modeling process.

the truss that lie off the neutral axis; as will be seen when the modeling process is described. In the case of the beam inputs, both the bending and axial inputs, u_1 and u_2 respectively, shown in Figure 2.2 are necessary to approximate the control authority that is provided by the active struts in the truss. Specifically, both axial and bending controls are needed to compensate for the axial and bending motions of the tip produced by the disturbances. In simple terms, it is sufficient at this point to recognize that the geometry and nature of the beam model in themselves provide a good approximation of the truss. In the following section, the specific modeling process of the truss, that is the process of creating the beam model, will be described in detail.

The most important aspect in acknowledging that the beam is a justifiable representation of the truss is the ability of the beam to capture the nature of realistic modeling errors for structural systems like the Interferometer. Even though the dynamics, the control topology, and the nature of the inputs, outputs, and disturbances of the beam are similar to those of the truss, there are fundamental limitations in trying to use a model based on the beam to control the truss just as there would be in trying to control the Interferometer with any model of it. For such systems, the expected modeling errors can be classified as either mismodeled or unmodeled dynamics no matter what modeling technique is used [32, 13]. Dynamics that are well known and modeled but whose exact parameters are unknown will be referred to as *mismodeled dynamics*. For example, the the first bending mode of the truss may be well modeled by the beam, yet the exact value of the frequency of the mode may only be known within a small percentage of the true value. On the other hand, dynamics that are not well known, poorly modeled, or neglected will be referred to as *unmodeled dynamics*. The local vibration modes of the struts in the truss may be at a sufficiently high enough frequency to neglect in the modeling process. In this respect, the beam contains unmodeled dynamics since it does not capture the local truss modes. In summary, the beam model of the truss is a typical nominal model of a structural system in that it contains both mismodeled and unmodeled dynamics.

The advantages of pursuing this philosophy for the sample problem are apparent.

First of all, explicit state space models of both the truss and beam are available due to the relative simplicity of the sample problem. Hence there is an exact knowledge of the modeling errors between the actual and nominal systems, and there is an actual system to apply controllers based on the nominal model to. This combination of factors allows for a somewhat controlled environment in which to study stability robustness. Whereas in a realistic scenario, the lack of an exact description of the uncertainty along with the difficulties of implementing compensator complicates the theoretical analysis of stability robustness.

The intent of this section has been to show that the sample problem allows for a simple yet realistic investigation of many critical issues in structural control. Parallels between the sample problem and the Interferometer testbed were given to solidify the usefulness and simplicity of using the sample problem. Further, the convention of using the beam as a nominal model of the truss was introduced as a means of investigating how to deal with the reality of uncertainty in structural models.

2.2 Modeling

The details of the models used throughout this work are presented in this section. From this point on, the beam will be considered a model of the actual truss system that is to be controlled. Hence, presenting the specifics of the beam modeling process is akin to describing the design plant model of a control system. Finite Element Modeling, scaling (signal normalization), and model order reduction are the major stages of the beam modeling process which are presented here. Furthermore, in keeping with the outlined philosophy, a model of the truss is also developed as a reference system to compare the beam models to and an evaluation model to apply beam based compensators to.

2.2.1 State Space Models Using Finite Element Data

Since analytical models of realistic systems like the Interferometer are generally derived from Finite Element methods, Finite Element methods will be used to model

the truss and beam systems. In this section, the general procedure for creating state space models of structural systems from Finite Element models will be presented. The following section will describe the actual modeling process of the truss that uses the method presented here.

Letting M, K, and C denote the mass, stiffness, and damping matrices, the standard, dynamic finite element equations of motion for a structure with n degrees of described by the vector $q(t)$ are

$$M\ddot{q}(t) + C\dot{q}(t) + Kq(t) = \mathcal{U}u(t) + \mathcal{D}d(t) \tag{2.1}$$

$$y(t) = \mathcal{Y}q(t)$$

$$q \in \mathbf{R}^n \qquad d \in \mathbf{R}^p$$

$$u \in \mathbf{R}^m \qquad y \in \mathbf{R}^\ell$$

The $\mathcal{U}$, $\mathcal{D}$, and $\mathcal{Y}$ matrices simply contain constant values that place the location of the controls, $u(t)$, disturbances, $d(t)$, and sensors $y(t)$, at the appropriate degrees of freedom in $q(t)$. In using these placement matrices, the u, d, and y vectors only contain the forces and measurements in the beam (truss) system shown in Figure 2.2 (2.1). Since the damping matrix is in general a difficult quantity to evaluate, a modal modeling approach will be used to create a state space model of the system described by (2.1).

By assuming that the damping in the system described by (2.1) is modal in nature, that is assuming the damping matrix is a linear combination of the mass and stiffness matrices

$$C = \alpha M + \beta K, \tag{2.2}$$

the solution to the following set of homogeneous differential equations

$$M\ddot{q}(t) + Kq(t) = 0. \tag{2.3}$$

provides the undamped natural frequencies of vibration, ω_i, and corresponding mode shapes, ϕ_i, of (2.1). Realize that evaluating the free vibration modes from (2.3) is only an intermediate step in arriving at a state space representation of (2.1). Assembling the modes, ϕ_i, into a matrix Φ and assuming that these eigenvectors are mass

normalized so that

$$\Phi^T M \Phi = I \tag{2.4}$$

yields the following useful results that are a consequence of the inherent orthogonality of the modes

$$\Phi^T C \Phi = \Gamma \triangleq \text{diag}\{2\xi_i\omega_i\} \quad \text{and} \quad \Phi^T K \Phi = \Lambda \triangleq \text{diag}\left\{\omega_i^2\right\}. \tag{2.5}$$

In Γ, ξ_i is the modal damping in the i^{th} structural mode of the system with frequency ω_i and mode shape ϕ_i. Using (2.4) and (2.5), the full equations of motion, (2.1), can be decoupled by premultiplying (2.1) by Φ^T and substituting a transformed

$$q(t) = \Phi\eta(t) \tag{2.6}$$

into (2.1)

$$\begin{aligned} I\ddot{\eta}(t) + \Gamma\dot{\eta} + \Lambda\eta &= \Phi^T\mathcal{U}u(t) + \Phi^T\mathcal{D}d(t) \\ y(t) &= \mathcal{Y}\Phi\eta(t) \end{aligned} \tag{2.7}$$

The advantage of using a modal representation of the equations of motion should now be clear. Only the modal damping ratio in each mode, ξ_i, is needed to specify the damping model of the system, which is a tremendous simplification over having to derive a damping matrix for structural systems.

Now getting a state space model is a simple manner of breaking (2.7) down into a set of first order differential equations. Letting

$$x(t) \triangleq \begin{pmatrix} \eta(t) \\ \dot{\eta}(t) \end{pmatrix} \tag{2.8}$$

be the states of the system, the decoupled set of equations (2.7) can be rearranged to obtain a state space model representation of (2.1) with modal damping

$$\begin{aligned} \dot{x}(t) &= Ax(t) + B_2u(t) + B_1d(t) \\ y(t) &= Cx(t) \end{aligned} \tag{2.9}$$

where

$$A \triangleq \begin{bmatrix} 0^{n\times n} & I^{n\times n} \\ -\Lambda & -\Gamma \end{bmatrix} \quad B_1 \triangleq \begin{bmatrix} 0^{n\times p} \\ \Phi^T\mathcal{D} \end{bmatrix} \quad B_2 \triangleq \begin{bmatrix} 0^{n\times m} \\ \Phi^T\mathcal{U} \end{bmatrix} \quad C \triangleq \begin{bmatrix} \mathcal{Y}\Phi & 0^{\ell\times n} \end{bmatrix} \tag{2.10}$$

Notice that this approach only requires knowledge of the placement of the inputs, outputs, and disturbances at the assumed degrees of freedom in the model and the frequency, damping, and shape of the structural modes in the system. Since the number of states in (2.9) is two times the number of degrees of freedom in the original model, (2.9) will be referred to as the full order model.

2.2.2 Full Order Finite Element Models for the Beam and Truss

With a procedure for creating state space models of structural systems at hand, this section will describe the process of deriving a model of the beam which, in keeping with the philosophy of the sample problem, will be considered the nominal model of the truss system. The details of a state space model for the truss, that will serve as the evaluation model for the beam, will also be described. In both the truss and the beam, a one percent damping ratio will be assumed for all the modes, $\xi_i = .01\ \forall i$, to account for the inherently low levels of damping in structural systems like the Interferometer [33].

Realize from the previous section that the major part of the modeling process is the computation of the natural modes of the system. For both the beam and truss, the modes were evaluated by using the ADINA finite element program to assemble the mass and stiffness matrices and solve the homogeneous set of equations (2.3) [34]. The essence of the modeling process then boils down to spatially discretizing the system, carefully deciding upon what kind of elements and mass model to use, and evaluating the necessary properties of the elements in order to provide the finite element code with the proper data to assemble the mass and stiffness matrices. Realize that once

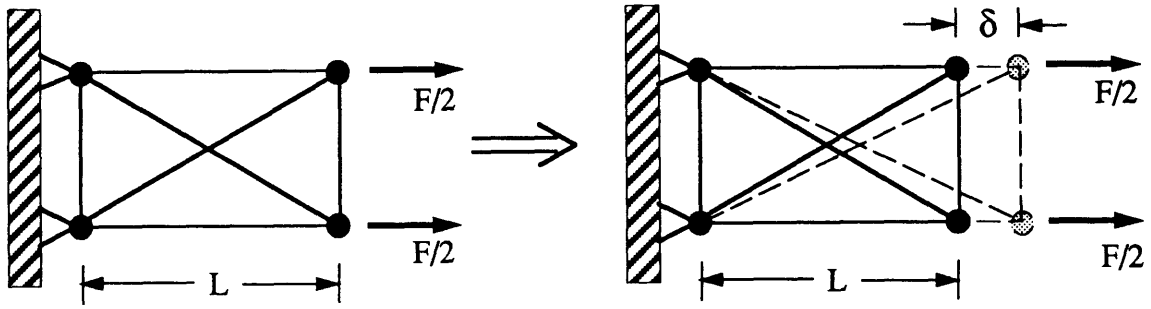

a.) Typical substructure under unit loading.

b.) Deformed substructure

Figure 2.4: Truss Substructure. Static test used to evaluate equivalent cross-sectional area.

the discretization of the system is decided upon, the $\mathcal{U}$, $\mathcal{D}$, and $\mathcal{Y}$ placement matrices can be trivially evaluated.

In terms of the philosophy of the sample problem, the values provided to the finite element program to evaluate the vibration modes of the beam should be chosen to mimic the dynamics of the truss system. In this way, the beam will serve as a model of the truss in that its dynamics will approximate those of the actual system. To this end, ten equally sized Bernoulli–Euler beam–column elements, one corresponding to each bay of the truss, were used in modeling the beam. In order to capture the dynamics of the truss in the beam model, the specific values of the beam element properties were derived by evaluating the equivalent beam properties of the truss system [35].

To exemplify how the equivalent structural beam properties were derived, consider Figure 2.4 that shows how the equivalent cross–sectional, A_c, of a beam–column approximation of the truss was calculated. In general, the substructure shown in Figure 2.4 is all that is needed to evaluate the equivalent beam properties of the truss, since the truss is composed of these symmetric, repeatable bays. Now to evaluate A_c, recall the simple proportional relation between an applied tensile load, F, and the axial deformation, δ, for a rod

$$F = \frac{EA_c}{L}\delta \tag{2.11}$$

where E is the Young's Modulus of Elasticity of the material and L is the length of the specimen. By evaluating the elongation of the substructure under a unit load, the cross–sectional area can be trivially backed out of (2.11)

$$F = 1 \Rightarrow A_c = \frac{L}{E\delta} \tag{2.12}$$

Similar simple static tests lead to the equivalent beam values of the bending moment of inertia, I_{xx}, and shear area, A_s of the truss [36]. However, the shear term was specifically excluded from the beam model to intentionally constrain it to be a lower fidelity model of the actual truss system. This is in keeping with the philosophy of the sample problem where it is desirable for the beam to contain unmodeled dynamics in order to mimic reality. Realize that the equivalent beam model would be a much better approximation of the truss had the shear properties been included [36].

As far as the mass properties of the beam model are concerned, a consistent mass model with lumped masses was used. The equivalent mass per unit length, ρA_c , of the beam was calculated by summing the mass of the struts in a repeatable section of the truss and dividing this sum by the substructure's length. To account for the mass of the joints in the truss, the mass of two truss joints was lumped at each node of the beam model. Finally by assuming the Young's Modulus, E, to be that of Aluminum, all the necessary values of the element properties were resolved and provided to ADINA to assemble the mass and stiffness matrices. A summary of these values is included in Figure 2.2.

In the case of the truss, the mass and stiffness matrices were assembled in a straight forward manner using the strut and joint characteristics shown in Figure 2.1. The nodes were located at the joints and mass loaded to accommodate for the mass associated with the joints. For the sake of simplicity, all the struts, including the active struts, were modeled as a Bernoulli-Euler beam elements. As with the beam, a consistent mass model was also used for the truss.

This brief explanation outlines how the mass and stiffness matrices of the beam and truss were created. Given the necessary data, ADINA provided the natural frequencies and mode shapes that were used along with the placement matrices to

form state space models from (2.9) and (2.10) for the beam and truss . As a first check on the fidelity of using the beam model to predict the dynamics of the truss, Figure 2.5 shows a comparison of the first few modes of vibration for the beam and truss that were evaluated from (2.3). Notice that in fact the beam does capture the shape and nominally predict the frequency of the first three bending modes and the first axial mode of the truss. Also notice that the fourth truss mode, which is a shearing mode, is not at all captured by the beam. This is to be expected since the necessary information the beam model needed to predict this mode was left out of the finite element model to be consistent with the philosophy of the sample problem.

In order to use the beam as a design plant model of the truss, the truss' actuators, sensors and disturbances must be included in the beam model so that it generates truss outputs, uses truss controls, and reacts to truss disturbances. Recall that the necessity of the beam model to produce truss inputs and measure truss outputs was seen in Figure 2.3 that depicts the philosophy of the sample problem. In essence, the beam model will be used to derive compensators for the truss for various reasons, and it is thus desirable to have a model that produces compensator that can be directly applied to the actual system they are designed for.

The process of modeling the truss inputs and disturbances in the beam involves deriving transformations from the truss inputs and disturbances to the beam inputs and disturbances so that

$$u_b(t) = T_u u_t(t) \tag{2.13}$$

$$d_b(t) = T_d d_t(t). \tag{2.14}$$

In these expressions, T_u and T_d are the input and disturbance transformations respectively while the b and t subscripts respectively denote the inputs and outputs for the beam and truss. The notation for u_b implies that

$$u_b = \begin{bmatrix} u_1 \\ u_2 \end{bmatrix}_{beam} \tag{2.15}$$

where u_1 and u_2 are defined in Figure 2.2. As mentioned, the inputs and disturbances that are specified for the beam in Figure 2.2 are the static equivalent of the truss

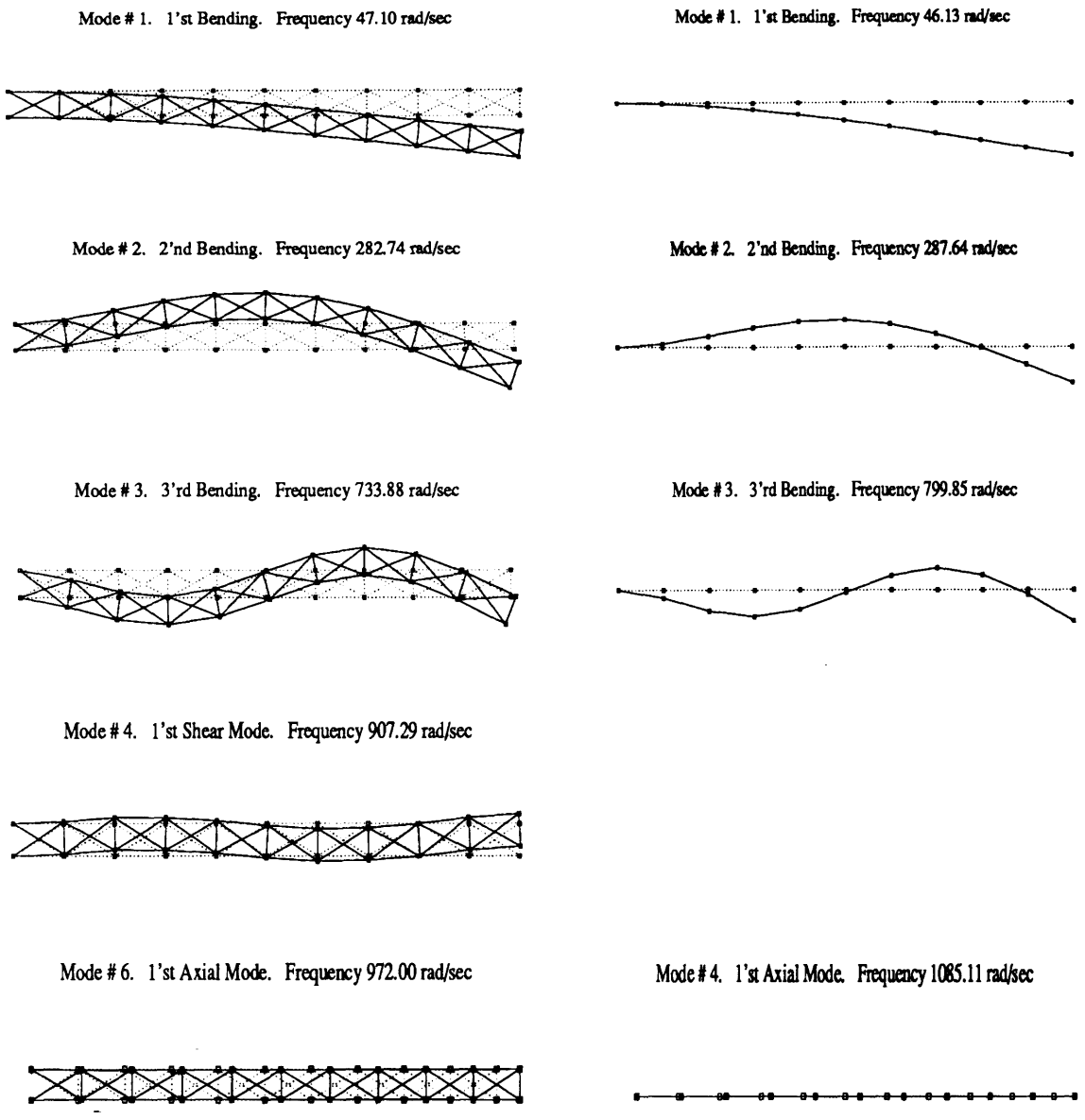

Figure 2.5: Comparsion of the undamped structural modes of the sample problem. Similar mode shape scale factors were used to depict all the modes.

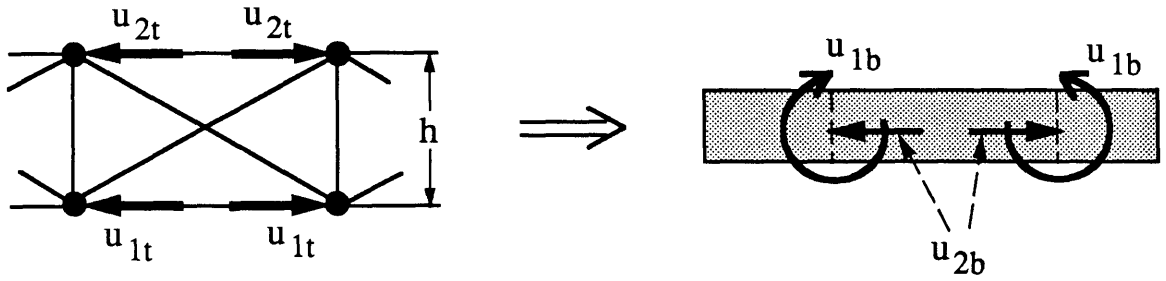

a.) Typical loading situation created by the active struts.

b.) Statically equivalent loading situation for the beam.

Figure 2.6: Statically equivalent loading situation for the truss and beam inputs.

inputs and disturbances reflected to the neutral axis of the truss. As result of this, T_u and T_d can be derived based on equivalent loading situations. To see how this was done for the sample problem, consider the equivalent loading situation used to derive T_u shown in Figure 2.6. Based on the static equivalence of the loads shown in Figure 2.6, T_u was evaluated to be

$$T_u = \begin{bmatrix} \frac{h}{2} & -\frac{h}{2} \\ 1 & 1 \end{bmatrix}. \tag{2.16}$$

Similar arguments lead to the disturbance transformation matrix, T_d.

On the other hand, the output transformations were derived based on geometric compatibility arguments. In order for the beam to capture the truss measurement off the neutral axis, it was necessary to measure the tip rotation of the beam as well as the axial and vertical displacements. Figure 2.7 shows the geometric compatibility used to derive the output transformation matrix, T_y,

$$y_t(t) = T_y y_b(t) \tag{2.17}$$

$$T_y = \begin{bmatrix} 1 & 0 & 0 \\ 0 & \frac{h}{2} & 1 \end{bmatrix} \tag{2.18}$$

where the b and t subscripts are used to differentiate the outputs of the beam and truss systems.

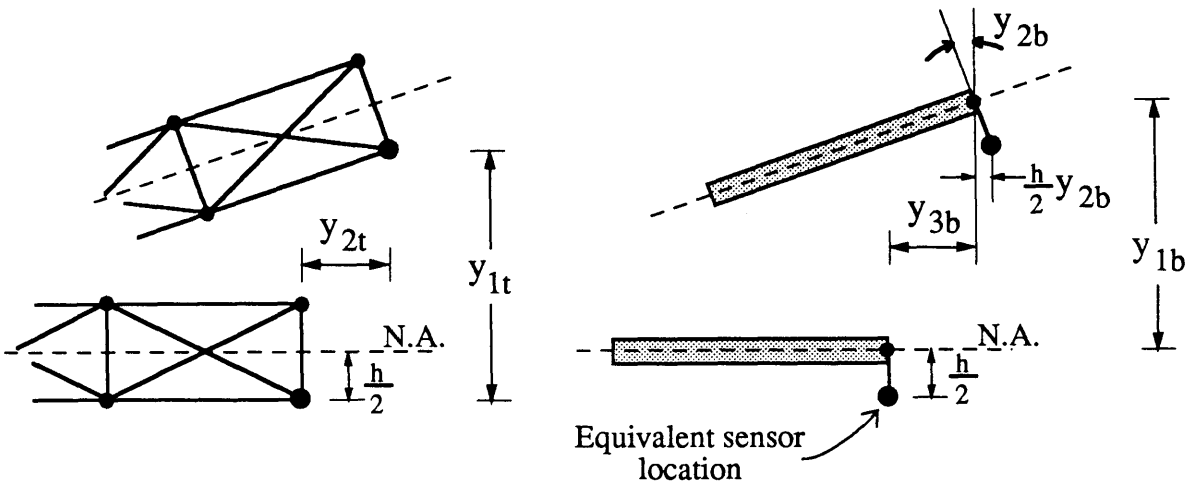

a.) Typical deformation in the truss system.

b.) Geometrically compatible deformation for the beam.

Figure 2.7: Geometric compatibility of the truss and beam outputs. The top figures show an exaggerated deformation from the undeformed configurations shown in the bottom figures. Here "N.A." denotes the neutral axis of the respective structures.

To finally arrive at a state space model of the beam that captures the input and output behavior of the truss, the transformations (2.13), (2.17), and (2.14) were applied to the inputs, outputs and disturbances of the full order state space system 2.9. In doing so, the transformation matrices T_u, T_d, and T_y were absorbed into the the B_2, B_1, and C matrices of the state space system. In terms of the block diagram of Figure 2.3 that clarifies the philosophy of the sample problem, the T_u matrix sits in the "Input Xfer" box and converts the truss controls generated by the "Beam Compensator" back to the beam inputs shown in Figure 2.2, and the T_y matrix sits inside the "Output Xfer" box and converts the beam outputs shown in Figure 2.2 into the truss outputs off of the neutral axis shown in Figure 2.1.

At this point in the modeling process, finite element models have been used to provide full order state space representations of the truss and beam. Whereas the truss system is driven by the "physical" inputs, outputs and disturbances, the beam model is driven by a model of those physical quantities. In the next section, the vector valued inputs, outputs and disturbances will be treated as signals that need

to be properly conditioned if they are to be used in multivariable control schemes.

2.2.3 Scaling the Signals

Unlike scalar systems, signals in a multivariable system are vector valued quantities. As a result of this, norms must be used to quantify the notion of a signal's size. The size of a vector, denoted by $\|\cdot\|$, depends upon the space in which it lies. Realizing that the signals of the sample problem are physical inputs, outputs, and disturbances, it makes sense to consider the class of bounded energy, or $\mathcal{L}_2$, signals. For an $\mathcal{L}_2$ signal $u(t)$, the size of $u(t)$, is dictated by its 2-norm

$$u(t) \in \mathbb{C}^m$$

$$\|u(t)\|_2 = \left(\int_{-\infty}^{\infty} u(t)^H u(t) \mathrm{d}t\right)^{\frac{1}{2}}. \tag{2.19}$$

At a specific frequency, ω , this norm is simply the standard Euclidean norm

$$\|u(\omega)\|_2 = u(\omega)^H u(\omega). \tag{2.20}$$

The 2-norm allows for a simple measure of how a vector valued signal propagates through a multivariable system. Consider a frequency domain representation of a general multivariable system

$$y(s) = G(s)u(s).$$

If a complex sinusoidal input at frequency ω

$$u(t) = \mathrm{u}e^{\jmath\omega t} \qquad \mathrm{u} \in \mathbb{C}^m \tag{2.21}$$

is applied to the system, the output and size of the output will be

$$y(t) = \mathrm{y}e^{\jmath\omega t} \qquad \mathrm{y} \in \mathbb{C}^l \tag{2.22}$$

$$\|\mathrm{y}(\omega)\|_2 = \|G(\jmath\omega)\mathrm{u}(\omega)\|_2.$$

Using the definition for the induced norm of a system and some singular value properties leads to the following bounds on the size of the output of the system

$$\|\mathrm{y}_{\max}(\omega)\|_2 = \max_{\|\mathrm{u}(\omega)\|_2=1} \|G(\jmath\omega)\mathrm{u}(\omega)\|_2 = \overline{\sigma}G(\jmath\omega) \tag{2.23}$$

$$\|\mathrm{y}_{\min}(\omega)\|_2 = \min_{\|\mathrm{u}(\omega)\|_2=1} \|G(\jmath\omega)\mathrm{u}(\omega)\|_2 = \underline{\sigma}G(\jmath\omega) \tag{2.24}$$

Hence, bounds on the output of a system over the space of all possible inputs such that $\|\mathsf{u}\|_2 = 1$ are easily evaluated by computing the maximum and minimum singular values, denoted $\overline{\sigma}$ and $\underline{\sigma}$ respectively, of a system matrix

$$\underline{\sigma}G(\jmath\omega) \leq \|\mathsf{y}(\omega)\|_2 \leq \overline{\sigma}G(\jmath\omega). \tag{2.25}$$

Evaluating the singular values of the system over a set of frequencies of interest constitutes the well known singular value plots that are analogous to Bode magnitude plots. Furthermore, inducing the norm of a system's sensitivity and complementary sensitivity transfer functions over appropriate signals leads to a loop shaping design paradigm for multivariable systems similar to that of scalar systems [37–39].

Realize, that this notion of size for a system's output is dependent on the input being in a ball in $\mathcal{L}_2$ at each frequency , that is $\|\mathsf{u}(\omega)\|_2 = 1 \ \forall\omega$. Various singular value plots between the inputs, outputs, and disturbances will be required to analyze and synthesize multivariable controllers for the sample problem. As a result of this, the input, output, and disturbance signals must all live in balls in $\mathcal{L}_2$ to properly interpret the singular value plots used to design controllers. Unfortunately, realistic signals do not live in balls in $\mathcal{L}_2$, and this is why it is necessary to scale the signals.

To exemplify what is meant by a ball in $\mathcal{L}_2$, why physical signals typically do not live in balls, and how to scale signals to be in balls consider $y(t) \in \mathbf{R}^2$, the output of the truss system. This example has the advantage of providing good physical insight into the task at hand. The real valued vector $y(t)$ at any instant, denoted simply by

$$y = \begin{pmatrix} y_1 \\ y_2 \end{pmatrix}, \tag{2.26}$$

has the following 2-norm

$$\|y\|_2 = y^T y = \left(y_1^2 + y_2^2\right)^{\frac{1}{2}}. \tag{2.27}$$

If a standard Euclidean basis for y is assumed and $\|y\|_2$ is set to unity, as is done when inducing the norm of a matrix, the resulting expression can be interpreted as the equation of a circle.

$$\|y\|_2 = 1 = y_1^2 + y_2^2 \tag{2.28}$$

If the signal had three components, $\|y\|_2 = 1$ would similarly give the equation of a sphere in $\mathbf{R}^3$. Even though it is difficult to visualize this interpretation of a vector norm for complex valued vectors of higher dimension, the concept still holds and is the basis for saying y is in a ball in $\mathcal{L}_2$ if $\|y\|_2 = 1$.

To get a grasp for why physical signals are usually not in balls, consider the outputs of the truss produced by the following static input load to the system.

$$u(0) = \begin{pmatrix} -1.0\ N \\ 1.0\ N \end{pmatrix} \tag{2.29}$$

Using a finite element routine, the outputs produced by this input were evaluated to be

$$y = y(0) = \begin{pmatrix} 3.51\ \mu m \\ .195\ \mu m \end{pmatrix}. \tag{2.30}$$

Notice that there is an order of magnitude difference in the size of the outputs. The large difference in the size of the outputs is a result of the physical nature of the truss system in which the vertical deformations, measured by y_1, are more predominant than the axial deformations, measured by y_2. Thus at any instant, the vector valued output will nominally lie in an ellipse in $\mathbf{R}^2$ as shown in Figure 2.8. As a result, any design based on the singular values of a the system with such an output would be misleading.

It is easy enough to alleviate this phenomena by simply normalizing each element of the output by its maximum allowable value, denoted by $\overline{y}_i$. The scaled output, $\tilde{y}$, can then be defined as

$$\tilde{y} = Q_y y \tag{2.31}$$

where Q_y is a diagonal, output scaling matrix

$$Q_y = \begin{bmatrix} \frac{1}{\overline{y}_1} & 0 \\ 0 & \frac{1}{\overline{y}_2} \end{bmatrix} \tag{2.32}$$

that contains the normalization factors used to scale the output. Realize that by normalizing each element of the signal, $\tilde{y}_1 = y_1/\overline{y}_1$ and $\tilde{y}_2 = y_2/\overline{y}_2$ will nominally be on the order of one but no greater than one at any instant. Hence the scaled input will lie in a disk in $\mathbf{R}^2$ as shown in Figure 2.9.

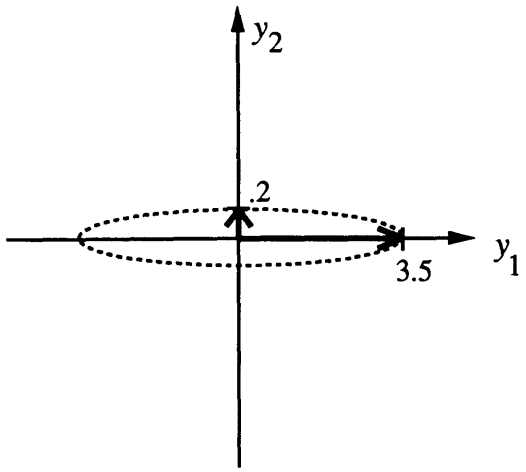

Figure 2.8: Unscaled Truss Outputs.

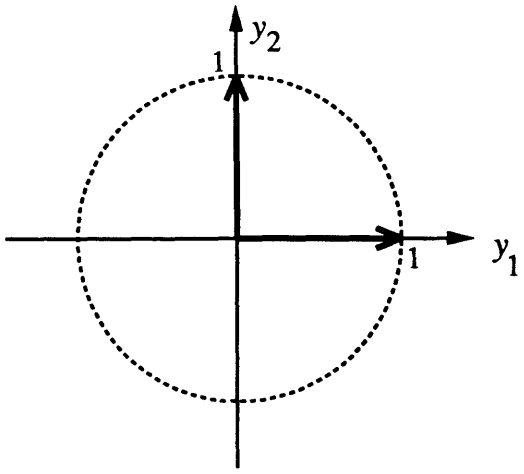

Figure 2.9: Scaled Truss Outputs.

Realize that this method of appropriately scaling the outputs can also be applied to the inputs and modeled disturbances. However, in the case of interest where the signals are complex sinusoids, it becomes necessary to ensure that the signals are in balls at all frequencies. Since frequency dependent scalings are undesirable though, the above scaling method is generally applied by choosing a particular frequency to scale the signals at to arrive at constant scaling transformations.

Given this brief exposition on the nuances of multivariable signals, the modeling process for the sample problem can continue. As described, the inputs, outputs, and disturbances of the beam model must all be in a ball in $\mathcal{L}_2$ for a proper interpretation of the singular values used in design. To begin the scaling process for the beam, notice that both inputs of the actual system are identical active struts. As a result of this, the actual input signals will generally lie in a ball in $\mathcal{L}_2$. Since the actual inputs were modeled in the beam system in Section 2.2.2, there is subsequently no need to scale the inputs of the beam model. For simplicity it was assumed that the actual disturbances also naturally occupy a ball in $\mathcal{L}_2$, and no scaling was performed for the beam disturbances. This is not at all the case with the beam outputs as already seen.

In essence, the method for scaling the beam outputs has already been outlined.

Only the frequency and maximum allowable outputs at that frequency need to be evaluated to arrive at a scaling matrix for the beam. In structural systems, DC ($\omega = 0$) is the logical frequency to evaluate the output normalizing factors at; since good approximations of the static behavior of the actual system are available in general. As a result of this, it is really only necessary to evaluate the output scaling matrix of the truss system, (2.32). Then the beam scaling can then be evaluated from the already defined transformation between the beam and truss outputs, (2.17). This procedure is more realistic, in terms of the sample problem philosophy, than evaluating a scaling matrix solely from the beam model, since it is based on estimating the behavior of the actual system. To arrive at the normalization values used in (2.32), the static deformation of the actual truss under an input load that produced the largest relative output was computed. Assuming a maximum allowable input of one Newton for the active struts, the largest tip deflection of the actual system in both directions is achieved when the active struts are actuated out of phase from each other. This is the load in (2.29) that was used in the previous analysis that produced the deformations in (2.30). Using the values of $y(0)$ in (2.30) for $\overline{y}_1$ and $\overline{y}_2$ in (2.32) yields the output scaling matrix for the truss model. It is important to realize that these values represent an ad hoc approach to properly conditioning the signals as an exact approach is intractable.

It is now a simple manner to incorporate the output scaling into the state space model of the beam. Using t and b subscripts to denote the truss and beam respectively, the output scaling matrix, Q_y can be lumped together with the output transformation matrix, T_y and reflected to the state measurement matrix, C, of the beam model in (2.9). From (2.31), (2.17), and (2.9)

$$\tilde{y}_t(t) = Q_y y_t(t) = Q_y T_y y_b(t) = Q_y T_y C x(t) \tag{2.33}$$

where the expression $Q_y T_y C$ is used as the output measurement matrix of the beam model that produces scaled truss outputs, which, as seen in Figure 2.3, is the desired output. Similarly, the output scaling was also included in the model of the actual system by reflecting Q_y to the C matrix of the truss model. While this modeling step

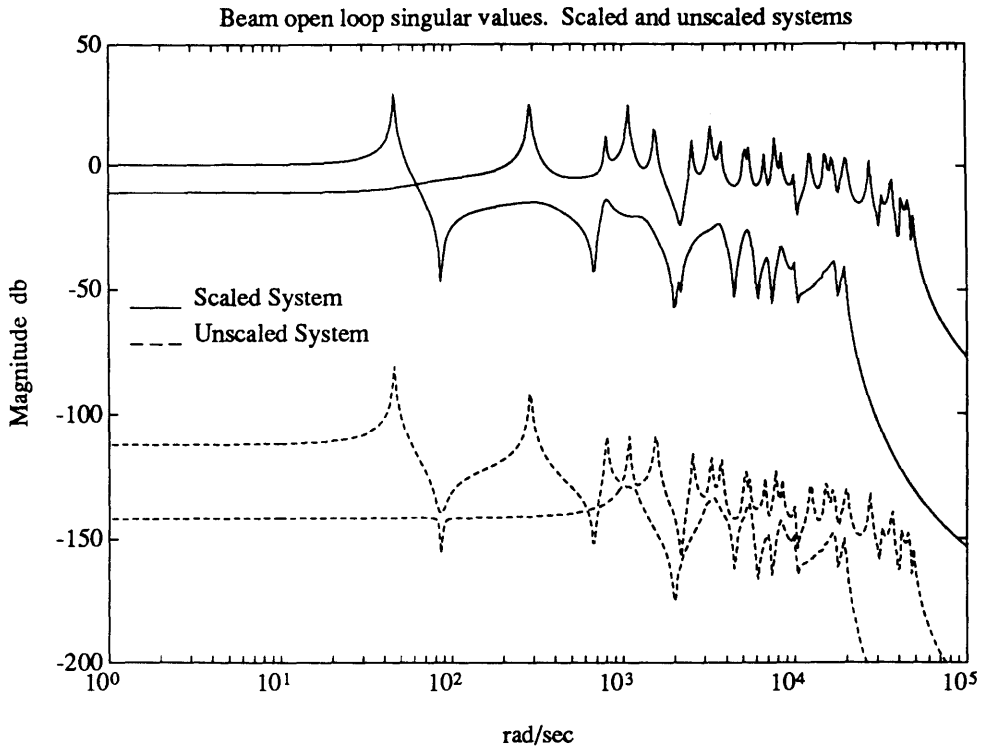

Figure 2.10: Comparison of the scaled and unscaled beam input to output loop singular values.

would not be applied in a realistic scenario, it is done here for the sake of comparing results between the beam and truss systems. For notational brevity throughout this work, it is assumed that the transformation and scaling matrices that were derived for the systems are included the B and C matrices of the standard state space models (2.9). A comparison of the input to output singular values for the scaled and unscaled beam system are shown in Figure 2.10. Notice that scaling does effect the singular values of the system and hence the analysis and synthesis of controllers.

At this point in the modeling process of the sample problem, full order finite element models of the truss and beam systems have been described. The exogenous signals of the truss system were modeled, scaled, and incorporated into the beam model so that it can be used to develop controllers for the actual truss system. Realize that the state space model as it now stands contains $2n$ states, where n is the dimension of q from (2.1). Large values of n, as is the case here, are undesirable for high authority multivariable control. In the next section model order reduction is

applied to the sample problem to arrive at a model suitable for control.

2.2.4 Model Order Reduction

The modeling approach used here is typical for structural systems and leads to models whose order increases with the complexity of the system. Unfortunately, high authority, multivariable control techniques nominally lead to compensators with orders at least as large as the order of the plant used in the design. Since controllers are intended to be implemented on actual systems and not the models used to derive them, model order reduction must be included in the design process to arrive at controllers that are realistically useful. Reducing the order of the design model is a common and simple technique used to arrive at low order controllers. The actual mechanics of the reduction process are quite simple. What is not simple is the selection of the dynamics to truncate to arrive at a reduced order model.

Before describing the criterion for truncating dynamics, it is useful to understand the specific mechanics that will be used in the model order reduction. To begin with, a frequency domain representation of the state space model (2.9) is used to facilitate a MIMO residue expansion of the model. Taking (2.9) into the frequency domain leads to

$$y(s) = G_1(s)d(s) + G_2(s)u(s) \tag{2.34}$$

$$G_1(s) = C(sI - A)^{-1}B_1 \tag{2.35}$$

$$G_2(s) = C(sI - A)^{-1}B_2 \tag{2.36}$$

where $G_1(s)$ and $G_2(s)$ respectively denote the performance and control loops transfer function matrices of the system. Using the knowledge that a state space model of a structural system derived from (2.1) contains n distinct pairs of complex conjugate modes leads to an equivalent expressions for the transfer function matrices in terms of their MIMO residue expansions.

$$G_1(s) = \sum_{i=1}^{n} \frac{F_{1_i}s + H_{1_i}}{s^2 + 2\xi_i\omega_i s + \omega_i^2} \tag{2.37}$$

$$G_2(s) = \sum_{i=1}^{n} \frac{F_{2_i}s + H_{2_i}}{s^2 + 2\xi_i\omega_i s + \omega_i^2} \tag{2.38}$$

In this representation, ω_i is the natural frequency of the i^{th} structural mode evaluated from (2.3), ξ_i is the assumed modal damping of the i^{th} structural mode, and F and H are the appropriate residues based on the partial fraction expansion. The values of F and H can be easily computed from an eigenanalysis of A

$$Av_i = \lambda_i v_i \tag{2.39}$$

$$w_i^T A = \lambda_i w_i^T \tag{2.40}$$

and the B and C matrices of the state space representation.

$$F_{1_i} = C\left(v_i w_i^T + v_i^* w_i^H\right) B_1 \tag{2.41}$$

$$F_{2_i} = C\left(v_i w_i^T + v_i^* w_i^H\right) B_2 \tag{2.42}$$

$$H_{1_i} = -C\left(v_i w_i^T \lambda_i + v_i^* w_i^H \lambda_i^*\right) B_1 \tag{2.43}$$

$$H_{2_i} = -C\left(v_i w_i^T \lambda_i + v_i^* w_i^H \lambda_i^*\right) B_2 \tag{2.44}$$

Here x^* denotes the complex conjugate of x, and x^H the complex conjugate transpose of x.

Realize that the response of the system is now represented as the weighted sum of the structural modes. Such a form has significant advantages when used to reduce the order of structural systems. If certain modes do not significantly contribute to the response of the system, they can simply be truncated from the model by neglecting the appropriate terms in the residue expansion. Since the number of states in these models is twice the number of structural modes, the order of the reduced model depends on how many modes are truncated. Once the undesirable modes are truncated, a reduced order model of the system can be obtained by reconstructing the state space from the modes that remain in the expansion. The specific process of reconstructing a state space will not be discussed here. A detailed account of this model order reduction technique, including the specifics on reconstructing the state space, can be found in [40].

At this point, it is simply a matter of deciding which structural modes to keep in the design model to arrive at a reduced order representation of the beam system. Extensive literature exists on selecting the appropriate However, in an effort to con-

centrate on the stability robustness traits of the sample problem, none of the schemes in the literature were used. Rather, simple bandwidth arguments were employed to decide upon which dynamics to retain in the design model. With the intention of controlling the first few modes of the truss system, it was decided to retain all the structural modes one decade beyond the targeted bandwidth of the controller. From the input to output singular value plot of the beam system, Figure 2.10, one can see that this objective corresponds to a bandwidth of roughly $500 rad/sec$. Hence, all the structural modes above 5000 rad/sec were truncated from the beam model. Specifically for the beam model, this meant retaining the first nine structural modes and truncating the remaining 21 modes. Realize that this is not at all an optimal method of selecting which modes to truncate. However, the intent here is only to capture the effect of model order reduction in the sample problem, and for this objective the ad hoc selection of modes to truncate does suffice.

Up to now, the term "truncate" was judiciously used to describe what happened to the modes left out of the reduced order model. In fact, by truncating modes specific dynamics of the model are neglected. This can be seen by considering the structural modes to be arranged in increasing order of frequency and rewriting (2.37) and (2.38) in terms of the r retained modes and $n-r$ modes to be truncated.

$$G_1(s) = \sum_{i=1}^{r} \frac{F_{1_i}s + H_{1_i}}{s^2 + 2\xi_i\omega_i s + \omega_i^2} + \sum_{i=r+1}^{n} \frac{F_{1_i}s + H_{1_i}}{s^2 + 2\xi_i\omega_i s + \omega_i^2} \tag{2.45}$$

$$G_2(s) = \sum_{i=1}^{r} \frac{F_{2_i}s + H_{2_i}}{s^2 + 2\xi_i\omega_i s + \omega_i^2} + \sum_{i=r+1}^{n} \frac{F_{2_i}s + H_{2_i}}{s^2 + 2\xi_i\omega_i s + \omega_i^2} \tag{2.46}$$

Simply neglecting the second term of these expressions, which corresponds to the modes to be truncated, introduces errors in the reduced order model. The predominant effects of simply neglecting the truncated dynamics are an improperly modeled system response, inaccurate DC behavior, and mismodeled multivariable transmission zeros [41]. The magnitude of these errors can be seen in Table 2.1 that shows a comparison of the DC gain and the first few control loop zeros for the full order and reduced order models of the beam. The errors are not that drastic for this system, but this may not always be the case. In any event, the transmission zero and DC errors can be reduced by including the static contribution of the truncated modes in

Model Description		Full Order	No Static Correction	Static Correction
No. of States		60	18	18
$\|G_2(0)\|_2$		1.05	1.11	1.05
Zero # 1	*freq.*	86.3	85.9	86.3
	value	-.626 $\pm$ 86.3$\jmath$	-.621 $\pm$ 85.9$\jmath$	-.626 $\pm$ 86.3$\jmath$
Zero # 2	*freq.*	677.6	673.2	677.6
	value	-6.59 $\pm$ 677.6$\jmath$	-6.49 $\pm$ 673.2$\jmath$	-6.59 $\pm$ 677.6$\jmath$
Zero # 3	*freq.*	1376.8	1770.0	1363.7
	value	-1376.8	-15.3 + 1770.0$\jmath$	-1363.7
Zero # 4	*freq.*	1396.5	1770.0	1379.0
	value	1396.5	-15.3 - 1770.0$\jmath$	1379.0

Table 2.1: Comparison of the DC gain and multivariable transmission zeros for various models of the beam. Frequencies are in *rad/sec.*

the reduced order models.

Introducing the static contribution of the truncated modes into the reduced order model does not increase their order. Rather, it simply adds feed–forward terms to the modeled response of the system. The feed–forward, or D terms, are simply evaluated by setting the frequency to zero in the summation of the truncated modes in (2.45) and (2.46).

$$G_1(s) = \sum_{i=1}^{r} \frac{F_{1_i} s + H_{1_i}}{s^2 + 2\xi_i \omega_i s + \omega_i^2} + D_1 \tag{2.47}$$

$$G_2(s) = \sum_{i=1}^{r} \frac{F_{2_i} s + H_{2_i}}{s^2 + 2\xi_i \omega_i s + \omega_i^2} + D_2 \tag{2.48}$$

$$D_1 = \sum_{i=r+1}^{n} \frac{H_{1_i}}{\omega_i^2} \qquad D_2 = \sum_{i=r+1}^{n} \frac{H_{2_i}}{\omega_i^2} \tag{2.49}$$

In returning to a state space representation of the above truncated system there will be $2r$ states for the r retained structural modes and D terms in both the control and disturbance loops to account for the truncated dynamics.

$$\dot{x}(t) = Ax(t) + B_2 u(t) + B_1 d(t) \tag{2.50}$$

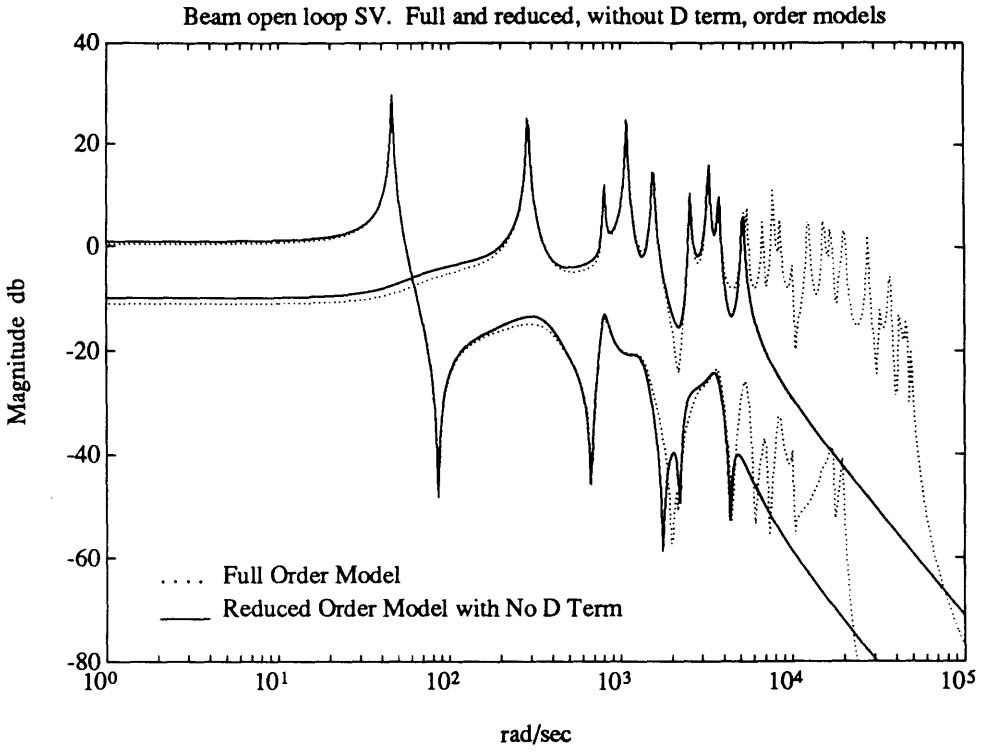

Figure 2.11: Comparison of the beam open loop input to output singular values for the full order model and the reduced order model without the static correction term.

$$y(t) = Cx(t) + D_2u(t) + D_1d(t) \tag{2.51}$$

For the sake of notational brevity, no new notation is used to distinguish the state matrices of this reduced order representation of the beam from the full order representation (2.9). Further in reconstructing the state space representation from the truncated partial fraction expansion, it is possible to preserve the structure of the original A matrix. This means that the A matrix of (2.50) will have the same form as the A matrix of (2.10) but will only contain the frequencies and damping ratios of the r retained modes.

As a means of comparing the reduced and full order models, consider Figures 2.11 and 2.12 that that compare the open loop singular values of $G_2(j\omega)$ for the reduced and full order models of the beam. Notice that the poles of the reduced order models corresponding to the retained modes are identical to those of the full order model. This is to be expected since the truncation of modes does not affect the denominators

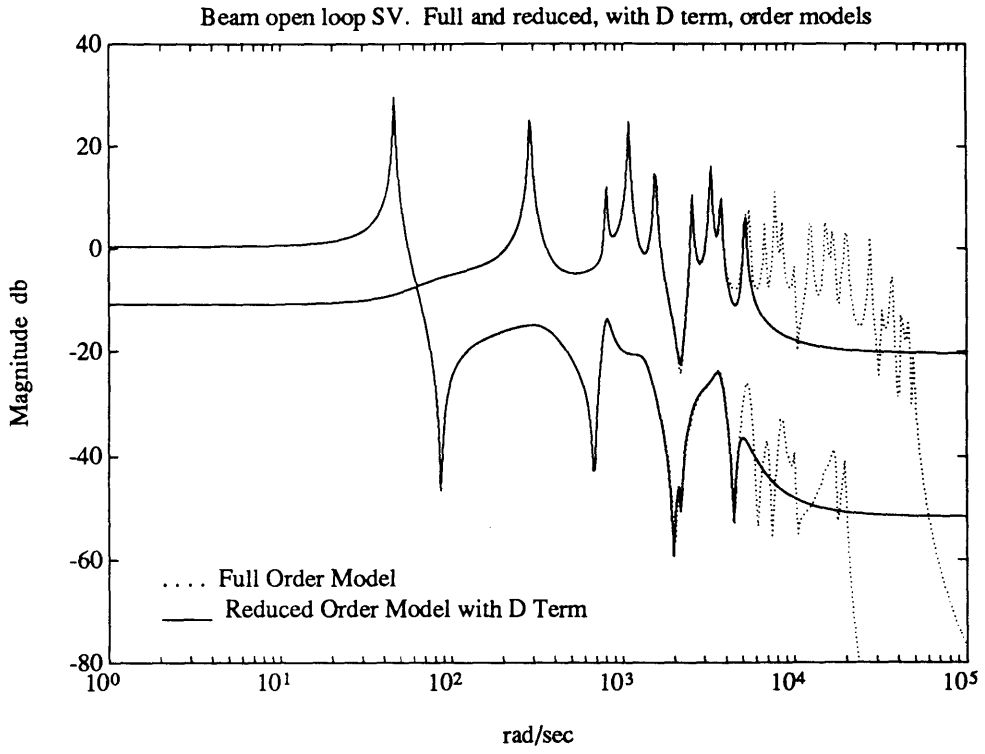

Figure 2.12: Comparison of the beam open loop input to output singular values for the full order model and the reduced order model with the static correction term.

of the retained terms in the residue expansion (2.48). Furthermore, the DC error in the reduced model with no static correction is visible in Figure 2.11, while there is no visible DC error in Figure 2.12. These same attributes apply to the third and fourth transmission zeros of the control loop, as seen in Table 2.1, Figure 2.11, and Figure 2.12. In general, the reduced order model with the static correction provides an almost exact representation of the full order system up to its truncation frequency.

The added fidelity the D terms contribute to the reduced order model should now be apparent. However, the inclusion of the D terms in the state space representation has implications that must be discussed. Consider first the D_1 term in the disturbance loop of the model. The presence of this term in (2.51) requires the disturbances to be directly fed forward to the outputs of the system. Such a procedure is pure nonsense since the disturbance signals are not available in real life. This situation is simply a case where the mathematics of creating lower order models conflicts with the physics

of the real world. For this reason, the D_1 term will be neglected in the model of the beam throughout the remainder of the work. The implications of this on the fidelity of the model are inconsequential. Basically, there will be some DC and transmission zero errors in the disturbance loop similar to those of the control loop discussed above. However, the main focus of this thesis is on stability robustness, and the ramifications of neglecting the D_1 term on the overall performance will not be discussed.

Unlike the D_1 term, there is nothing physically wrong with including the D_2 term in the output of the model. By their nature, the control signals are available and can be directly fed to the outputs. Unfortunately though, the presence of the D_2 terms in the model will complicate the controller synthesis process, as most control synthesis results are based on a state space models of the form (2.9) [22]. However, these complications are not limitations, and it is simply a manner of generalizing the existing theory to account for the D_2 term in the designs. Aside from the mechanics of synthesizing controllers, the D_2 term introduces an all pass characteristic to the control loop of the design model. That is the open loop models will not roll off, as seen in Figure 2.12. From a stability robustness point of view, this is a very undesirable trait. Without getting into the details of this issue which will be discussed in the sequel, systems that don't roll off in the region of unmodeled dynamics are extremely susceptible to instabilities. Most physical systems have a natural roll off built into them that helps maintain stability in the presence of unmodeled dynamics. By including the D_2 term in the control loop of the model, the beam system will not possess this quality, and controllers based on it will be more prone to drive the truss unstable. On the other hand from a modeling point of view, the all pass attribute introduced by the D_2 term is beneficial. Specifically, notice from Figure 2.12 that there are still dynamics past the truncation frequency of the reduced order model. The reduced order model with the static correction does not predict these dynamics, but rather by its all pass nature it contains the knowledge that there are still significant dynamics beyond the truncation frequency. Conversely, the reduced order model without the static correction rolls off as if there were no more dynamics beyond the truncation frequency. This is not at all the case, and it would be inappropriate

to design compensators based on the reduced order model without the D_2 term. Realizing this, the D_2 term in the control loop will remain in the design model of the beam throughout this work. If it is not possible to design sufficient compensators given the model with the D_2 term, then it is unreasonable to expect that the design objectives could be met with high authority control schemes.

In summary, the beam design plant model will be denoted as

$$\begin{aligned} \dot{x}(t) &= Ax(t) + B_2u(t) + B_1d(t) \\ y(t) &= Cx(t) + D_2u(t) \end{aligned} \tag{2.52}$$

throughout the remainder of the work. Recall that the model captures the input, output, and disturbance attributes of the truss, has scaled outputs for a proper interpretation of the singular values used in design, and contains 18 states with a static correction in the control loop to account for the truncated dynamics. The specific values of the state space matrices in (2.52) are included in Appendix A for reference. In keeping with the philosophy of the sample problem, a mathematical model of the truss was analogously created to have a reference actual model for the beam. The form of the truss model is identical to that of beam model. Using the same method and criterion to reduce the order of the truss lead to an evaluation model with 60 states and a static correction, D_2, term. The nominal reason for reducing the order of the evaluation system was to have an evaluation model with dynamics over the same range as the design model. This step is not consistent with the philosophy of considering the truss to be the actual system. Rather, it is a simplifying measure that reduces the complexity of interpreting comparisons between the truss and beam models. The values of the state space matrices for the truss evaluation model used throughout the sequel are also included in Appendix A for reference.

As of now, the modeling of the actual truss system is nearly complete. The only step of the modeling process that has not been discussed in this chapter is the modeling of the uncertainty in the beam model. This is the topic of Chapter 3.

Chapter 3

Assessing the Uncertainty

Given a mathematical model of a physical system, the designer must evaluate its fidelity and limitations before synthesizing controllers. This is especially true for structural systems whose lightly damped and modally rich nature makes them quite susceptible to closed loop instabilities [28]. To see this, consider a comparison of the Nyquist plots for a single mode

$$g(s) = \frac{\omega_n^2}{s^2 + 2\xi\omega_n s + \omega_n^2} \tag{3.1}$$

with typical structural damping, $\xi = 1\%$, and typical servo damping[1], $\xi = 20\%$. For $\omega_n = 1\ rad/sec$, a blow up of the Nyquist plots near the critical point is shown in Figure 3.1. Notice how close the Nyquist plot for the lightly damped system comes to the critical point, assumed to be at (-1,0) here, as compared to the Nyquist plot of the heavily damped system. Since stability robustness is a measure of the distance to the critical point, it is obvious that the lightly damped system is much more susceptible to instabilities than the heavily damped one. Also, since there is less distance to the critical point from the Nyquist plot of the lightly damped system, there is less room for error in the model of the lightly damped system. Thus, the accuracy of models for structural systems does play a key role in assuring closed loop stability. Further, the modally rich nature of structural systems means that there are many occasions where the Nyquist plot zooms near the critical point, and hence there are more chances

[1]This value is typical of the damping in a Phugoid mode of an aircraft.

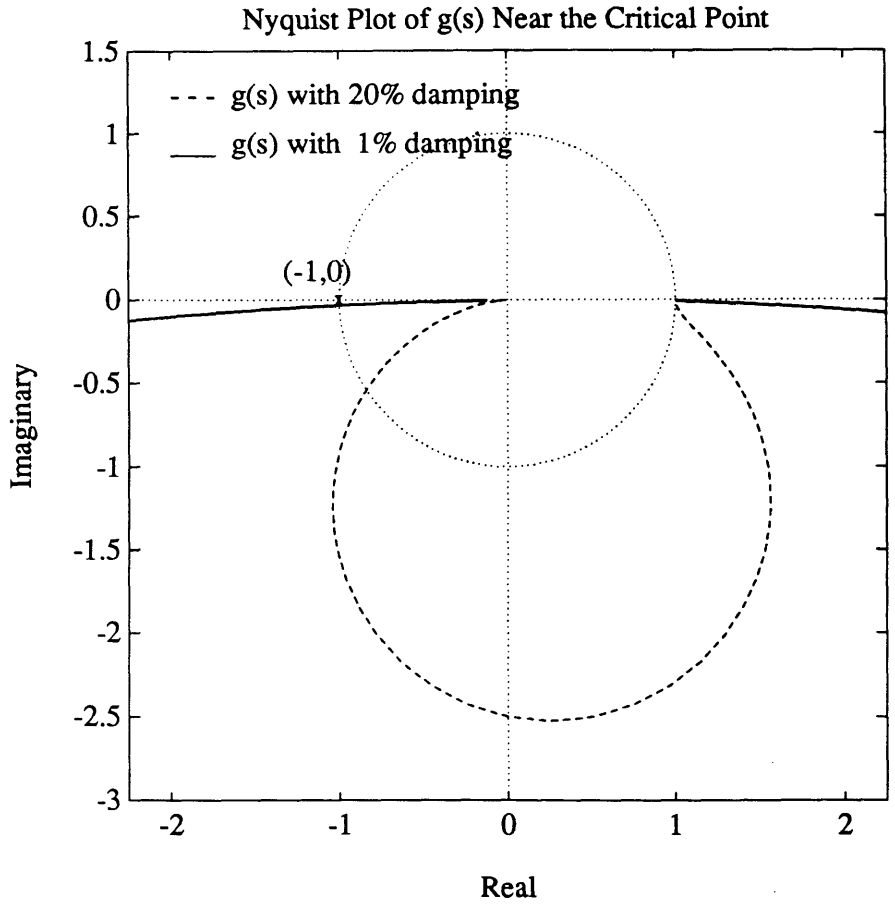

Figure 3.1: Comparison of Nyquist plots with typical structural damping and typical servo damping near the critical point. Only the map of $g(j\omega)$ for $\omega \in (0, \infty)$ is shown to maintain clarity.

for the system to become unstable. Acknowledging these characteristics, it becomes necessary to employ stability constraints in the synthesis of controllers for structural systems. Various robustness techniques for guaranteeing closed loop stability will be analyzed in Chapter 4. Before embarking on such a study, the nature of the uncertainties in a model of a system must be well understood. The focus of this chapter is thus an in depth study of the modeling errors that will occur in models of systems like the Interferometer testbed.

The logical way to begin an investigation of a model's fidelity is to make use of the available a priori information. The nature of the system and the choice of modeling process both provide insight into how accurate a model has to be and how accurate

a model is. As outlined above, the nature of structural systems necessitates models that are as accurate as possible. However, as was alluded to in the philosophy of the sample problem, accurate models of structural systems are hard to come by. In fact, the accuracy of a structural model varies depending on the modeling process used. For example, models derived from experimental measurements are typically more accurate than models derived from finite elements in the frequency range where good data is available, while experimental models do not offer the physical significance that finite element models provide. Hence a good qualitative measure of the accuracy of a structural model is often provided by the assumptions and limitations of the actual modeling process.

As an example of how a structural model's fidelity can be analyzed, consider the approximate modeling process of the truss system. In assuming a beam model for the truss there are specific truss dynamics that are not accounted for in the design model, such as the dynamics of the individual struts in the truss, in addition to the shear modes that are purposely neglected in accordance with the philosophy of the sample problem. The design model will thus contain unmodeled dynamics at intermediate frequencies. Furthermore, Finite Element modeling itself imposes limitations on the accuracy of the beam model. Once the wavelength of the vibrations are on the order of the element size, the finite element model is quite inaccurate. As a result, the fidelity of the beam model is inherently quite poor at high frequencies. Combining this information with knowledge of the unmodeled shear modes, it is obvious that the beam based model of the truss is only reasonably accurate at low frequencies. That is not to say that the model is exact at low frequencies. The process of approximating the truss properties along with the inability of finite element models to exactly predict low frequency behavior leads to slight errors between the first few modes of the beam and actual truss; as seen in Figure 2.5. In this respect, the low frequency dynamics of the actual system are well known but are mismodeled. This simple evaluation of the modeling process provides good qualitative information about the accuracy of the beam model, but qualitative information alone is not sufficient for dealing with the uncertainty.

Multivariable stability robustness techniques require explicit uncertainty descriptions. Once a qualitative feel for a model is available, a further measure of its accuracy can be obtained by quantifying the qualitative errors. The ability to predict the size of the expected errors helps determine how close the Nyquist plot of the actual system gets to the critical point, which in turn provides a means to quantify how much modeling error a feedback design can safely tolerate. Without a quantitative description of the uncertainty, control system designs would have to be overly conservative to ensure that the Nyquist plot stayed away from the critical point. While it is necessary to quantify the modeling errors, it is not at all a straight forward process to do so. Exact descriptions of the uncertainty are unrealistic. If some error was exactly known, it would not be uncertain and could certainly be used in the design model. As a result of this reality, uncertainty models are usually derived from insight and engineering judgment gained in the modeling process and from a qualitative description of the uncertainty. Even though uncertainty models are often ad hoc estimates of a model's accuracy, they are necessary components of robust control design.

The sample problem presented in Chapter 2 provides a simple framework in which to understand the ad hoc nature of uncertainty descriptions. For the time being, consider the realistic situation where there is no model of the actual truss system available. As discussed above, the beam design model is only accurate at low frequencies with unmodeled dynamics at higher frequencies. To quantify the model's fidelity it is necessary to specify how accurate the beam model is at low frequencies and what the frequency range of accurate dynamics is. Since the beam model can not predict the shear modes of the truss, an upper bound on the frequency range of accurately modeled dynamics could be set by estimating the frequency of the first truss shear mode. Beyond that frequency, the beam model will definitely contain unmodeled dynamics. Below that frequency, there will be errors in the values of the frequency, residue, and damping of the beam's axial and bending modes. Having used an equivalent modeling procedure to capture the input/output topology and the axial and bending characteristics of the truss, it is safe to assume that the values of frequency, residue, and damping for the first few beam modes are well modeled

and accurate to within five percent of the actual truss values. However, it is possible that the beam will approximate modes in the truss with large errors (greater than ten percent) in frequency, damping and residue. Such errors would be classified as unmodeled dynamics since the behavior is poorly modeled. If there were such uncertainties below the frequency of the first shear mode of the truss, a more accurate upper bound on the frequency range of accurately modeled dynamics would be set in the vicinity of the poorly modeled modes. In a realistic modeling situation, this uncertainty description is typical of the level to which the accuracy of a model could be characterized without experimental validation.

Up to now a simple and realistic exposition of uncertainty modeling has been described. Given a model of a system, the designer must understand the limitations and assumptions in the modeling process in order to quantify the uncertainties in at best an ad hoc manner. In an effort to become more comfortable with this heuristic modeling procedure, the sample problem setup was used to validate the realistic uncertainty modeling process for the beam already described. In the following sections, the beam model is compared to the actual truss system model to verify the realistic uncertainty model and to understand how the uncertainties manifest themselves in many of the common tools of control system design. Understanding specifically how the expected modeling errors effect the common analysis tools of robust control design will provide an extra dimension of engineering judgment when it comes time to evaluate the fidelity of models for actual systems like the Interferometer testbed.

3.1 Individual SISO Transfer Functions

Even though individual scalar transfer functions are not useful in multivariable controller synthesis, they do provide useful information about the model used in design. With the widespread availability of spectral analyzers, it is a simple matter to measure scalar transfer functions between the inputs and outputs of the actual, physical system being modeled. Given this ability, experimental scalar transfer functions can either be used to derive multivariable state space models [9, 10] or validate math-

ematically created models. Pursuing the later avenue by comparing measured and modeled transfer function serves as a more precise means of quantifying the accuracy of a design model. A wise control system designer would surely compare the scalar transfer functions of their model to the readily available, experimentally measured ones.

In order to understand what added information this technique provides, the individual scalar transfer functions of the truss open loop dynamics, which mimic experimentally measured data in the sample problem framework, were compared to the corresponding scalar transfer functions of the nominal beam based model of the truss. Neglecting the disturbance term in (2.52) and taking it into the frequency domain leads to the input/output relation

$$y(s) = G_2(s)u(s) \tag{3.2}$$

in which $G_2(s)$ can be written in a form conducive to evaluating the scalar transfer functions necessary for the desired comparison

$$G_2(s) = C(sI - A)^{-1}B_2 + D_2 = \begin{bmatrix} g_{11}(s) & g_{12}(s) \\ g_{21}(s) & g_{22}(s) \end{bmatrix}. \tag{3.3}$$

Comparing the Bode plots for each $g_{ij}(s)$ where

$$y_i(s) = g_{ij}(s)u_j(s) \qquad i,j = 1,2 \tag{3.4}$$

between the truss and beam systems, shown in Figures 3.2 and 3.3, provides a representative comparison of the "measured" and modeled transfer functions. Since the truss Bode plots could be experimentally measured in the real world, the plots of Figures 3.2 and 3.3 do represent a realistic way to asses the fidelity of the beam design model.

As far as the assessment of the uncertainty goes, notice that the low frequency mismodeled and high frequency unmodeled dynamics are plainly seen in these plots. The plots demonstrate that there are slight errors in the frequency of the first two poles and the first zero, but that the beam model in general does a good job of predicting the dynamics below $700 rad/sec$ or so. Given the experimental measurements, the

specific discrepancies between the frequency and damping of the well modeled beam and truss poles could be evaluated using standard modal testing techniques [42]. On the other hand, beyond 700 rad/sec there are significant errors in each transfer function at various frequencies. Specifically notice that while the third bending mode, near 700 rad/sec, is captured in the beam model, it is poorly modeled. Further since the scalar poles shown in these plots are no different than the poles of the multivariable system, a more accurate lower bound on the range of unmodeled dynamics than the first shear mode of the truss would be the frequency of the third bending mode of the truss, approximately 700 rad/sec. Realize that while there is an equally large error in the frequency of the second zero in each of the scalar transfer functions, the frequency of these scalar zeros can not be used as a measure of the multivariable system's fidelity.

In summary, these scalar bode plots have graphically led to a more accurate division of the region of mismodeled and unmodeled dynamics. From here on in, the dynamics below 700 rad/sec will be considered mismodeled while those above 700 rad/sec will be classified as unmodeled. Even though this method of comparing scalar frequency response functions is readily applicable in the real world and useful in assessing the uncertainty in a model, it should be understood that scalar transfer functions have little use in multivariable controller synthesis.

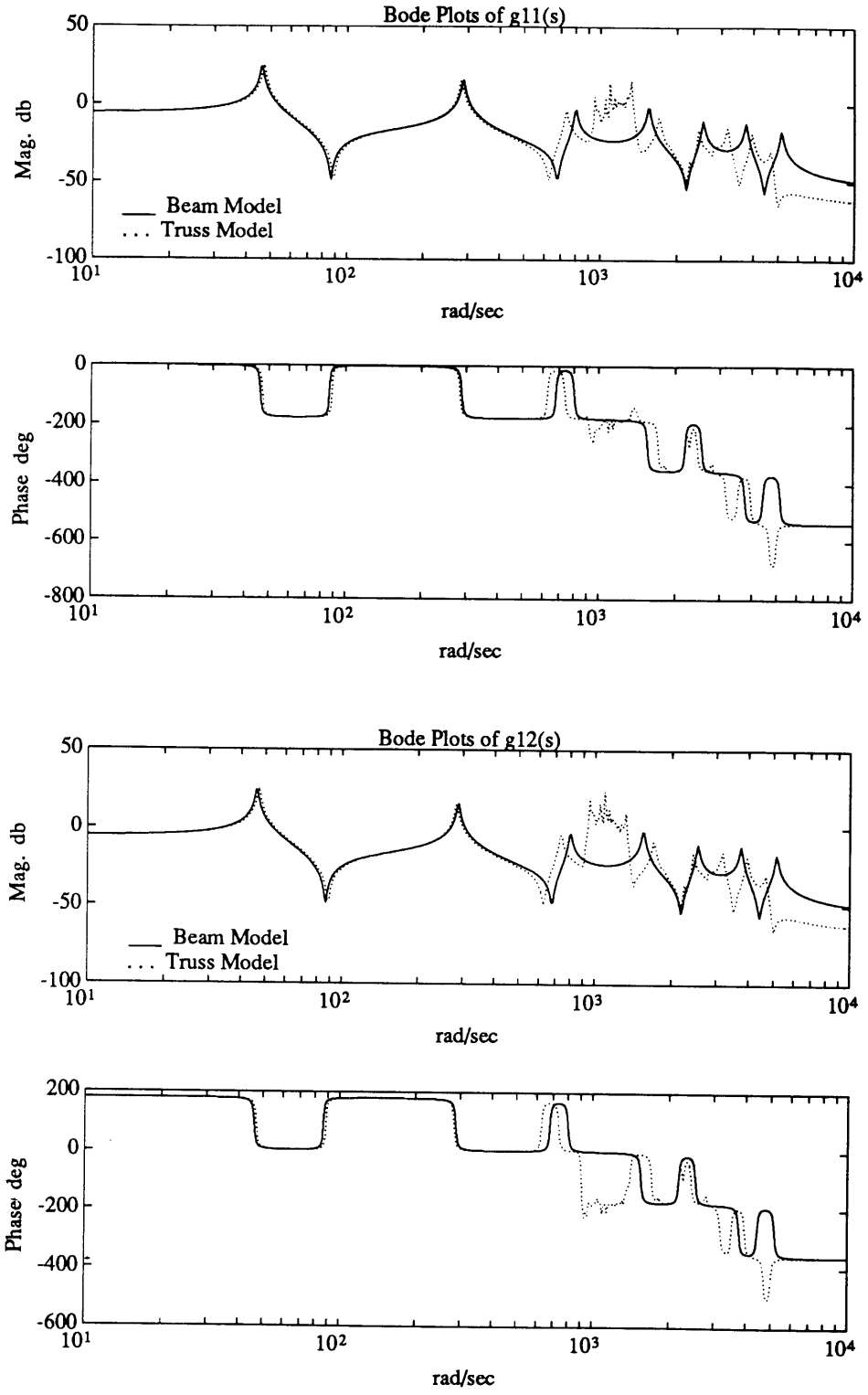

Figure 3.2: Comparison of scalar, control loop transfer functions for the beam and truss.

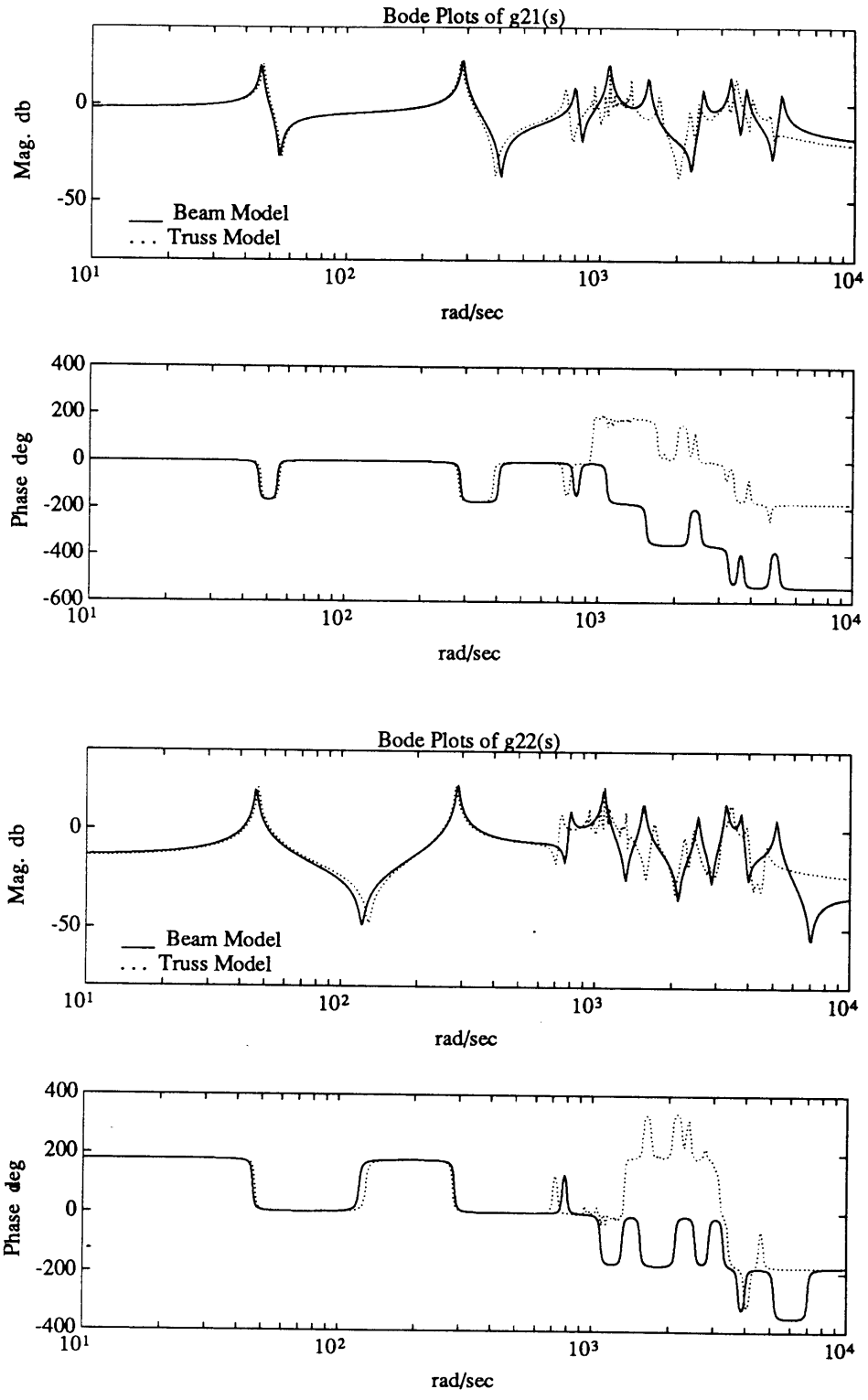

Figure 3.3: Comparison of scalar, control loop transfer functions for the beam and truss.

3.2 Multivariable Magnitude Information

As mentioned in section 2.2.3, the appropriate measure of magnitude for a multivariable transfer function matrix that can be used in frequency response analysis is provided by singular values of the transfer function matrix. In fact, multivariable control system design relies heavily on singular value information. For this reason it is important to understand how modeling uncertainties manifest themselves in the singular value plots used in design. Unfortunately, singular values can not be easily measured in the laboratory like their analogous scalar frequency responses. Hence there is no transparent way in which to asses how modeling uncertainties affect the singular values of a model. Herein lies the usefulness of the sample problem. By comparing the singular values for the truss and beam models, it should become apparent how the expected uncertainties manifest themselves in the singular values. To this end, a comparison of the open loop singular values of $G_2(s)$ for the beam and truss is shown in Figure 3.4.

While Figure 3.4 is an unrealistic measure of the of the beam model's fidelity, it does verify the heuristically derived uncertainty model. First of all, notice that this plot looks very similar to the realistic, scalar, magnitude Bode plot comparisons of Figures 3.2 and 3.3. The high frequency unmodeled dynamics begin at around 700 rad/sec, and the low frequency dynamics are well modeled but contain slight errors in the frequency and residue of the modes. In essence, the singular value comparison confirms the ad hoc description of the uncertainties and shows that the errors manifest themselves in ways similar to the scalar magnitude Bode plots. It is reassuring to know that the errors which appear in the commonly used singular value plots as a result of the modeling process can be predicted from the measurable, scalar transfer functions.

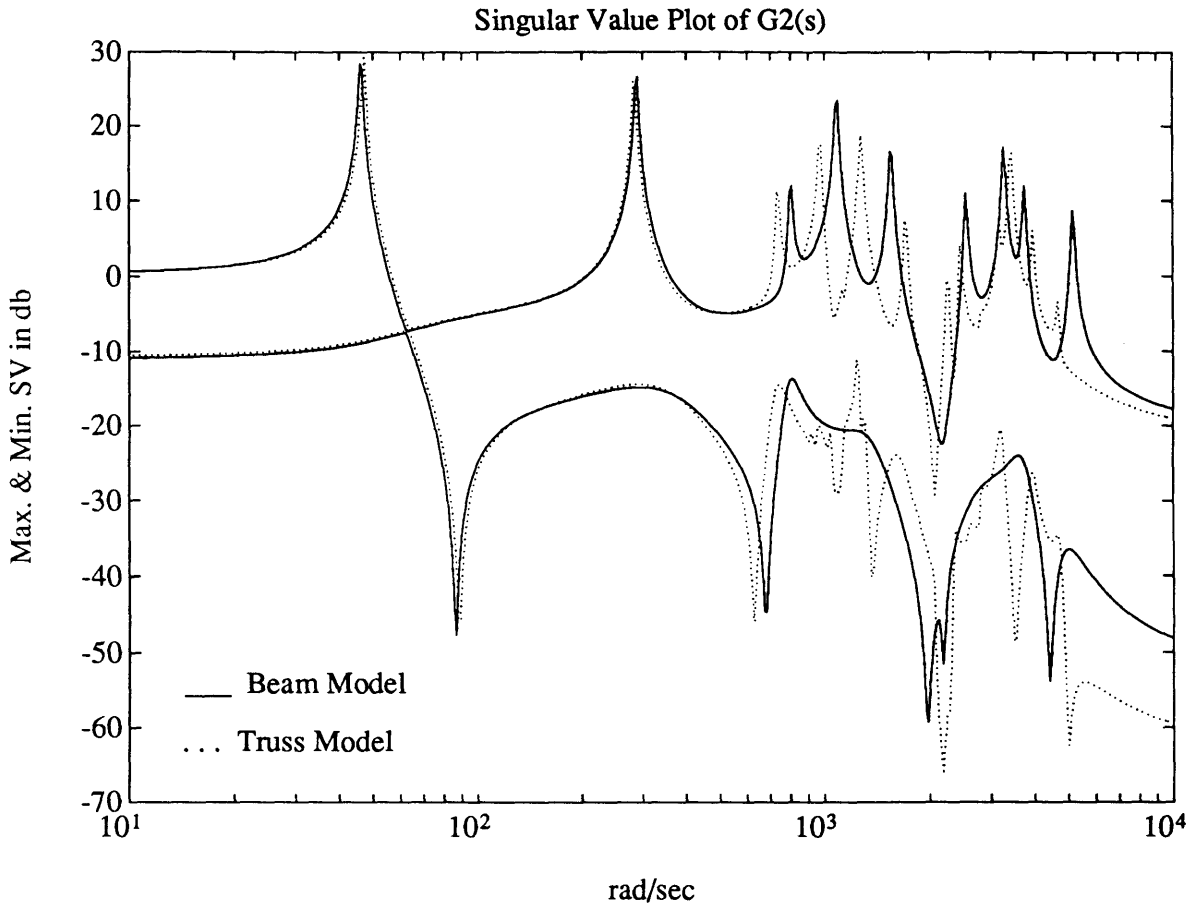

Figure 3.4: Comparison of the open loop singular values of $G_2(s)$ for the beam and truss.

3.3 Multivariable Phase Information

Having presented a means to analyze magnitude errors in a multivariable model, it would seem reasonable to also assess the phase fidelity of multivariable models. In scalar systems, phase information is a common and useful tool in the analysis and synthesis of controllers. Yet there is no widely accepted notion of phase for multivariable systems. If phase data were available for multivariable models, designers would have access to additional information about their systems. Such data could provide directional information about the system as well as an additional means of quantifying the modeling errors. More importantly, utilization of phase information in multivariable designs might lead to less conservative stability robustness measures, as it does in the scalar case.

While it is obviously worthwhile to quantify phase information for multivariable systems, no clear cut or universally accepted method for doing so exists to date. None the less, a few individuals have attempted to elicit phase information out of multivariable models in the past. MacFarlane and his colleagues proposed the use of principal phases to help analyze the stability properties of multivariable systems [43]. For a given matrix the principal phases are the arguments of the eigenvalues of the unitary part its polar decomposition. Computing the maximum and minimum principal phases and singular values of the return difference matrix, $I + G(s)K(s)$, for values of s around the Nyquist D_r contour leads to a principal region in the S–Plane within which the locus of eigenvalues of the return difference matrix must lie. Since the multivariable Nyquist criterion [15] is based on the determinant of the return difference matrix, an equivalent stability criterion based on the principal region can be derived from the fact that the determinant of a matrix is equivalent to the product of its eigenvalues. In this respect, the principal phases simply allow for a different way to check the closed loop stability of a system. Unlike scalar phase information, principal phases do not provide a measure of how signals pass through a system and will thus not be pursued in the task of assessing the uncertainty.

Freudenberg and Looze also investigated the notion of phase in multivariable systems [39]. Since their work mainly focused on extrapolating the Bode Gain–Phase Theorem to multivariable systems, they needed to characterize a relationship between gain and phase in multivariable systems. In so doing, they determined expressions that relate the phase difference between vector valued signals. In the scalar case, the phase difference between the input and output signals of a system is uniquely determined from the phase of the system's transfer function. Along with the magnitude of the transfer function, this phase difference is the quantity that provides useful information about scalar systems. Freudenberg and Looze showed that the phase difference between the input and output signals of a multivariable system is not only determined by the transfer function matrix but also by the direction in which the vector valued input lies. It is well known that the singular values of a transfer function matrix provide useful information about the magnitude of the

outputs of a multivariable system. In special cases, the relative phases between the inputs and outputs of a multivariable system can also be determined solely by the transfer function matrix of a system. To make use of this fact it is necessary to consider the direction in which the inputs lie. In the following section, the singular value decomposition is employed to find input directions that provided simple and physically meaningful measures of the phase difference between the outputs and inputs of multivariable systems. Once compiled, this information will be used to help asses the uncertainties in multivariable models

3.3.1 The Singular Value Decomposition and Multivariable Phase Information

A brief review of the singular value decomposition and some of its associated properties is in order to facilitate the discussion on multivariable phase. Given a multivariable system

$$y(s) = G(s)u(s) \tag{3.5}$$

with a complex sinusoidal input

$$u(t) = \mathsf{u}e^{\jmath\omega t} \qquad \mathsf{u} \in \mathbb{C}^m, \tag{3.6}$$

the output will also be a complex sinusoid

$$y(t) = \mathsf{y}e^{\jmath\omega t} \qquad \mathsf{y} \in \mathbb{C}^\ell \tag{3.7}$$

with

$$\mathsf{y}(\omega) = G(\jmath\omega)\mathsf{u}(\omega). \tag{3.8}$$

The singular value decomposition of $G(\jmath\omega)$ at each frequency, ω, is represented as

$$G(\jmath\omega) = U(\jmath\omega)\Sigma(\omega)V^H(\jmath\omega) \tag{3.9}$$

where the ordered, non–zero singular values of G

$$\sigma_1 > \sigma_2 > \ldots > \sigma_k > 0 \tag{3.10}$$

sit on the diagonal of the $l \times m$ matrix Σ that is otherwise populated by zeros, and the columns of the unitary matrices U and V contain the orthonormal eigenvectors of GG^H and G^HG respectively. Using the following notation for the left and right singular vectors

$$U = [\mu_1 \; \mu_2 \; \ldots \; \mu_j \; \ldots \; \mu_l] \tag{3.11}$$

$$V = [\nu_1 \; \nu_2 \; \ldots \; \nu_j \; \ldots \; \nu_m] \tag{3.12}$$

it should be clear that $\mu_i^H \mu_j = \delta_{ij}$ and $\nu_i^H \nu_j = \delta_{ij}$ where

$$\delta_{ij} = \begin{cases} 1 & i = j \\ 0 & i \neq j \end{cases} . \tag{3.13}$$

At this point all the mathematics needed to find input directions that provide useful multivariable phase information are at hand.

The singular value decomposition of G provides the special input directions that allow the relative phases between the inputs and outputs to be computed solely from the transfer function matrix. By forcing the input of the system (3.5) to lie along the direction of the j^{th} right singular vector of G, the direction, magnitude, and phase of the output can be trivially computed from the j^{th} singular value and j^{th} left singular vector of G. To see this let $\mathsf{u} = \nu_j$ in (3.6), which specifies the input direction. Then the value of y is simply obtained from the singular value decomposition of G and some matrix multiplication

$$\mathsf{y} = G\mathsf{u} = U\Sigma V^H \nu_j = \sigma_j \mu_j. \tag{3.14}$$

Writing the elements of the left and right singular vectors in polar notation

$$\mu_{ij} = |\mu_{ij}| e^{\jmath \psi_{ij}} \qquad \psi_{ij} \triangleq \angle \mu_{ij} \tag{3.15}$$

$$\nu_{ij} = |\nu_{ij}| e^{\jmath \gamma_{ij}} \qquad \gamma_{ij} \triangleq \angle \nu_{ij} \tag{3.16}$$

allows for a more detailed picture of how these special input signals pass through the system (3.5). For a sinusoidal input along the j^{th} right singular vector

$$u_i(t) = |\nu_{ij}| \sin(\omega t + \gamma_{ij}) \qquad i = 1, 2, \ldots, m \tag{3.17}$$

the corresponding steady state output, as a result of (3.14), is given by

$$y_i(t) = \sigma_j |\mu_{ij}| \sin(\omega t + \psi_{ij}) \qquad i = 1, 2, \ldots, \ell. \tag{3.18}$$

Hence by constructing specific inputs from the right singular vectors of G, the phase of the steady state outputs, ψ_{ij}, is solely determined by the left singular vectors of G. Further, realize that the specific output phases, ψ_{ij}, are not absolute but dependent on the specific input directions, ν_j, which are determined by the input phases, γ_{ij}. In this respect, the output phases, ψ_{ij}, are an appropriate measure of the relative phase between the input and the output of a multivariable system. Therefore, the values of the $\psi_{ij}(\omega)$ provide the sought after measure of phase for multivariable systems.

While this measure of phase for a multivariable systems is easy to evaluate, it is also physically meaningful. Consider the singular vectors associated with the maximum and minimum singular values of G, $\overline{\sigma} = \sigma_1$ and $\underline{\sigma} = \sigma_k$ respectively. Constructing the i input sinusoids, (3.17), for $j = 1$ and $j = k$ provides the inputs that produce the maximum and minimum amplification of the outputs of the system, which are given by (3.18) for $j = 1$ and $j = k$. This in turn allows for a time domain interpretation of the behavior of the system that corresponds to the frequency domain representation of the singular value plots. Even though the phase information provided by the singular value decomposition is readily available and meaningful, it should not be considered a straightforward extrapolation of the scalar Bode phase. Rather the output phases, $\psi_{ij}(\omega)$, should be considered a special, yet useful, means of investigating phase in multivariable systems for very particular inputs.

As of now, the phase discussion has focused on a specific frequency ω. Plotting the relative output phases, $\psi_{ij}(\omega)$ for $i = 1, 2, \ldots, \ell$, as a function of frequency, as is done in the scalar case, provides a useful way of representing information about a multivariable system. However, a proper representation of the phase requires that the output phase be relative to the same input at each frequency. In scalar systems, the input is inherently assumed to be one, e^{j0°, at each frequency so that the output phase is simply that of the transfer function. On the other hand, the notion of a fixed input in multivariable systems is not as simple due to the vector valued nature of the

inputs. Hence before presenting multivariable phase plots, it is necessary to reconcile how to fix the input so that the output phases are relative to the same input at each frequency.

By exploring some vector space concepts, a method of constraining the vector valued inputs to provided consistent output phases can be derived. In the following discussion only unit length ($\|\cdot\|_2 = 1$), complex vectors, like the left and right singular vectors, are considered. To begin with, realize that the direction of a complex, unit vector is determined by the relative, rather than absolute, phase of its elements. In fact, multiplying a complex vector by a scalar complex number, say $e^{j\theta}$, does not change its direction; since the relative phases amongst the elements will be the same. Hence, this notion of direction introduces some ambiguities when comparing two vectors. Since the direction of a vector is unchanged by the multiplication of a scalar, the comparison of two vectors can not be carried out on an element by element basis. If the relative phase amongst the elements in the vectors is the same and the absolute phase of corresponding elements is different, the vectors will still lie along the same direction. For example, the vectors

$$\nu_1 = \begin{pmatrix} .664 + .242j \\ .354 + .612j \end{pmatrix} = \begin{pmatrix} .707e^{j20^\circ} \\ .707e^{j60^\circ} \end{pmatrix} \tag{3.19}$$

and

$$\nu_2 = \begin{pmatrix} .696 - .122j \\ .613 + .353j \end{pmatrix} = \begin{pmatrix} .707e^{-j10^\circ} \\ .707e^{j30^\circ} \end{pmatrix} \tag{3.20}$$

both lie along the same direction since the relative phase of the elements in $\hat{\nu}_2 = e^{j40^\circ}\nu_2$ is the same as that in ν_1. To eliminate this arbitrariness of phase before comparing the vectors, it suffices to fix the phase of one element in each vector to be the same. In the example, setting $\angle\nu_{1j} = 0^\circ$ requires that $\angle\nu_{11}$ and $\angle\nu_{12} = 0^\circ$ to compare ν_1 and ν_2 without an arbitrariness of phase. Multiplying ν_1 by e^{-j20° and ν_2 by e^{j10° gives

$$\tilde{\nu}_1 = \begin{pmatrix} .707 \\ .542 + .454j \end{pmatrix} = \begin{pmatrix} .707e^{j0^\circ} \\ .707e^{j40^\circ} \end{pmatrix} \tag{3.21}$$

and

$$\tilde{\nu}_2 = \begin{pmatrix} .707 \\ .542 + .454\jmath \end{pmatrix} = \begin{pmatrix} .707e^{\jmath 0^\circ} \\ .707e^{\jmath 60^\circ} \end{pmatrix}, \tag{3.22}$$

which makes it clear that ν_1 and ν_2 lie in the same direction. This method of alleviating the the arbitrariness of phase when comparing two unit complex vectors is the fix that allows the output phase to be compared to the same input at each frequency for both scalar and multivariable systems.

To see how the above method can be used to provide a proper interpretation of the output phase as a function of frequency, consider first how to apply it to the scalar case. For $\mathsf{u} \in \mathbb{C}^1$ and $\mathsf{y} \in \mathbb{C}^1$, equations (3.5) to (3.8) provide a general description of the frequency response of a scalar system. As is usually the case, the phase of u is fixed to be 0° for all frequencies. If at some frequency, ω_f, the $\angle \mathsf{u}(\omega_f) = \theta$ rather than the specified value of 0°, the output phase would not be $\angle g(\jmath\omega_f)$, as it is when $\angle \mathsf{u}(\omega) = 0^\circ$. Multiplying $\mathsf{u}(\omega_f)$ by $\mathrm{e}^{-\jmath\theta}$, so that $\angle \mathsf{u}(\omega_f) = 0^\circ$, and $g(\jmath\omega_f)$ by $\mathrm{e}^{\jmath\theta}$, to maintain equivalence in (3.8), corrects for the phase anomaly at ω_f yet does not change the value of the output phase. Furthermore, the output phase at ω_f

$$\angle \mathsf{y}(\omega_f) = \angle \mathrm{e}^{\jmath\theta} g(\jmath\omega_f)\mathsf{u}(\omega_f)\mathrm{e}^{-\jmath\theta} = \angle \mathrm{e}^{\jmath\theta} g(\jmath\omega_f). \tag{3.23}$$

is now relative to the same input phase as the outputs at all the other frequencies. Realize that this method is a simple scalar version of the vector case described above.

Just as there should not be any differences between the input phases at each frequency in the scalar case, there should not be any ambiguities between the input vectors at each frequency in the multivariable case. Fortunately, the issue of consistent inputs in the multivariable case only requires some additional notation given the scalar example. Recall from (3.18) that there are ℓ output phases for each of the k inputs specified by (3.17), and for the time being consider only the output phases relative to an input defined by the j^{th} right singular vector. To properly plot the $\psi_{ij}(\omega)$ for $i = 1, 2, \ldots, \ell$ as function of frequency, it is necessary to fix the phase of one element in $\nu_j(\omega)$ to be the same at each frequency; since the input is defined by the right singular vector, ν_j. In practice, this can be done by carefully monitoring the phase of the ν_{1j} element in the computation of the singular value decomposition of G and

assuring that it maintains some predetermined value, $\gamma_{1j}(\omega_o)$, at each frequency. If at some frequency, ω_f ,the phase of a particular $\nu_{1j}(\omega)$ strays from its predetermined value

$$\gamma_{1j}(\omega_f) \neq \gamma_{1j}(\omega_o), \tag{3.24}$$

and there will be an ambiguity between the inputs defined by $\nu_j(\omega_o)$ and $\nu_j(\omega_f)$; as seen in (3.19) and (3.20). Letting $\theta = \gamma_{1j}(\omega_o) - \gamma_{1j}(\omega_f)$ and multiplying $\nu_j(\omega_f)$ by $e^{j\theta}$ will remove the phase arbitrariness between $\nu_j(\omega_f)$ and $\nu_j(\omega_o)$. However in so doing, it is necessary to maintain the equality of (3.14) by multiplying G by $e^{-j\theta}$

$$y(\omega_f) = e^{-j\theta}G(j\omega_f)\nu_j(\omega_f)e^{j\theta} = \sigma_j(\omega_f)\mu_j(\omega_f)e^{-j\theta}. \tag{3.25}$$

Carrying out this method at each frequency removes the ambiguity associated with the complex input vectors, $\nu_j(\omega)$, and provides output phases, $\psi_{ij}(\omega)$ for $i = 1, 2, \ldots, \ell$, that are relative to similar inputs at each frequency, ω. Of course this procedure must also be applied to each of the k possible input directions to yield a complete set of consistent output phases that provide additional information for multivariable systems.

At this point, a summary of the concepts that tie the results of this section together is in order before continuing with the task of assessing the uncertainty. The primary result of this section has been the development of a method to extract some phase information out of multivariable systems. Seeking a measure of phase analogous to the scalar Bode phase lead to the concept of computing the relative phase between the input and output vectors of a system. Since the output phase of a multivariable system depends on the direction of the input as well as the transfer function matrix, a singular value decomposition of the transfer function matrix was used to provide input directions that allowed for an easy and physically meaningful way to compute the output phases of a system. In order to create proper plots of these relative output phases, it was necessary to ensure that the outputs were relative to the same input at each frequency. Monitoring and adjusting the phase of one element in each of the complex valued inputs provided a method to ensure unambiguous output phase plots. In a nut shell, the singular vector output phases, $\psi_{ij}(\omega)$, are the phases of the

$i = 1, 2, \ldots, \ell$ outputs of a multivariable system relative to a set of specific inputs whose directions are specified by the $j = 1, 2, \ldots, k$ right singular vectors. A Matlab function that evaluates $\psi_{ij}(\omega)$ is included in Appendix B and is used in the following section to help assess the uncertainty in the sample problem.

3.3.2 Multivariable Phase for the Sample Problem

While the output phase provided by the singular value decomposition does not have a clear cut role in multivariable controller synthesis, it still provides an additional means to quantify the fidelity of models. Given the proper equipment in a realistic scenario, the specific inputs defined by the right singular vectors of a model, (3.17), could be applied to an actual system. Measuring the corresponding output phases and comparing them to the ones derived from the left singular vectors, $\psi_{ij}(\omega)$, would then serve as a measure of how good the model predicts the actual behavior under specific vector inputs. In the range of mismodeled dynamics it seems reasonable to expect good agreement between the experimental and analytically predicted phases with minor discrepancies occurring in the vicinity of the structural modes. If this were the case, regions for the unmodeled and mismodeled dynamics could be established by finding the frequencies at which there are vast differences and good agreement between the expected and measured output phases. In actuality, this experiment requires the ability to simultaneously measure ℓ outputs and produce m sinusoidal inputs with an accurate amount of relative phase between each input. While this is no small task, the sample problem allows for an easy way to investigate what information could be inferred from such an experiment.

Mimicking the proposed experiment with the sample problem not only helps assess the uncertainties in the beam model but also helps clarify the proposed concept of multivariable phase. To begin with, the necessary inputs, $\nu_j(\omega)$, were assembled from a singular value decomposition of the open loop beam model (3.3)

$$G_2(\jmath\omega) = U(\jmath\omega)\Sigma(\omega)V^H(\jmath\omega) \tag{3.26}$$

$$U(\jmath\omega) = [\mu_1(\omega)\ \mu_2(\omega)] \qquad V(\jmath\omega) = [\nu_1(\omega)\ \nu_2(\omega)]\,. \tag{3.27}$$

Applying an input to the beam system along the maximum right singular vector direction, given by (3.17) for $j = 1$, yields the suggested measure of multivariable phase, ψ_{i1} for $i = 1, 2$. The corresponding phase for the truss system was computed by applying the same input to the truss model via (3.5) to (3.8) with $\mathsf{u}(\omega) = \nu_1(\omega)$

$$\angle \mathsf{y}_{1_t}(\omega) = \angle G_{2_t}(\jmath\omega)\nu_1(\omega), \tag{3.28}$$

where the t subscript is used to distinguish the beam and truss values. Using the notation

$$\alpha_{i1}(\omega) \triangleq \angle \mathsf{y}_{i1_t}(\omega) \tag{3.29}$$

to denote the relative output phases of the truss system clarifies which phases to compare. For the input along the maximum singular value direction, the beam model predicts a set of outputs with phases $\psi_{i1}(\omega)$ for $i = 1, 2$. Applying the same input to the truss model yields a set of outputs with phases $\alpha_{i1}(\omega)$ for $i = 1, 2$. A comparison of $\psi_{i1}(\omega)$ and $\alpha_{i1}(\omega)$ for the vertical, $i = 1$ and axial, $i = 2$, outputs is shown in Figure 3.5, and a similar comparison for the outputs relative to an input along the minimum right singular vector direction, ν_2, is shown in Figure 3.6. Realize that these plots are intended to mimic "realistic" data that will help assess the fidelity of the beam model.

Without a doubt, the phase information presented in Figures 3.5 and 3.6 confirms the ad hoc uncertainty description of the sample problem discussed earlier in this chapter. There is excellent agreement between the phases of the beam and truss in the low frequency region of mismodeled dynamics. As expected though, there are small phase discrepancies, the blips in Figure 3.6, between $\psi_{i2}(\omega)$ and $\alpha_{i2}(\omega)$ at the frequency of the first and second bending modes of the systems, 46 rad/sec and 282 rad/sec respectively. The occurrence of these phase blip anomalies can be attributed to the beam's inability to precisely capture the true amount of axial deformation in the truss during bending vibrations. As far as the unmodeled dynamics are concerned, the phase plots clearly show a sizable differences in the outputs of the beam and truss at various frequencies beginning at around 700 rad/sec, the approximate frequency of the third truss bending mode. Further, since the phase plots only

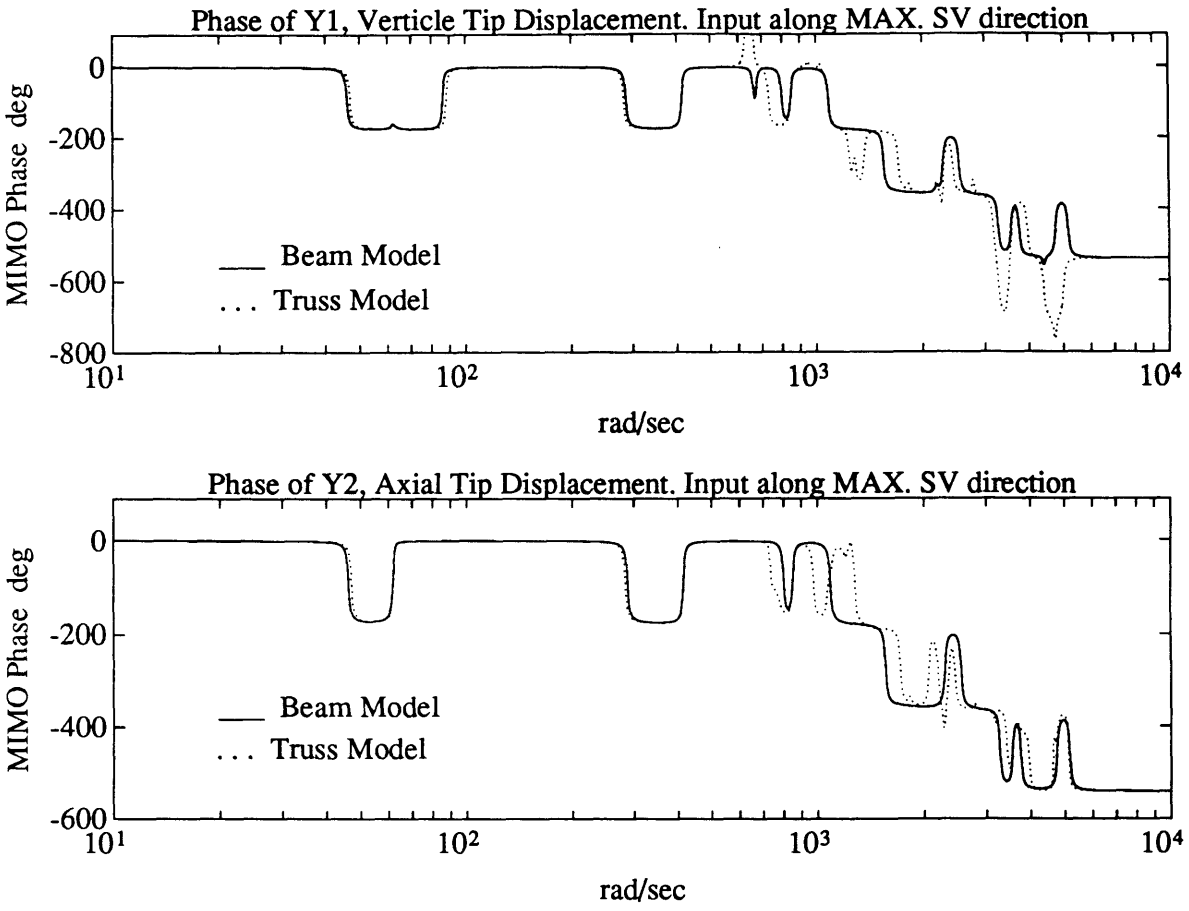

Figure 3.5: Comparison of the output phases for the beam, $\psi_{i1}(\omega)$, and truss, $\alpha_{i1}(\omega)$, given an input along the direction of the maximum right singular vector of the beam.

provide information for two very specific inputs, it is not at all conservative to specify a lower bound on the unmodeled dynamics to be at 700 rad/sec; as was estimated from the scalar transfer functions. It should be clear that the multivariable phase plots do provide additional information that helps asses the beam model's fidelity.

Even though the multivariable phase plots of Figures 3.5 and 3.6 look similar to the Bode phase plots in Figures 3.2 and 3.3, they are not a strict extrapolation of their scalar counterparts. Conceptually, both sets of phase plots allow for a measure of how signals pass through the actual systems. Indeed the expected modeling uncertainties manifest themselves in similar ways in both the scalar and multivariable phase plots. However, at a mathematical level, the theoretical usefulness of the scalar phase information is, given the current state of control theory, more useful

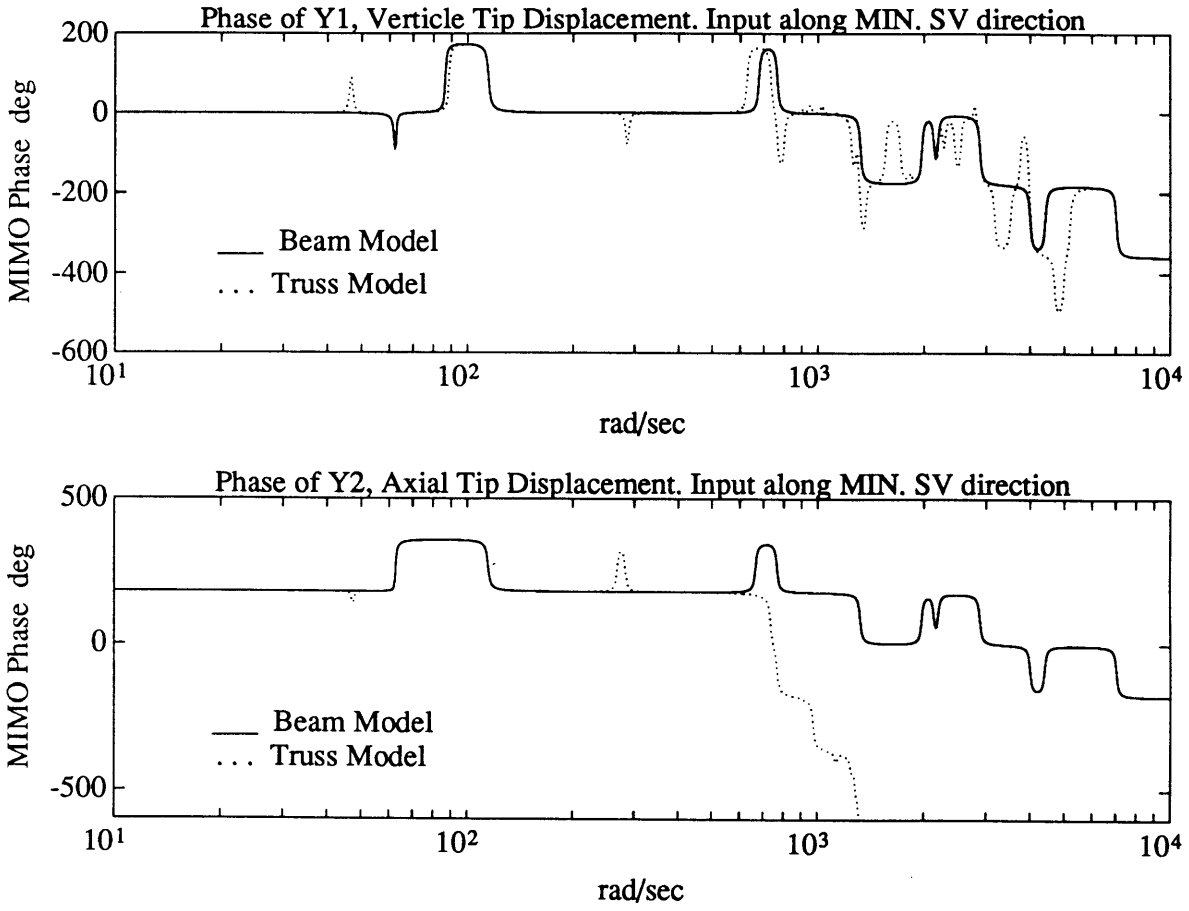

Figure 3.6: Comparison of the output phases for the beam, $\psi_{i2}(\omega)$, and truss, $\alpha_{i2}(\omega)$, given an input along the direction of the minimum right singular vector of the beam.

than the multivariable version of phase information. In a nut shell, the scalar Bode phase comes from the frequency response function of a model, which is extensively used in analyzing and synthesizing controllers. On the other hand, the multivariable phase information is based on having specific inputs defined by the singular value decomposition of a model's transfer function matrix. Unlike the scalar case, such a method provides very limited information about a system and has no clear cut role in synthesizing controllers. However, the information is truly multivariable, unlike the scalar data presented in section 3.1, since the output phases are those resulting from a vector valued input to the system. In conclusion while the multivariable phase information provides an added way to assess the fidelity of a multivariable model, its role in robust controller synthesis is unclear.

3.4 Parametric Uncertainties

In lieu of the popular loop shaping paradigm for control system design, primarily graphical methods have been used to assess the fidelity of structural models up to now. That is not to say that all design schemes rely on graphical techniques. In fact, a vast branch of control theory exists that deals with parameters in models rather than graphs of models to develop controllers. Parameter methods are useful when dealing with systems with quantifiable uncertainty, as bounds on the uncertain parameters can be accounted for directly in the analysis and synthesis of controllers [20, 44, 45]. Further, parameter methods provide a natural way in which to quantify mismodeled dynamics. For these reasons it is necessary to assess the nature of mismodeled dynamics in structural systems.

Unlike the uncertainties in the region of unmodeled dynamics, the uncertainties in the region of mismodeled dynamics are quit measurable. To get a feel for this, consider the modeling process of the sample problem. The structural properties of the beam used to assemble the mass and stiffness matrices of the sample problem contain errors as a result of the equivalent modeling process. At the simplest level, the elements in the mass and stiffness matrices are thus uncertain but nominally correct. A possible uncertainty description for the beam's mismodeled dynamics could then be quantified by defining upper and lower bounds for the structural properties used to derive the mass and stiffness matrices. While an uncertainty description based on the structural properties is easy to define, it becomes too complex to be of any use by the time a state space model is formed; since the uncertain parameters appear in non–trivial ways in the elements of the state space matrices. Alternatively, a more compact description of the mismodeled dynamics can be defined by placing bounds on the frequency, damping and residues of the mismodeled modes in a model. Bounds on the frequency and damping of the mismodeled modes can be readily obtained by estimating the accuracy of the poles of a system. In a realistic scenario, measurements of the scalar input to output transfer functions provide good estimates of the values of the poles that can be compared to the values of the poles predicted by a mathematical model

	Truss	Beam	Error
Frequency of pole #1	47.1	46.1	2.1%
Frequency of zero #1	88.5	86.3	2.5%
Frequency of pole #2	282.7	287.6	1.7%
Frequency of zero #2	628.9	678.0	7.8%

Table 3.1: Comparison of frequencies for the mismodeled poles and zeros, in *rad/sec*, for the sample problem.

and used to define the desired bounds. As far as the sample problem is concerned, a comparison of the frequency of the mismodeled poles for the truss and beam, shown in Table 3.1, provides a quantifiable measure of the uncertainty in the modes. Recall that there is no damping uncertainty in the sample problem, as the damping was fixed to be the same in all the modes of both systems. Unfortunately, obtaining bounds on the multivariable residues of the mismodeled modes is not as straightforward and is currently an open topic of research. However, the uncertainties in the residues can be realized as errors in the frequency of the multivariable transmission zeros. The magnitude of these errors for the sample problem is also show in Table 3.1 for reference. Realize that these pole and zero errors have already been identified as the low frequency discrepancies in the graphical assessment of the uncertainty in the previous sections. The main point here is that there is usually a lot of information about the uncertainty in the region of mismodeled dynamics. Information that could be quantified and used to define an uncertainty model that is well suited for parametric design methods.

By this point, a wide variety of methods have been explored and used to asses the uncertainty of lightly damped structural systems. The sample problem provided both a means to verify realistic ways of quantifying uncertainties and a means to exemplify how the uncertainties manifest themselves in the common tools of controller design. In essence, this chapter has provided useful insight into the accuracy of typical structural models. The next logical topic to discuss then is how to take this knowledge of the uncertainties and use it to design compensators that will not destabilize the actual

systems they are applied to. Chapter 4 will cover how to deal with the unmodeled and mismodeled dynamics that are inevitable in any model of a system.

Chapter 4

Dealing With the Uncertainty

Given a mathematical model of a physical system and a quantifiable description of the uncertainty in the model, designers must ensure that their feedback control systems will not destabilize the actual system. In more common terms, the designs must exhibit *stability robustness.* To date, there exists a broad spectrum of methodologies for ensuring stability robustness in the presence of unmodeled and mismodeled dynamics. This Chapter will analyze the applicability, usefulness, and limitations of various stability robustness techniques when applied to lightly damped, structural systems.

The analysis will be executed with a strong emphasis on the Nyquist domain interpretation of stability. For this reason, it is fruitful to briefly review the Multivariable Nyquist Theorem for a nominal model $G(s)$ with a compensator $K(s)$.

Theorem 4.1 (Multivariable Nyquist Theorem) [15, *page 59*] *The closed loop system depicted in Figure 4.1 is stable if and only if the number of counterclockwise encirclements of the critical point,* $(-1, 0)$, *by*

$$\mathcal{N}(s) \triangleq -1 + \det\left[I + G(s)K(s)\right] \qquad s \in D_r$$

is equal to the number of unstable poles of $G(s)K(s)$, *where* D_r *is the Nyquist contour*[1] *shown in Figure 4.2.*

Notice that the Multivariable Nyquist Theorem requires knowledge of a specific

[1]The indentations on the imaginary axis are made to avoid the open–loop $j\omega$-axis poles.

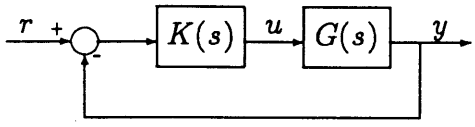

Figure 4.1: Standard feedback control system.

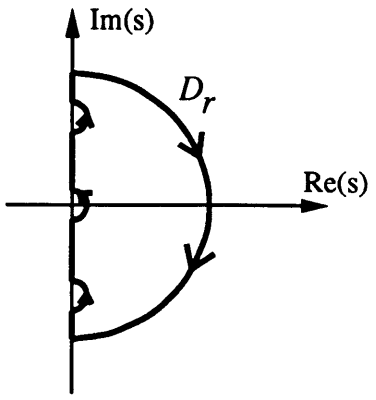

Figure 4.2: The Nyquist contour, D_r.

compensator, which can not be unraveled from the determinant operation in general. As a result of this, the scalar Nyquist criterion will be used from time to time to illustrate a point. Using lower case notation to differentiate a multivariable system from a scalar system, the Scalar Nyquist Theorem can be stated as follows.

Theorem 4.2 (Scalar Nyquist Theorem) [46] *The closed loop system depicted in Figure 4.1, where $G(s)$ and $K(s)$ are now represented by $g(s)$ and $k(s)$ to explicitly denote a scalar system, is stable if and only if the number of counterclockwise encirclements of the critical point, $(-1,0)$, by*

$$t(s) \triangleq g(s)k(s) \qquad s \in D_r$$

is equal to the number of unstable poles of $t(s)$, where D_r is the Nyquist contour shown in Figure 4.2.

Just as the Nyquist plot of (3.1) clearly showed how susceptible lightly damped structural systems are to closed loop instabilities, Nyquist plots of $\mathcal{N}(s)$ can be used to visualize and interpret various methods of guaranteeing closed loop stability. In the process of analyzing stability robustness, the notation $\tilde{G}(s)$ will be used to represent the dynamics of the actual or perturbed model. As a preliminary step to describing how to visualize stability robustness in the Nyquist framework, it is necessary to assume that the actual loop transfer function, $\tilde{G}(s)K(s)$, has the same number of open loop unstable poles as the loop transfer function of the nominal model of the

system, $G(s)K(s)$. If this is the case and the nominal closed loop system is stable, an instability in the actual closed loop system dictates that the number of encirclements of the critical point by the Nyquist plot of the nominal system has changed. In this respect, stability robustness can be viewed as a means of assuring that the number of encirclements of the critical point by $\mathcal{N}(s)$ and

$$\tilde{\mathcal{N}}(s) \triangleq -1 + \det[I + \tilde{G}(s)K(s)] \tag{4.1}$$

are the same. Since there is no way to create a Nyquist plot for the actual system, various error models can be used to estimate where the locus of $\tilde{\mathcal{N}}(s)$ for s evaluated along D_r lies. Graphically, this leads to the visualization of a region around each point on the Nyquist plot of the nominal system within which are the possible locations of the actual system at each frequency. If this region contains the critical point at any frequency, there may be a change in the number of encirclements and hence a closed loop instability. In this respect, stability robustness can be ensured if the uncertainty region never contains the critical point. Having a mathematical description of the region, or where the Nyquist plot of the actual system lies, provides information that can be used to design compensators that will not allow the Nyquist plot of the actual system to have a different number of encirclements of the critical point than the nominal system. Thus in this Nyquist interpretation of stability there are two key aspects to consider in analyzing stability robustness theory: How to cast the uncertainty description into a useful form that provides a measure of where the Nyquist plot of the actual system lies, and how to use this information to design compensators that will not destabilize the actual closed loop system.

This graphical interpretation of stability robustness will be heavily exploited throughout this Chapter. Concrete examples of what the uncertainty region looks like for various error models will be presented along with the associated conditions on the compensator needed to maintain stability. Focusing the study on how to deal with the unmodeled and mismodeled uncertainties in the sample problem will explicitly exemplify the applicability, usefulness, and limitations of various robustness techniques. Furthermore since the sample problem captures the inherent character-

istics of realistic systems like the Interferometer testbed, this Chapter will provide valuable insight into how to ensure robustly stable control systems for lightly damped structures.

4.1 Robustness for Unmodeled Dynamics

Strong and useful stability robustness techniques exist for unmodeled dynamics. Common to all of these techniques is the use of an unstructured uncertainty model to represent the modeling errors and an associated sufficient condition that must be met to ensure stability robustness. Illustrating this first in the scalar case and then extrapolating to the multivariable case will provide a clear visualization of the applicability, usefulness, and limitations of stability robustness tests for unmodeled dynamics. Once these are understood, the assessment of the uncertainty in the sample problem from Chapter 3 will be used to exemplify how to form specific uncertainty models needed to apply the stability robustness results presented.

4.1.1 Additive Error in Scalar Systems

In the scalar case, the additive error model allows for a clear visualization of how to deal with unmodeled dynamics that also applies to the multivariable case in which the visualization is not as clear. Using $\Delta_a(s)$ to denote an additive perturbation in the nominal model, the actual model with an additive error is defined as

$$\tilde{g}(s) = g(s) + \Delta_a(s). \tag{4.2}$$

To see how stability robustness can be maintained in the presence of these errors, consider Figure 4.3 that shows a portion of the Nyquist plots of $t(\jmath\omega)$ and

$$\tilde{t}(\jmath\omega) = \tilde{g}(\jmath\omega)k(\jmath\omega), \tag{4.3}$$

a candidate actual system, near the critical point. At a specific frequency ω_o, $t(\jmath\omega_o)$ and $\tilde{t}(\jmath\omega_o)$ are scalar complex numbers, and it is useful to visualize them as vectors

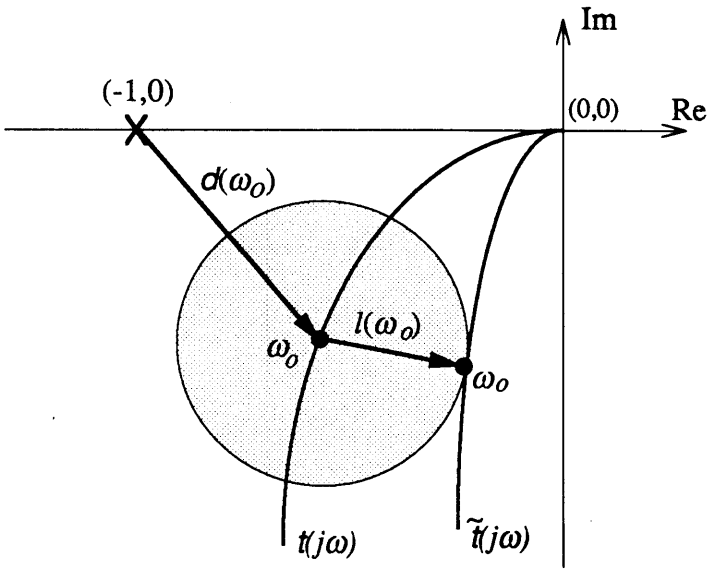

Figure 4.3: Portion of the Nyquist plot for a scalar nominal system, $t(s)$ and a typical actual system, $\tilde{t}(s)$, with a representation of the additive error and unstructured uncertainty disk at ω_o.

with a basis consisting of the real and imaginary axes of the complex plane. In doing so, both the error vector,

$$l(\omega_o) = \Delta_a(j\omega_o)k(j\omega_o) = \tilde{t}(j\omega_o) - t(j\omega_o), \tag{4.4}$$

and the distance from the critical point to the nominal model at ω_o, $d(\omega_o)$, can also be visualized as vectors; as shown in Figure 4.3. Now as long as the magnitude of the error vector is smaller than the distance to the critical point at each frequency, that is as long as

$$|l(\omega)| = |\Delta_a(j\omega)|\,|k(j\omega)| < |d(\omega)| = |1 + t(j\omega)| \qquad \forall\omega, \tag{4.5}$$

the actual closed loop system will be stable since there can not be a change in the number of encirclements of the critical point by the actual system. In this respect, (4.5) provides a sufficient condition for guaranteeing stability robustness in the presence of additive perturbations.

In the additive error stability robustness condition of (4.5), only the magnitude of the additive error is needed to test the robustness of a control system. Since the the additive error robustness condition only requires knowledge of the magnitude of

the error and does not use the specific structure of the error model, it is classified as an unstructured error robustness test. An inherent characteristic of unstructured robustness tests is that the the phase of the error model is irrelevant. In the additive error case represented in Figure 4.3 this means the error vector, $l(\omega_o)$, centered at $t(\omega_o)$ with length $|l(\omega_o)|$ can point in any direction in the complex plane, and as long as the condition of (4.5) is met the actual closed loop system will be stable. This interpretation of the allowable error leads to the visualization of an uncertainty disk centered at each point of the Nyquist plot of the nominal system, as shown for ω_o in Figure 4.3. Alternatively then, the stability robustness condition of (4.5) can be visualized as a means of ensuring that the uncertainty disk with magnitude $|l(\omega)|$ at each frequency does not contain the critical point. If this is the case for all frequencies, the distance to the critical point will always be greater than the size of the additive error no matter what direction the error lies in.

The concept of an uncertainty disk and an associated condition to make sure that the critical point does not lie in the disk at any frequency is at the heart of all the unstructured error stability robustness tests. In fact, it is the visualization of an error disk at each frequency of the nominal model that exemplifies the applicability of unstructured uncertainty models to unmodeled dynamics. Recall that unmodeled dynamics refer to the poorly modeled or unknown dynamics in a system. Hence, specifying phase, or directional, information about these errors is completely inappropriate. Rather since the only relevant information about the modeling uncertainty the stability robustness test needs is the magnitude of $\Delta_a(\omega)$, it is by no means conservative to use an unstructured uncertainty model to handle the unmodeled dynamics. Physically speaking, by admiring an unstructured modeling error the designer assumes that the actual plant can lie anywhere within the disk of radius $|l(\omega)|$ around the nominal system at each frequency, which is not a bad assumption in the frequency range where the nature of the dynamics are unknown or poorly modeled. For these simple reasons, unstructured uncertainty models are completely appropriate for unmodeled dynamics.

By now, the the means of assuring stability robustness for unstructured uncer-

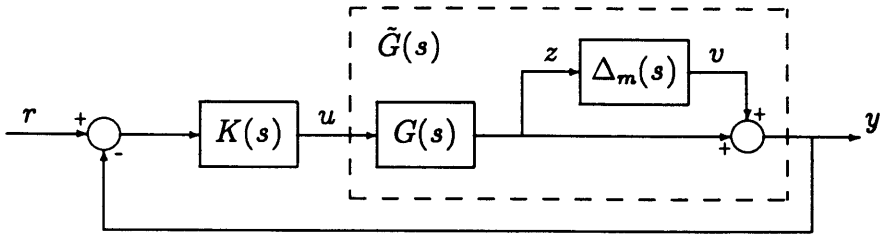

Figure 4.4: Nominal system with a multiplicative perturbation, $\Delta_m(s)$ at the plant output.

tainty models, the interpretation of unstructured uncertainty as a disk in the Nyquist domain, and the applicability of unstructured uncertainty models to unmodeled dynamics should be clear. The same insight applies in the multivariable case even though the mathematics do not allow for a strict graphical representation, as presented in the scalar case here.

4.1.2 Relative Error in Multivariable Systems

While the previous section on additive errors in scalar systems illustrated the inherent characteristics of unstructured error stability robustness tests, this section deals with popular multivariable stability robustness conditions that are often used in controller synthesis. To begin with, it is more useful to consider the class of relative errors so that the compensator can be separated from the expression of the uncertainty required by the additive error stability robustness criterion of (4.5). A typical and frequently used relative error model is the multiplicative error reflected to the plant output. Using $\Delta_m(s)$ to denote a multiplicative perturbation in the nominal model, the actual system that arises from modeling the uncertainties as a multiplicative perturbation at the output of the nominal system is

$$\tilde{G}(s) = [I + \Delta_m(s)]G(s). \tag{4.6}$$

A block diagram of a nominal system with an output multiplicative error perturbation is shown in Figure 4.4. For this model of the uncertainties the well known multiplica-

tive error stability robustness criterion provides sufficient conditions for maintaining closed loop stability in the actual system.

Theorem 4.3 (Multiplicative Error Stability Robustness Criterion) *The closed loop system with a multiplicative error perturbation at the plant output*

$$\tilde{C}(s) = \left[I + \tilde{T}(s)\right]^{-1} \tilde{T}(s) \tag{4.7}$$

shown in Figure 4.4 is robustly stable if and only if the following conditions are satisfied.

1. *(a) $\tilde{T}(s) = \tilde{G}(s)K(s)$ and $T(s) = G(s)K(s)$, the nominal and actual loop transfer function matrices, have the same number of unstable poles.*

   (b) The purely imaginary poles of $\tilde{T}(s)$ and $T(s)$ are identical.

   (c) The nominal closed loop system,

$$C(s) = [I + T(s)]^{-1} T(s), \tag{4.8}$$

   is stable.

2.

$$\overline{\sigma}\,[C(\jmath\omega)] < \frac{1}{\overline{\sigma}\,[\Delta_m(\jmath\omega)]} \qquad \forall\omega \tag{4.9}$$

Proof (loosely): A formal proof of this theorem can be found in [16, *Theorem 3*]. However, it is necessary to present a sketch of the proof since certain aspects of it will be used to illustrate the theorem's applicability, usefulness, and limitations.

To begin, condition *1* provides the technical assumptions needed to ensure that a closed loop instability in the actual system dictates a change in the number of encirclements of the critical point by $\tilde{N}(s)$. Given that the technical assumptions of condition *1* are met, there can not be a change in the number of encirclements of the critical point by $N(s)$ as long as the Nyquist plot of $\tilde{N}(s)$ does not contain the critical point for all possible perturbations $\Delta_m(s)$. Hence under condition *1*, the actual closed loop system will remain stable if

$$\tilde{N}(\jmath\omega) \neq -1 \quad \forall\omega \qquad \text{or} \qquad \det[I + \tilde{T}(\jmath\omega)] \neq 0 \quad \forall\omega. \tag{4.10}$$

Now substituting (4.6) into this sufficient condition gives

$$\det\Big[I + [I + \Delta_m(\jmath\omega)]\, T(\jmath\omega)\Big] \neq 0 \qquad \forall\omega \tag{4.11}$$

which can be reduced to

$$\det\left[I + T(\jmath\omega)^{-1} + \Delta_m(\jmath\omega)\right] \det T(\jmath\omega) \neq 0 \qquad \forall\omega. \tag{4.12}$$

Employing the singular value property

$$\underline{\sigma}(A) > \overline{\sigma}(B) \Rightarrow \det(A + B) \neq 0 \tag{4.13}$$

reduces (4.12) to a sufficient condition that ensures that the Nyquist plot of $\tilde{\mathcal{N}}(s)$ will not contain the critical point

$$\underline{\sigma}\left[I + T(\jmath\omega)^{-1}\right] > \overline{\sigma}\left[\Delta_m(\jmath\omega)\right] \qquad \forall\omega. \tag{4.14}$$

Finally using the facts that

$$\underline{\sigma}(A) = \frac{1}{\overline{\sigma}(A^{-1})} \qquad \text{if } A^{-1} \text{ exists} \tag{4.15}$$

and

$$\left[I + T(\jmath\omega)^{-1}\right]^{-1} = C(\jmath\omega) \tag{4.16}$$

to rewrite (4.14) leads to condition *2* of the theorem. This completes the sketch of the sufficiency part of the proof.

The necessity part of the proof requires a clear understanding of the language used in the theorem. First of all, realize that the theorem only guarantees robust stability for the specific class of multiplicative perturbations at the output of the nominal system and that the theorem does not state that the actual closed loop system will be unstable if its conditions are not met. Rather the theorem only states that the actual closed loop system will not be robust to a multiplicative uncertainty at the plant output if its conditions are not satisfied. To prove the necessity of the theorem, it is thus adequate to show that there does exist a multiplicative perturbation that will lead to a closed loop instability if the conditions of the theorem are not met.

Using $\Delta_o(s)$ to represent such a perturbation and $\tilde{T}_o(s)$ to denote the corresponding actual loop transfer function, realize that if

$$\det[I + \tilde{T}_o(j\omega_o)] = \frac{\tilde{\phi}_{CL}(j\omega_o)}{\tilde{\phi}_{OL}(j\omega_o)} = 0 \tag{4.17}$$

the actual closed loop system will be unstable since there will be a closed loop pole of the actual system with frequency ω_o on the imaginary axis in the S-plane. In this expression, $\tilde{\phi}_{CL}(s)$ and $\tilde{\phi}_{OL}(s)$ respectively denote the closed loop and open loop characteristic equations of the actual system. Further, a $\Delta_o(j\omega_o)$ that satisfies (4.17) can be found by solving the following optimization problem.

$$\begin{aligned} \Delta_o \;=\; & \arg \min_{\Delta} \overline{\sigma}(\Delta) \\ & \text{s.t } \det[I + T^{-1} + \Delta] = 0 \end{aligned} \tag{4.18}$$

The solution to this problem, [15, *Problem A, page 23*], can be constructed form a singular value decomposition of $I + T^{-1}(j\omega_o) = U\Sigma V^H$

$$\Delta_o(j\omega_o) = U \begin{bmatrix} E & 0 \\ 0^T & -\sigma_\ell \end{bmatrix} V^H \tag{4.19}$$

where σ_ℓ is the smallest singular value of $I + T^{-1}(j\omega_o)$ and E is an arbitrary matrix satisfying $\overline{\sigma}(E) < \sigma_\ell$. This choice of Δ_o shows that there does exists an admissible multiplicative perturbation, which by definition is the smallest perturbation that could destabilize the actual system, that violates the assumptions of the theorem and leads to a closed loop instability. In this respect, it is necessary to satisfy condition *2* to be robust to multiplicative perturbations at the output of the nominal system. □

In essence, the details of this theorem provide the fundamental concepts needed to understand the applicability, usefulness, and limitations of using relative error models to guarantee stability robustness in the presence of unmodeled dynamics. As in the scalar additive error case, the multivariable, multiplicative error, stability robustness condition only requires knowledge of the magnitude of the perturbation, $\overline{\sigma}\Delta(j\omega)$, at each frequency. As a result, the interpretation of an uncertainty disk at each frequency still holds. In the multivariable version though, the radius of the disk,

$\overline{\sigma}\Delta(j\omega)$, must be smaller than the magnitude of the worst possible error, $\overline{\sigma}\Delta_o(j\omega)$, at each frequency to remain robustly stable. In this way, the robustness criterion of Theorem 4.3 protects the nominal system from the worst possible perturbation no matter what direction it lies in. This lack of structure makes such stability robustness tests appropriate for unmodeled dynamics for the same reasons as in the scalar additive error case already discussed.

As far as the usefulness of the of this stability robustness test is concerned, realize that even though Theorem 4.3 is quite applicable to unmodeled dynamics the dynamics of $\tilde{G}(s)$ and thus $\Delta_m(s)$ are not precisely known. If they were, such knowledge could be used to obtain a more accurate nominal model. To actually make use of the stability robustness theorem, it is sufficient to define a weight, $w_m(s)$, that bounds the size of the perturbations

$$|w_m(j\omega)| > \overline{\sigma}\Delta_m(j\omega) \qquad \forall\omega \tag{4.20}$$

so that the stability robustness criterion (4.9) becomes

$$\overline{\sigma}C(j\omega) < \frac{1}{|w_m(j\omega)|} \qquad \forall\omega. \tag{4.21}$$

The weight, $w_m(s)$, can be readily defined using engineering judgment and intuition, as will be seen in the next section. Also realize that the technical assumptions of Theorem 4.3 are not very restrictive. This is especially true for structural systems that typically do not have any unstable or purely imaginary open loop poles. Finally unlike the additive error robustness condition (4.5), the multiplicative error model is more useful for multivariable systems since the nominal design sits on one side of the robustness criterion, (4.9), with the error model on the other.

While the multiplicative error stability robustness theorem is applicable and useful for unmodeled dynamics, it does have limitations. The primary limitation is that the theorem only provides a measure of robustness for unstructured uncertainties. As was seen in Chapter 3, there is a lot of information, which translates into structure in the error model, available for the mismodeled dynamics. As a result, applying the multiplicative error robustness criterion to the mismodeled dynamics would introduce

unnecessary conservatism into the design process. This will be seen and explored in more detail in the following sections. Further since the nature of Theorem 4.3 is not well suited for mismodeled dynamics, it should really only be applied or trusted over the range of unmodeled dynamics. Hence, the $\forall\omega$ qualifier in (4.9) should be practically interpreted as for all frequencies where the modeling errors should be represented as unstructured perturbations. Another limitation of Theorem 4.3 is that it only applies to a multiplicative error description at the output of the nominal plant, which might not be the most realistic way to represent the unmodeled dynamics depending on the system at hand. Fortunately, the same methods used to derive Theorem 4.3 can be used to arrive at similar stability robustness criterion for division and multiplicative, relative errors at any point in the loop of the system. A list of several such robustness tests is available in References [17] and [15]. Since the same methods are used to arrive at the various relative error, unstructured uncertainty, robustness criterions, they will all be applicable to unmodeled dynamics, useful to implement, and over conservative for mismodeled dynamics; as is the multiplicative error discussed here. Hence, only the stability robustness criterion of Theorem 4.3 will be discussed when dealing with the unmodeled dynamics of the sample problem.

At this point, the relevant theory that can be used to guarantee stability robustness in the presence of unmodeled dynamics has been presented along with a Nyquist domain interpretation of the theory. In the following section, the framework of the sample problem will be used to tie together the mathematics of the theory with the practical implementation aspects of the theory.

4.1.3 Unstructured Uncertainty Models for the Sample Problem

Having illustrated the applicability of unstructured robustness tests to unmodeled dynamics, all that remains to show is how to practically use the theory to deal with the uncertainty. As discussed, the unstructured, relative error stability robustness criterions are suited for the task, and, as they are all similar, only the criterion given

in Theorem 4.3 for multiplicative errors at the nominal plant output will be considered. Recall that it is intractable to have an exact description of $\Delta_m(s)$ required by Theorem 4.3, and that it was thus suggested that a weight that bounds the maximum singular value of the error model, (4.20), could be used in its place. The task at hand then becomes defining the weight $w_m(s)$ so that the multiplicative error stability robustness criterion can be applied via (4.21) to guarantee stability robustness for unmodeled dynamics. Depending on the flavor of the design methodology one intends to use, the possible ways of defining the weight varies. In a $\mathcal{H}_\infty/\mu$-synthesis framework, the weight is incorporated directly into the design model to guarantee stability robustness, and it thus must be a proper transfer function. Alternatively, in a more hands on approach any weight can be defined that appropriately bounds the error, and then any design process can be used to develop a compensator which can be tested for its robustness by directly applying Theorem 4.3. In the following neither approach will be emphasized. Rather some occasional comments pointing out the role that the desired synthesis method has on the weight selection will be provided. Also using the framework of the sample problem, both a realistic definition of $w_m(s)$ and an exact representation of $\Delta_m(s)$ will be pursued to bring into focus the contrast between the exactness of the theory and the harsh realities of modeling the uncertainty. Herein lies the usefulness of the assessment of the uncertainty provided in Chapter 3.

First of all, a realistic approach to defining a suitable $w_m(s)$ for a multiplicative perturbation at the output of the beam model will be pursued. In this situation, Figure 4.4 with $G(s)$ replaced by $G_2(s)$, the beam open loop dynamics, serves as a block diagram representation of the sample problem in which the disturbances are neglected, $d = 0$, and $\tilde{G}(s)$ represents the truss open loop dynamics. To begin the weight definition process, recall from Chapter 3 that the unmodeled dynamics of the beam were targeted to be all the dynamics above approximately 700 rad/sec, which corresponds to the region of the third bending mode of vibration. However, no notion of the size of the errors was presented as there was no concept of how to classify the errors other than a frequency range at the time. Considering that the fidelity of a finite element model decreases with frequency and that the high frequency, local strut

modes of the truss are not captured in the beam, it makes sense to choose a weight, or error model, whose magnitude increases with frequency. Having made this decision, a hands on weight could be defined as

$$w_m(s) = ks^n \qquad \text{for } s = \jmath\omega,\ \omega \in (700, \infty)\ rad/sec. \tag{4.22}$$

where the positive integer, n, dictates how rapidly the size of the errors increase with frequency and the gain, k, provides a way to specify the size of the uncertainty at some critical frequency. Once a desirable rate of increase for the error is determined and an approximation of how large $|w_m(\jmath\omega_o)|$ has to be at a specific frequency, ω_o, the gain in (4.22) can be determined via

$$k = \frac{|w_m(\jmath\omega_o)|}{\omega_o^n}. \tag{4.23}$$

Such an error model is wholly consistent with the discussion of Theorem 4.3. For $\omega < 700\ rad/sec$ the dynamics are well modeled, and as discussed it would be inappropriate to consider an unstructured error model there. Hence, the frequency range specification in (4.22) serves as a means to restrict the error bound to the region of unmodeled dynamics where the stability robustness result of Theorem 4.3 is applicable. Further, the simple form of (4.22) compliments the frequency range specification since the amount of information about the unmodeled dynamics is limited.

Given the form and frequency range of the weight, a value for the gain, k, must be evaluated in a realistic manner to complete the error bound model. Since the magnitude of (4.22) will be the smallest at $\omega = 700 rad/sec$, it would be wise to choose a gain that ensures that $|w_m(\jmath\omega)|$ is large enough to bound $\overline{\sigma}\Delta_m(\jmath\omega)$ at $\omega = 700\ rad/sec$. The value of n can then be chosen to make sure that the magnitude of (4.22) bounds the size of the multiplicative perturbation at the remaining frequencies of interest. Unavoidably the choice of k necessitates some sort of estimate of $\overline{\sigma}\Delta_m(700\jmath)$, the actual multiplicative error at $700\ rad/sec$, to get a sufficient yet non conservative value for the gain. Fortunately, the size of $\overline{\sigma}\Delta_m(700\jmath)$ can be estimated by creating a pseudo actual model that nominally estimates the dynamics of the truss around $700\ rad/sec$, denoted as $\tilde{G}_2'(s)$, and evaluating

$$\overline{\sigma}\Delta_m(\jmath\omega) = \overline{\sigma}\left\{[\tilde{G}_2'(\jmath\omega) - G_2(\jmath\omega)]G_2^{-1}(\jmath\omega)\right\} \tag{4.24}$$

at $\omega = 700\, rad/sec$. Note that (4.24) was obtained by solving for $\Delta_m(s)$ in (4.6) and using the correct sample problem representations for the nominal and actual systems for $G(s)$ and $\tilde{G}(s)$. Now the task of choosing a suitable value for k boils down to creating a model of the pseudo actual system that is accurate around $700 rad/sec$, that is $\tilde{G}_2'(s)$, in a realistic way. To do so, recall from the scalar Bode plots of Section 3.1 that the error in the beam model around 700 rad/sec is a result of the inability of the beam based model of the truss to correctly predict the frequency of the third bending mode of the truss. Thus an approximate actual model can be created by directly incorporating a more accurate estimate of the frequency of the third bending mode into the beam based model of the truss. The nature of the modeling process used to create a state space model of the beam is well suited for this task since the frequencies of the modes of vibration appear directly in the A matrix of the state space representation via the Λ and Γ matrices of (2.5). Hence, replacing the beam's poor approximation of the frequency of vibration of the third bending mode with a more accurate estimate of the true frequency in the Λ and Γ matrices of (2.5) and carrying out the same modeling procedure that lead to $G_2(s)$ will produce a model that almost captures the true truss dynamics in the vicinity of 700 rad/sec or, in other words, the pseudo actual system $\tilde{G}_2'(s)$. Realize that such a representation of the actual system will only be valid near the third bending mode of vibration because the dynamics of this lightly damped mode dominates the response of the system in its vicinity. In a truly realistic scenario, the frequency of the third bending mode of the truss needed to compute $\tilde{G}_2'(s)$ could be estimated from experimentally measured, scalar Bode plots as alluded to in Section 3.1. However, given a model of the truss there is no reason not to use its exact value of 733.8 rad/sec given in Figure 2.5. Using this value to create $\tilde{G}_2'(s)$ as described, the value of (4.24) was evaluated to be 32 db at 700 rad/sec. With this approximation of the size of the multiplicative error at 700 rad/sec, a viable value for k can be evaluated by letting $|w_m(700\jmath)| = 32\ db$ in (4.23) and allowing $n = 1$ for a first estimate of how fast the error increases with frequency. In doing so, the definition of the hands on error bound will be complete

$$w_m(s) = 0.0569s \qquad \text{for } s = \jmath\omega,\ \omega \in (700, \infty)\ rad/sec, \tag{4.25}$$

and the size of the error bound will be approximately correct at its smallest value. It is important to realize that the process used to define the above error bound did not rely on any unrealistic information.

Now given this specific error bound model, the robustness of beam based compensators to unmodeled dynamics could be tested by verifying if (4.21) for $w_m(s)$ in (4.25) is satisfied for $\omega > 700\ rad/sec$. Using this hands on error bound typically leads to an iterative design process where various compensators are simply tested for their robustness once they are designed. Alternatively, the $\mathcal{H}_\infty/\mu$-synthesis design methodology is a more efficient, yet more complex, method of designing compensators that directly incorporates the unstructured stability robustness criterion as a constraint that the compensator must satisfy in the optimization scheme used to synthesize controllers. Since the bound on the multiplicative error is directly incorporated into the plant dynamics in the $\mathcal{H}_\infty/\mu$-synthesis framework, $w_m(s)$ must be a proper transfer function. Thus the hands on error bound, (4.22), can not be used in the $\mathcal{H}_\infty/\mu$-synthesis framework to implement Theorem 4.3.

With the more formal $\mathcal{H}_\infty/\mu$-synthesis design framework in mind, a weight that is a proper transfer function and bounds the size of the multiplicative error at the output of the beam model could be defined as

$$w_m(s) = k\frac{(s/a+1)^n}{(s/b+1)^n}. \tag{4.26}$$

Realize that there is a great deal of freedom involved in choosing a proper weight and (4.26) will simply serve as a candidate weight to illustrate the implications of using a proper transfer function to bound the magnitude of the multiplicative error. Unlike the hands on bound, this weight is defined for all frequencies. Hence, the shape of the magnitude of $w_m(s)$ should be large enough in the range of unmodeled dynamics to bound $\overline{\sigma}\Delta_m(j\omega)$ and small enough in the range of mismodeled dynamics, where the errors are not unstructured, to minimize the constraints on the compensator. Choosing the value of the DC gain in in (4.26), k, to be very small takes care of the later specification while the previous analysis that lead to the approximate size of $\overline{\sigma}\Delta_m(700j)$ can be used to choose the values of a, b and n to take care of the

former. Also, as before, it would make sense to have an error bound that increases with frequency in the range of unmodeled dynamics. Obviously then b and a should be chosen such that $a < b$. As a consequence of all these specifications, the magnitude of the proper weight will surely be one at some frequency. Since this is the case for most proper, realistic weights, the stability robustness condition (4.21) imposes a bandwidth[2] constraint on the closed loop system because

$$\overline{\sigma}C(j\omega_o) < 1 \tag{4.27}$$

for some frequency ω_o to maintain stability robustness. Given these insights, it is obvious that the values of the parameters in (4.26) will have a profound effect on both the stability robustness and performance of a control system designed with the stability robustness condition serving as a constraint in the controller synthesis.

Evaluating the parameters of (4.26) for the sample problem using only realistic data, like that provided by the scalar transfer functions of the actual truss system, will complete the definition of a weight which is heuristically different than (4.25) yet similarly useful for bounding the multiplicative error at the output of the beam model. Knowing that the beam model predicts the low frequency behavior of the truss rather well, the DC gain of (4.26) was set at $-30\ db$, $k = .0316$. Further, the corner frequency of the poles were set at a sufficiently high enough frequency, $b = 2000$, so that the magnitude of (4.26) would be large enough over the range of unmodeled dynamics to bound the actual multiplicative error while still increasing in magnitude over the first portion of the range of unmodeled dynamics. In choosing a value for n in (4.26), realize that it controls the bandwidth of the closed loop and the frequency range of where the magnitude of the error bound is small, large, and in transition from small to large. A large value for n would specify a high bandwidth and produce a sharp weight in which there was a quick transition from small magnitudes in the range of mismodeled dynamics, where Theorem 4.3 is over conservative, and the range of unmodeled dynamics where a good bound is needed. Even though large values of

[2]Recall that the bandwidth of a system is represented as the frequency at which the magnitude of the closed loop transfer function is one, $||C(j\omega)||_2 = 1$, and beyond which the system rolls off.

n are beneficial in specifying accurate bounds on the multiplicative error, they are undesirable since the order of compensators in the $\mathcal{H}_\infty/\mu$-synthesis design framework increases with the order of the weights used in the design. Thus a value of $n = 2$ was chosen for the sample problem to provide a reasonably sharp transition without an unreasonably high order weight. With these specifications and the previous estimation of the size of the actual multiplicative error at 700 rad/sec, the value of the poles, a, in (4.26) were chosen so that $|w_m(700\jmath)| = 32\ db$. Putting all this together, the candidate, proper weight of (4.26) becomes

$$w_m(s) = .0316\frac{(s/19.7+1)^2}{(s/2000+1)^2}. \tag{4.28}$$

As with the hands on weight of (4.25), this model represents a realistic bound on the multiplicative error at the output of the beam model.

At this point, the task of defining realistic weights to practically use Theorem 4.3 has been accomplished. Either (4.25) or (4.28) could be used in conjunction with (4.21) to check the stability robustness of compensators designed using the beam based model of the truss to high frequency unmodeled dynamics. Since these weights will be used to design stably robust control systems in Chapter 5, it is quite instructive to compare their size to the size of the actual multiplicative error between the beam and truss models. Using t and b subscripts to denote the truss and beam models respectively, acknowledging that the truss is the actual model, and solving (4.6) for $\Delta_m(s)$ leads to an expression for the exact output multiplicative error between the truss and beam models

$$\Delta_m(s) = [G_{2_t}(s) - G_{2_b}(s)]G_{2_b}^{-1}(s). \tag{4.29}$$

Given the mathematical model of the truss, $\overline{\sigma}\Delta_m(\jmath\omega)$ in (4.29) can be evaluated on a frequency by frequency basis, an unrealistic computation for physical systems, to evaluate the realistically defined weights. To this end, Figure 4.5 shows a comparison of the size of the exact multiplicative error, $\overline{\sigma}\Delta_m(\jmath\omega)$, from (4.29) and the magnitude of the bounds for the multiplicative error, $|w_m(\jmath\omega)|$, motivated by a hands on design approach, (4.25), and an $\mathcal{H}_\infty/\mu$-synthesis motivated approach, (4.28). A copy of

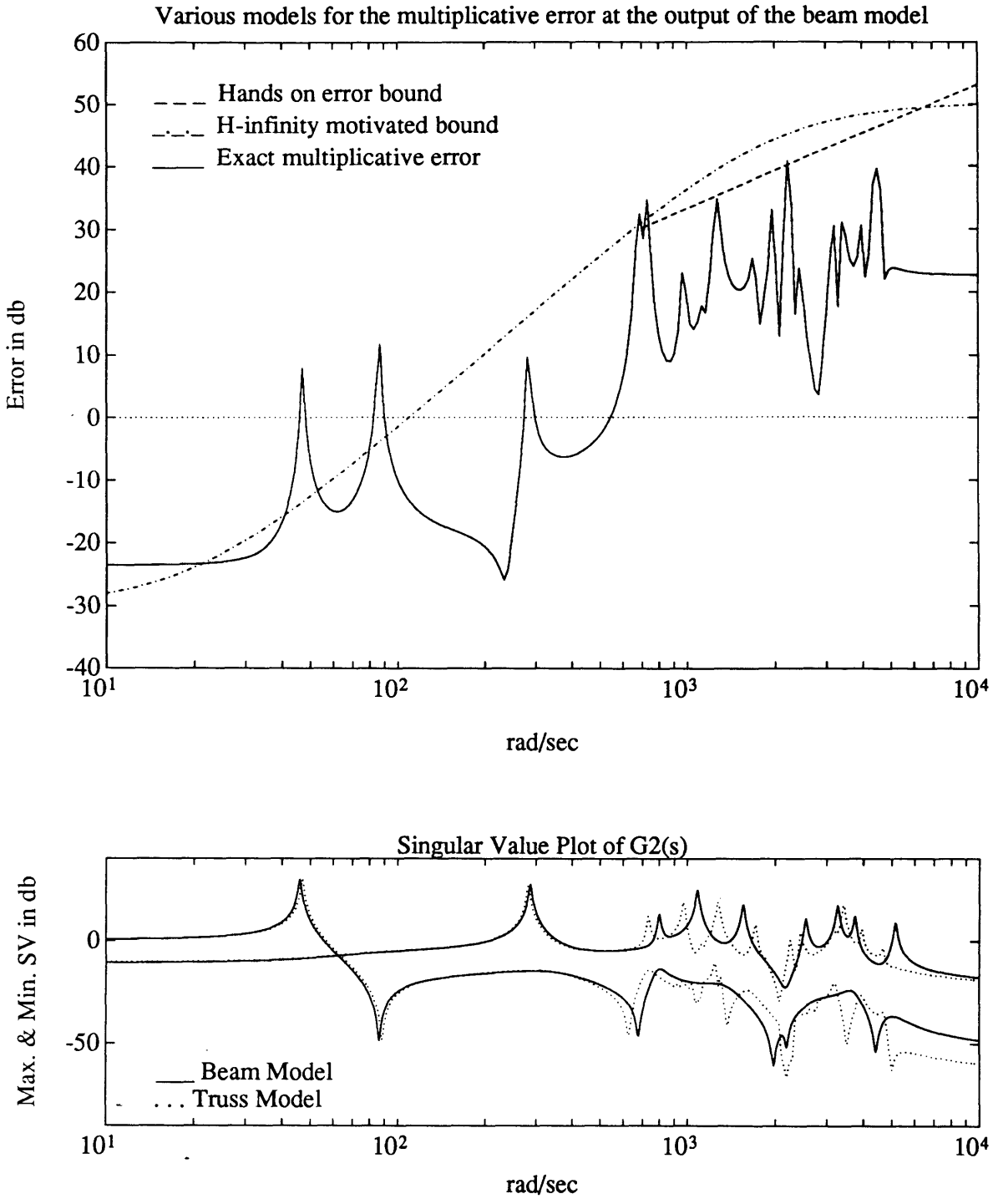

Figure 4.5: *Top:* Comparison of error models for a multiplicative perturbation at the output of the beam model: Hands on error bound is $|w_m(j\omega)|$ from (4.25), H-infinity motivated bound is $|w_m(j\omega)|$ from (4.28), and exact multiplicative error is $\overline{\sigma}\Delta_m(j\omega)$ from (4.29). *Bottom:* Comparison of the open loop singular values of $G_2(s)$ for the beam and truss.

Figure 3.4 that compares the open loop singular values of the beam and truss models is also included in Figure 4.5 to directly show how the errors between the beam and truss systems manifest themselves in a multiplicative error model.

Figure 4.5 clearly brings into focus the contrast between the exact error model specified in Theorem 4.3 and the realistic weights that can actually be used to implement the theory. Notice that in general the realistically defined weights do a good job of bounding the exact multiplicative error between the beam model and actual truss system in the range of unmodeled dynamics. Granted the actual multiplicative error is slightly larger than both bounds in the vicinity of 700 rad/sec, but this is to be expected given the limited information and approximate method used to estimate the size of the error at $700 rad/sec$. Similarly the specification of $700 rad/sec$ as the lower bound on the frequency range of unmodeled dynamics is not precisely correct as seen in both plots of Figure 4.5. This is a result of the poorly modeled, lightly damped transmission zeros that directly precede the poles corresponding to the third bending mode of the truss. However, given that there is no simple way to estimate the actual multivariable transmission zeros as there is for estimating the actual poles, it would not have been realistic to specify a different value for the lower bound on the frequency range of unmodeled dynamics. Since the range of mismodeled dynamics and the size of the multiplicative error are not really know precisely, there inevitably will be some uncertainty involved in defining suitable bounds on the size of the multiplicative error as seen in Figure 4.5. These factors show that even though unstructured error robustness tests guarantee stability robustness for unmodeled dynamics they must be exercised with care because it is difficult to accurately bound the size of the perturbations needed to implement them.

Another attribute of Figure 4.5 is that the bandwidth constraint imposed by the proper weight, (4.28) can clearly be seen. If the stability robustness condition, (4.21), along with the proper transfer function weight, (4.28), were included as a constraint in the controller synthesis, the controller would be forced to roll off just after the first structural mode. Hence the performance of the controller would be sacrificed to provide stability robustness for the unstructured uncertainties at the

output of the design model characterized by (4.28). In an actual design procedure, this attribute of the proper weight could be used as a design knob to tune the inherent performance/robustness trade off in a control system design.

Further insight into the accuracy of the weights and dealing with the uncertainty in a model is provided by the plot of the actual multiplicative error between the truss and beam models in Figure 4.5. As expected, the size of the actual multiplicative error does grow as the frequency increases. The constant level of error past $6000\,rad/sec$ in Figure 4.5 is simply an artifact of the model reduction applied to both the beam and truss models. Further, notice that the size of the error in the vicinity of the lightly damped poles and zeros of the system is quite large. In essence these large spikes in the multiplicative error for the lightly damped poles and zeros is a way of saying that perturbations in the poles and zeros near the imaginary axis are dangerous due to their proximity to the right half S–plane. In the case of the first bending mode at $46\ rad/sec$ there is only a 2% error in the frequency of vibration between the truss and beam models with no error in the damping ratio, yet the multiplicative error is nearly $10\ db$ large at that frequency. If the true multiplicative error were used in the stability robustness criterion of Theorem 4.3, the closed loop system would have to roll off before the first mode of vibration to guarantee stability robustness even though it is well modeled. This is a direct example of why the unstructured error stability robustness tests are conservative for mismodeled dynamics. The following section on dealing with the mismodeled dynamics will explore this issue in more detail. For the time being it is sufficient to acknowledge that Figure 4.5 provides a compact picture of the various error models required to implement the stability robustness criterion of Theorem 4.3.

As of now, an in depth study of the means to deal with unmodeled dynamics has been presented along with a detailed description of the applicability, usefulness, and limitations of the methods for doing so. Before continuing onto how to deal with the mismodeled dynamics, a brief review of the main concepts presented so far in this chapter is in order. The theory of stability robustness was presented with a Nyquist interpretation in which stability robustness can be guaranteed by defining

a region in which the actual system is assumed to lie and ensuring that the region does not contain the critical point at each frequency. Then it was shown in the scalar case that an appropriate region for unmodeled dynamics is a disk since the designer only has to specify the size of the errors at each frequency to guarantee stability robustness. Extrapolating these concepts to the multivariable case led to Theorem 4.3 that provided necessary and sufficient conditions to ensure stability robustness for multiplicative perturbations at the output of a nominal model. Implementation of Theorem 4.3, which is typical of all unstructured error stability robustness results, requires the definition of a weight that bounds the size of the multiplicative error at the output of the nominal model. Using the framework of the sample problem, two realistic weights were defined and compared to the actual multiplicative error to bridge the gap between the stability robustness theory and its implementation. In the process of outlining the methods to deal with the unmodeled dynamics, it was pointed out that the results are very conservative when applied to mismodeled dynamics. The following section will complete the stability robustness picture by discussing how to deal with the mismodeled dynamics in lightly damped structural systems.

4.2 Robustness for Mismodeled Dynamics

Unlike the case with unmodeled dynamics, there is still no widely accepted method that can be implemented to design control systems that are robust to the mismodeled dynamics in a model. However, many results addressing the issue of parameter uncertainty in multivariable systems exist and can be applied to the problem of guaranteeing stability robustness for mismodeled dynamics. In [20, *Chapter 1*], Hagood provides a thorough overview and classification of the various methods that have been proposed and are currently being researched to deal with parameter uncertainties. Rather than reiterating this summary, the inherent difficulties of developing techniques to handle mismodeled dynamics will be illustrated here using the Nyquist domain interpretation of stability robustness. Once the difficulties are understood, the applicability, usefulness, and limitations of using structured singular values [18]

to deal with mismodeled dynamics will be presented. Investigating the structured singular value technique is valuable because it lends itself nicely to the frequency domain overtones of this chapter and contains similar intrinsic characteristics to the other parameter uncertainty robustness techniques reviewed in [20]. As was done with the unmodeled dynamics, the assessment of the uncertainty in Chapter 3 will be used to create specific, structured singular value uncertainty models for the sample problem to put this method into perspective with the unstructured robustness methods already presented.

4.2.1 Visualizing Mismodeled Dynamics in the Nyquist Domain

Graphically representing some typical mismodeled dynamics in the Nyquist domain will help clarify the difficulty of guaranteeing stability robustness in their presence and further exemplify why the unstructured stability robustness conditions are too conservative for dealing with them. Recall that the two key elements involved in the Nyquist interpretation of stability robustness are an uncertainty region within which the actual plant may lie and associated conditions to ensure that the region never contains the critical point. Hence the first step toward visualizing the difficulty of dealing with mismodeled dynamics will be the construction of a typical, yet realistic, region within which an actual system might lie at a given frequency in the range of mismodeled dynamics. By constructing a region, the difficulties involved in deriving non-conservative conditions to maintain stability robustness in the presence of mismodeled dynamics will become apparent.

The region within which the actual plant may lie in the Nyquist domain for a nominal system with mismodeled dynamics can be directly constructed from the additional information available about the modeling error in the range of mismodeled dynamics. As was described in the assessment of the uncertainty in Section 3.4, this additional information can be conveniently cast into a parametric uncertainty model in which individual variables in the nominal model that contribute to the

mismodeled dynamics are bounded from above and below. Letting $\alpha \in \mathbf{R}^q$ denote a vector of uncertain variables, a nominal plant with parametric uncertainty will explicitly be denoted as $G(\alpha, s)$ where each element in α, α_i, has an upper and lower bound denoted respectively as $\underline{\alpha_i}$ and $\overline{\alpha}_i$. The uncertain parameters and their upper and lower bounds represent the additional information about the uncertainties in the range of mismodeled dynamics that must be specified by the designer. Using such a description of the uncertainty naturally leads to the concept of a set of actual systems that is parameterized by all the possible values of the uncertain variables in the nominal model. Expressing this in mathematical terms, the actual system, $\tilde{G}(s)$, that arises from describing the uncertainties as parametric errors in the nominal system can be represented as

$$\tilde{G}(s) = \{G(\alpha, s) \ : \ \underline{\alpha_i} \leq \alpha_i \leq \overline{\alpha}_i \quad \forall \alpha_i\} . \tag{4.30}$$

Realize that the nominal design model,

$$G(\hat{\alpha}, s) \triangleq G(s) \tag{4.31}$$

in which $\hat{\alpha}$ denotes the nominal values of the uncertain variables, is contained in the set of actual plants $\tilde{G}(s)$. With such a description of the uncertainty, a region within which the Nyquist plot of the actual system will lie at a specific frequency can be trivially constructed by evaluating $\tilde{N}(j\omega)$ in (4.1) for $\tilde{G}(j\omega)$ in (4.30). Conceptually, this is how the mismodeled dynamics uncertainty regions can be visualized in the Nyquist domain.

To actually construct such a region in the multivariable case, realize that evaluating $\tilde{N}(j\omega)$ for $\tilde{G}(j\omega)$ in (4.30) requires knowledge of a specific compensator, $K(s)$, that can not be untangled from the determinant operator. As a result, the visualization of the inherent difficulty of dealing with the mismodeled dynamics in the multivariable case will be warped by whatever design procedure produces the compensator. Further since the aim here is to understand how to design compensators that are robust to mismodeled dynamics, the visualization of the region of mismodeled dynamics will be constructed for a scalar system to minimize these complications [3]. The benefit

[3]Specific visualizations of the mismodeled dynamic region for multivariable systems will be pre-

of working with a scalar system is that there is no loss of generality in studying the Nyquist plot of the system without the compensator, that is the locus of $g(s)$ instead of $t(s) = g(s)k(s)$ for $s \in D_r$, since the effect of any compensator influences the Nyquist plot of $t(s)$ in a straight forward manner. Furthermore by creating the region for the following scalar system

$$g(s) = \frac{\rho}{s^2 + 2\xi\omega_n s + \omega_n^2} \tag{4.32}$$

without any unmodeled dynamics, there will not be a vast loss in generality to the multivariable case; as the open loop dynamics in both scalar and multivariable systems are dominated by lightly damped poles in their neighborhood.

Creating a mismodeled dynamics region for the example, nominal model, (4.32), requires an uncertainty description and values for the parameters in the model. As was discussed in Section 3.4, it is convenient to express the uncertainty as bounds on the frequency, damping, and residue of the modes in the range of mismodeled dynamics. To this end, the uncertain variables of the nominal model, (4.32), were chosen to be

$$\alpha = \begin{pmatrix} \omega_n \\ \xi \\ \rho \end{pmatrix}. \tag{4.33}$$

The nominal values of these parameters and the amount of uncertainty in them were arrived at by the desire to remain consistent with the sample problem, the need to have a clear visualization of the uncertainties in the Nyquist domain, and the constraint to maintain realistic levels of uncertainty in the variables. Choosing the the nominal value of the natural frequency of the mode, $\hat{\omega}_n$, to be the same as the frequency of vibration of the first bending mode of the beam, which is mismodeled, maintains consistency with the sample problem. Similarly from the assessment of the uncertainty in the sample problem, a $\pm 5\%$ error in the nominal value of the natural frequency was chosen to provide a realistic amount of uncertainty in the modal frequency. A realistic value of structural damping, $\hat{\xi} = 1\%$, with a realistic level of

sented in Chapter 5 using the sample problem.

	α	$\hat{\alpha}$	Error	$\underline{\alpha}$	$\overline{\alpha}$
Natural freq.	ω_n	46.	$\pm 5\,\%$	43.7	48.3
Damping ratio	ξ	.01	$\pm 50\,\%$	.005	.015
Residue	ρ	2116.	$\pm 5\,\%$	2012.	2218.

Table 4.1: Mismodeled uncertainty description of the nominal system (4.32). Frequencies are in *rad/sec*.

uncertainty in the damping ratio, a $\pm .5\%$ variation in the percentage of damping ratio, was also used. This level of error in predicting the damping ratio for well modeled modes comes from an extensive experimental study of the structural dynamics of a lightly damped truss structure [47]. To further allow for a clean visualization, the nominal value of the residue, $\hat{\rho}$, was defined to give (4.32) a unity DC gain. As far as the uncertainty in the residue is concerned, a $\pm 5\%$ error in the nominal value of the residue was chosen by realizing that the amount of error in the mismodeled poles and zeros of the sample problem were nearly the same. These nominal values as well as their upper and lower limits are summarized in Table 4.1. Given such an uncertainty description for the nominal model, (4.32), the actual plant that arises from classifying the uncertainties as (4.33) is

$$\tilde{g}(s) = \{g(\alpha, s) \; : \; \underline{\alpha_i} \leq \alpha_i \leq \overline{\alpha}_i \quad \forall \alpha_i\}\,. \tag{4.34}$$

Evaluating (4.34) at a specific frequency, ω_o, over the range of its possible values defined by α will produce a region in the Nyquist plane within which the actual plant should lie at ω_o.

An actual Nyquist plot that will help clarify the difficulties of dealing with mismodeled dynamics and allow for another visualization of the conservatism of applying unstructured error models to mismodeled dynamics is shown in Figure 4.6. This figure contains the Nyquist plot of the nominal model, $g(\hat{\alpha}, \jmath\omega)$, near the critical point, the mismodeled uncertainty region describing the possible locations of the actual plant, $\tilde{g}(\jmath\omega_o)$, at $\omega_o = 50\ rad/sec$, and the error disk associated with a multiplicative error model between the nominal model and a typical actual model from the set (4.34) at ω_o. In order to draw the uncertainty disk in the Nyquist plane centered at $g(\hat{\alpha}, \jmath\omega_o)$ with

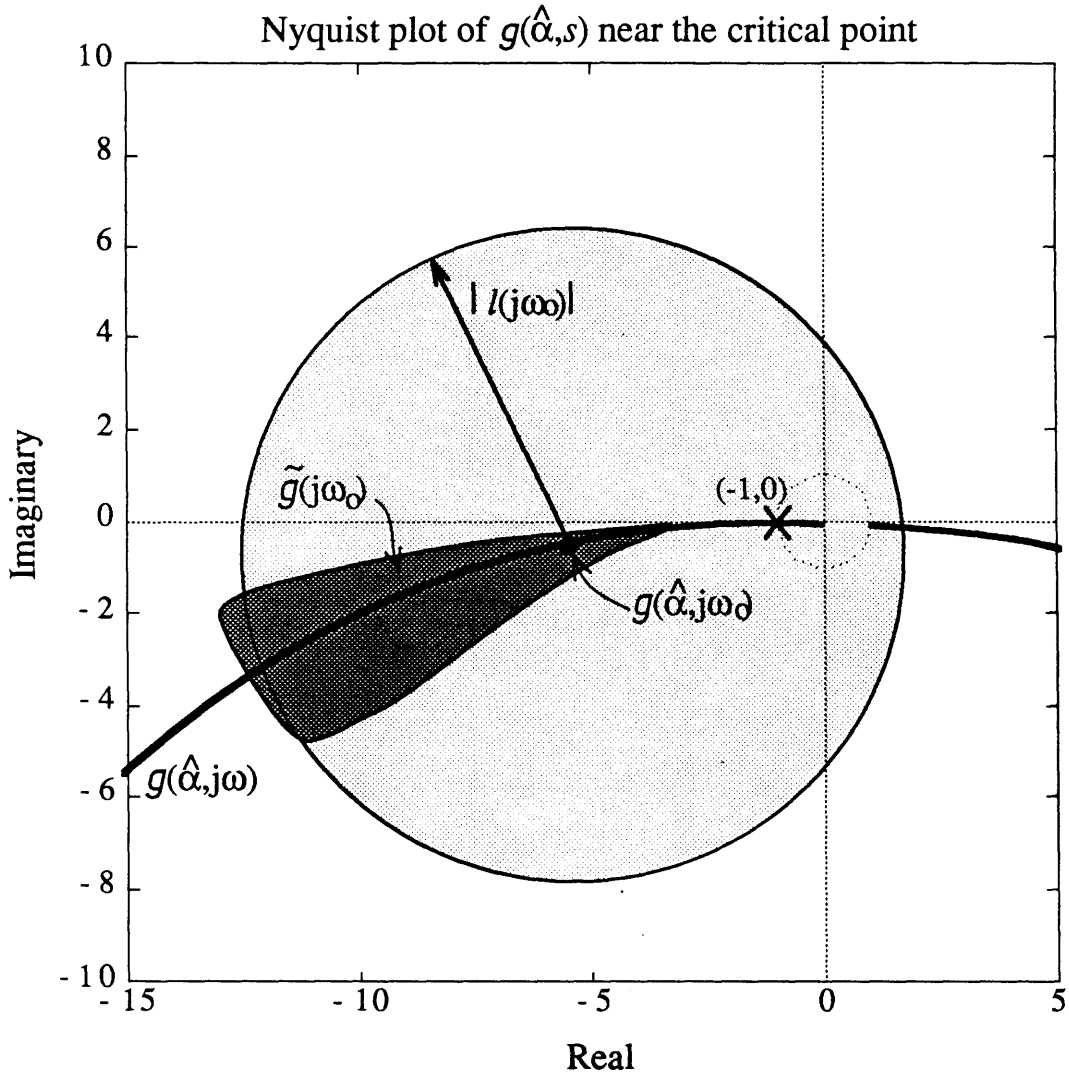

Figure 4.6: Blow up of the Nyquist plot of $g(\hat{\alpha}, s)$ near the critical point. The dark region indicates the possible locations of the actual plant, $\tilde{g}(j\omega_o)$ at $\omega_o = 50 rad/sec$. The shaded disk represents the multiplicative error, with radius $|l(\omega_o)|$ given by (4.39), between the nominal model and an actual model, assumed to be $g(\underline{\alpha}, s)$.

a radius of $|l(\omega_o)|$, it was necessary to use an additive error model, as in Section 4.1.1, that was equivalent to the desired multiplicative error model. Equating the actual models assumed in using an additive, (4.2), and multiplicative, (4.6), perturbation to describe the uncertainty in the nominal model,

$$g(s) + \Delta_a(s) = [1 + \Delta_m(s)]g(s), \tag{4.35}$$

leads to an expression that relates the additive and multiplicative errors

$$\Delta_a(s) = \Delta_m(s)g(s). \tag{4.36}$$

Based on this result, a multiplicative error can be visualized by an additive error disk in the Nyquist domain centered at $g(\jmath\omega)$ with a radius of

$$|l(\omega)| = |\Delta_m(\jmath\omega)g(\jmath\omega)|. \tag{4.37}$$

Now by assuming that the lower limit of all the uncertain parameters, $\underline{\alpha}$, defined the typical actual plant for our example, the multiplicative error used to create the error disk shown in Figure 4.6 was defined to be

$$\Delta_m(s) = [g(\underline{\alpha}, s) - g(\hat{\alpha}, s)]\, g(\hat{\alpha}, s)^{-1}, \tag{4.38}$$

and the radius of the resulting error disk, from (4.37), was evaluated to be

$$|l(\omega_o)| = |\Delta_m(\jmath\omega_o)g(\hat{\alpha}, \jmath\omega_o)|. \tag{4.39}$$

Notice that the conservatism of using unstructured error models to describe mismodeled dynamics is directly captured in Figure 4.6. Not only does the error disk associated with the multiplicative error encompass a much larger region than the true region of mismodeled dynamics it also contains the critical point. In other words, with this unstructured error model there may be a different number of encirclements of the critical point by the actual system and thus a closed loop instability. However, the realistic region of errors in the system, depicted by $\tilde{g}(\jmath\omega_o)$ in Figure 4.6, is no where near the critical point. Hence, any compensator that would be designed to meet the stability robustness criterion for this multiplicative error would be unnecessarily

conservative in that it would provide robustness for unrealistic errors. As an aside, realize that the large multiplicative error disk in Figure 4.6 is akin to the large spikes in the exact multiplicative error plot between the beam and truss seen in Figure 4.5 at the low frequency, mismodeled poles and zeros. In essence, the large multiplicative error disk, in contrast to the much smaller region of mismodeled dynamics, illustrates the conservatism of using unstructured error models for mismodeled dynamics.

To begin to understand why it is difficult to ensure robustness for the mismodeled dynamics, notice that the mismodeled dynamics region does not contain the critical point nor is it near the critical point. As a result, the closed loop system is not in danger of an instability resulting from the mismodeled dynamics in the nominal model at ω_o. None the less, it would still be beneficial to have some theory that can be employed to design compensators that provide guaranteed robustness to such uncertainties. This is especially true for lightly damped systems due to the proximity of the Nyquist plot to the critical point as seen in Figure 4.6. Unfortunately, the measure of whether or not the mismodeled dynamics region contains the critical point is not as simple as comparing the size of the errors to the distance to the critical point as is done for unstructured uncertainties. Further realize that the region of mismodeled uncertainties can not be defined by one quantity like the unstructured uncertainties that are specified solely by the radius of the error disk. This is clearly seen in Figure 4.6 in which the shape of the mismodeled dynamics region, arrived at by evaluating the nominal model over the entire range of possible values for the uncertain variables, has a complicated form even for the small number of uncertain variables in (4.32). Furthermore since the form of the mismodeled dynamics region is a function of all the uncertain variables in the model, the shape of the region will become more complicated as the number of uncertain variables increases. This is not to mention the fact that in the multivariable case of interest, the shape of the mismodeled dynamics region is further complicated by the nature of the determinant operation needed to evaluate $\tilde{\mathcal{N}}(\jmath\omega)$ for $\tilde{G}(\jmath\omega)$ in (4.30). Given that there is no simple way to describe the shape of a realistic region within which the actual plant may lie in the domain of mismodeled dynamics, it is obviously not simple to test if the region of

unmodeled dynamics contains the critical point. In essence, the difficulty in ensuring robustness for mismodeled dynamics is a result of an inability to simply and concisely describe the possible locations of the actual plant in the Nyquist domain, and the resulting difficulty in testing whether or not the hard to describe region of actual plants contains the critical point.

Another useful feature of Figure 4.6 is that it provides a microcosm of the different approaches to dealing with the uncertainty in a system. On one hand are the approaches that led to the unstructured error robustness tests used to guarantee stability robustness for unmodeled dynamics. Recall that these tests were arrived at by postulating an error model that lead to simple and useful conditions for assuring stability robustness. Once the nature of these tests were understood it became obvious that they are well suited for dealing with unmodeled dynamics. In essence, they classify the uncertainty as a disk around each point in the nominal system that can not contain the critical point if stability robustness is to be guaranteed. As seen in Figure 4.6, the disk is an overly conservative description of the uncertainty in the region where there is additional information about the errors in a model of a system. On the other hand, another approach to dealing with modeling errors begins by defining a realistic and less conservative error model using the additional information about the modeling errors. Given a realistic uncertainty model, the objective then becomes to find conditions to guarantee stability robustness for the realistic and less conservative error description. As pointed out above, this is not necessarily an easy task as seen by the complex shape of the mismodeled dynamics region in Figure 4.6.

These arguments bring out a bottom line trade off that is inherent in deriving ways to deal with the mismodeled dynamics. At one extreme, realistic uncertainty models do not lend themselves to easily implementable stability robustness tests even though they accurately describe the uncertainty. At the other extreme, implementable stability robustness conditions can easily be derived by choosing a convenient error model that typically provides robustness for an over conservative and unrealistic description of the uncertainty. As is usually the case in engineering design, some compromise between the extremes of the trade off will be needed to achieve the desired result of

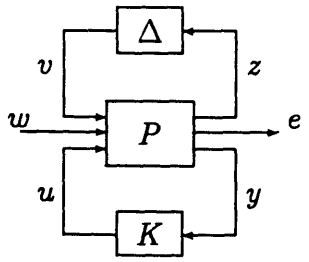

Figure 4.7: P–Δ : The general feedback system description.

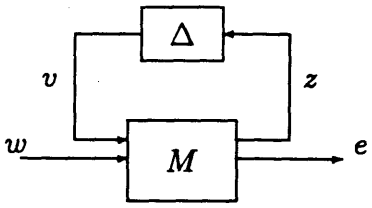

Figure 4.8: The Closed loop general feedback system description.

a useful and non–conservative way to guarantee robustness to mismodeled dynamics. All these aspects will be apparent in the following section that discusses how the structured singular value can be used to deal with the mismodeled dynamics in a model.

4.2.2 The Structured Singular Value and Mismodeled Dynamics

In this section, the key aspects of the structured singular value theory that are pertinent to understanding its use in dealing with the mismodeled dynamics will be presented. More in depth descriptions of the theory can be found in [17,48,18]. The structured singular value, also known as μ, framework is a logical extension of the concepts used in deriving the unstructured error stability robustness criterion to allow structured uncertainty models. Rather than working with a standard feedback description of the system and considering a single complex perturbation, like the multiplicative error at the plant output shown in Figure 4.4, the μ framework considers the more general system description depicted in Figure 4.7 and described in [49] that allows for multiple perturbations in the model of a system. Since the model description of Figure 4.7 will be referred to often throughout the sequel, it will be referred to as the P–Δ system. Any linear interconnection of control inputs (u), measured outputs (y), external inputs (w), performance variables (e), transfer functions, scalings, weights, parameter variations, and perturbations can be rearranged into the P–Δ system description by considering z and v to respectively be the inputs and outputs of the various perturbations in the model. For a realistically defined uncertainty de-

scription, the Δ matrix in general will be block diagonal and contain real blocks to account for parametric uncertainties as well as complex blocks to handle unmodeled dynamics and performance specifications. In other words, Δ will be a member of a set like

$$X_{\mathcal{K}} = \left\{ \Delta = \text{diag}\,(\delta_1, \delta_2, \ldots, \delta_m, \Delta_1, \Delta_2, \ldots, \Delta_n) \;:\; \delta_i \in \mathbf{R},\; \Delta_j \in \mathbf{C}^{k_j \times k_j} \right\}. \quad (4.40)$$

Further in the structured singular value framework, it is convention to force Δ to be a norm bounded matrix, that is $\overline{\sigma}(\Delta) < 1$, by including appropriate scalings and weights in the general system P. In doing so, the allowable set of perturbations is a bounded subset of (4.40)

$$\mathbf{B}X_{\mathcal{K}} = \{\Delta \in X_{\mathcal{K}} \;:\; \overline{\sigma}(\Delta) < 1\} \quad (4.41)$$

Realize that this uncertainty description is really nothing more than a way to capture both unstructured uncertainty models, such as (4.6), and parametric uncertainty models, such as (4.30), in one unifying framework.

Before presenting the specific structured singular value stability robustness results, it is necessary to define some more notation. The nominal closed loop system, denoted by M and shown in Figure 4.8, will be assumed to be stable for a given compensator K. In order to facilitate the stability robustness results, M will be partitioned into a 2×2 block–structured matrix

$$\begin{pmatrix} z(s) \\ e(s) \end{pmatrix} = \begin{bmatrix} M_{11}(s) & M_{12}(s) \\ M_{21}(s) & M_{22}(s) \end{bmatrix} \begin{pmatrix} v(s) \\ w(s) \end{pmatrix} \quad (4.42)$$

in which

$$M_{ij}(s) = P_{ij}(s) + P_{i3}(s)\,[I - K(s)P_{33}(s)]^{-1}\,K(s)P_{3j}(s) \qquad i,j = 1,2 \quad (4.43)$$

and the P_{ij} notation similarly originates from the 3×3 block structure of the P–Δ system.

The stability robustness results in the μ framework take on the same flavor as the multiplicative error stability robustness theorem already presented. That is, they provide necessary and sufficient conditions for the nominal closed loop system to be

stably robust to the uncertainty description given by the P–Δ system for Δ belonging to (4.41). Using concepts similar to those used to derive Theorem 4.3, a sufficient condition based solely on the size of the perturbation, $\overline{\sigma}(\Delta)$, could be derived to ensure stability robustness in the presence of $\Delta \in \mathbf{B}X_{\mathcal{K}}$ [18, *Theorem RSU*]. However, this test, like the multiplicative error stability robustness criterion, assumes that Δ is a full matrix and ignores any structure in Δ arrived at by realistically modeling the uncertainties. As a result, such a test would provide robustness for an unrealistic class of perturbations. In an effort to reduce this conservatism, a better measure of the size of the smallest perturbation needed to cause a closed loop instability in the nominal model with a structured uncertainty description was defined as the reciprocal of the structured singular value.

Definition 4.1 (Structured Singular Value, μ) [48] *The structured singular value for a complex matrix M, denoted by $\mu(M)$, is* 0 *if there exists no $\Delta \in X_{\mathcal{K}}$ such that* $\det(I - \Delta M) = 0$, *and*

$$\mu(M) \triangleq \left(\min_{\Delta \in X_{\mathcal{K}}} \{\overline{\sigma}(\Delta) \; : \; \det(I - \Delta M) = 0\} \right)^{-1} \tag{4.44}$$

when there does exist a $\Delta \in X_{\mathcal{K}}$ such that $\det(I - \Delta M) = 0$.

With this measure of the size of the perturbation needed to cause an instability, the following theorem provides necessary and sufficient conditions for stability robustness in the presence of a structured uncertainty description.

Theorem 4.4 (Structured Stability Robustness Theorem) [18] *The nominally stable closed loop system, M, partitioned as in (4.42) and shown in Figure 4.8 will be robustly stable to all uncertainties $\Delta \in \mathbf{B}X_{\mathcal{K}}$ if and only if*

$$\mu\left[M_{11}(j\omega)\right] < 1 \qquad \forall \omega \tag{4.45}$$

As in the case of Theorem 4.3 the language of this result is very deliberate. If (4.45) is violated at any frequency, the actual closed loop system will not necessarily be unstable. Rather the closed loop control system will not be robust to the errors in

the nominal model defined by Δ. However if (4.45) is satisfied for all frequencies and the actual system is included in the set of possible plants defined by the nominal model and its uncertainty description Δ, the actual closed loop system will be stable.

As of now, a means to classify multiple uncertainties in a nominal model and a means to test for stability robustness in their presence has been presented. The remainder of this section will address the applicability, limitations and usefulness of applying the μ analysis framework presented here to the problem of dealing with mismodeled dynamics in a model. Before doing so it is worthwhile to interpret the structured singular value results presented thus far in terms of the Nyquist domain interpretation of stability robustness used throughout the rest of this chapter. Basically, the interconnection structure of the P–Δ system description that leads to $\Delta \in \mathbf{B}X_{\mathcal{K}}$ is analogous to the region within which the actual plant may lie, and condition (4.45) is the test that ensures the uncertainty region will never contain the critical point. Further since the notion of an uncertainty region and an associated test is applicable to any stability robustness results and since the μ analysis framework allows the inclusion of parametric error models, the applicability, limitations, and usefulness of μ will be typical of the applicability, limitations, and usefulness of many of the other methods that are being researched to deal with mismodeled dynamics.

To begin assessing how the μ results can be used to deal with the mismodeled dynamics, realize that by its very nature the μ framework is applicable to mismodeled dynamics. As already discussed, parametric error models are quite appropriate descriptions for mismodeled dynamics. Further, parametric errors in the values of various elements in the A, B, and C matrices of a nominal state space model can be directly incorporated into the general feedback structure of figure 4.7 [20], which in turn leads to the real valued perturbations in $X_{\mathcal{K}}$. In this way the added knowledge about the mismodeled dynamics can be directly incorporated into an error model that is both realistic and theoretically useful for assuring stability robustness. Unfortunately, only linear combinations of the errors are allowed in forming an uncertainty description for Δ. This imposes a limitation for high order structural systems in which the uncertain variables of interest typically do not represent themselves in a

linearly related fashion; as will be seen in the following section. Thus the structured singular value framework is applicable to mismodeled dynamics, but it is still not general enough to specify any mismodeled dynamic uncertainty model.

Unfortunately, the inability to specify any uncertainty model is not the main limiting factor of the μ framework. Rather the inability to compute $\mu[M_{11}(j\omega)]$ for $\Delta \in \mathbf{B}X_{\mathcal{K}}$ is the primary limitation to using Theorem 4.4. Only for very specific forms of Δ can the structured singular value be computed. As a result, an intense amount of research has gone into computing tight upper and lower bounds on μ to make the framework useful in general. A current summary of the cases in which μ and the bounds on μ can be computed can be found in [19]. Needless to say for the case of interest in which Δ contains real perturbations from representing the mismodeled dynamics as parametric bounds on values in the state space representation, μ can not be computed and the current bounds on μ for such a Δ can be arbitrarily conservative. Given the insight gained in looking at a typical region of mismodeled dynamics in the Nyquist domain, this inability to compute μ for the uncertainty description of interest is to be expected. Simply put the inability to compute μ for $\Delta \in \mathbf{B}X_{\mathcal{K}}$ is analogous to not being able to easily determine whether or not the critical point lies within a realistic region of mismodeled dynamics in the Nyquist domain. Even though the inability to evaluate μ or bounds on μ at this time is the primary limitation of the method, the framework should not be dismissed because if μ were computable the problem of assuring stability robustness for realistic uncertainties would be nearer to resolution.

As far as the usefulness of the μ framework is concerned, it is obvious that it is not very useful at this point in time since μ can not be computed for the uncertainties of interest. Further since Theorem 4.4 is an analysis result that only applies for a given, specific compensator, the usefulness of using the μ framework to derive stably robust compensators is limited to a hands on iterative approach in which compensators are tested for their stability properties once they are designed. A procedure for synthesizing compensators that satisfy the conditions of Theorem 4.4 does not exist to date for the case where Δ contains real values. Although in the case where the real

uncertainties are "covered" by complex perturbations, compensators that are robust to such a fictitious and conservative description of the uncertainty can be synthesized using the so called D–K iteration scheme [18].

It should now be apparent that the structured singular value framework captures the inherent trade off involved in deriving ways to deal with mismodeled dynamics. While it is possible to realistically define the uncertainties in the μ framework, it is intractable to to carry out the computations needed to test the stability robustness properties of a compensator. At the other extreme, it becomes possible to compute μ and apply Theorem 4.4 to verify the robustness of a compensator by relaxing the realism of the uncertainty description. As seen, the penalty for using a mathematically tractable but physically unrealistic description of the uncertainty is an overly conservative stability robustness criterion. A fitting example of this arises when the system of Figure 4.4 is cast into the general system description of Figure 4.7 with

$$\Delta_m(s) = w_m(s)\Delta(s) \quad \text{and} \quad \overline{\sigma}\Delta(j\omega) < 1 \quad \forall\omega. \tag{4.46}$$

In this case, the stability robustness condition (4.45) can be reduced to (4.21), which was shown to be a very conservative test for stability in the presence of mismodeled dynamics. As is the case with many of the other methods that are being developed to deal with the mismodeled dynamics, the μ framework has potential to handle the mismodeled dynamics in a non conservative way but can not currently be implemented do to the inherent complexities of testing if the realistically defined uncertainties will lead to a closed loop instability.

4.2.3 Structured Uncertainty Models for the Sample Problem

This section will serve to solidify the applicability and limitations of using a structured uncertainty description to deal with the mismodeled dynamics in a structural model by casting the mismodeled dynamics of the beam into the P–Δ system description. Even though such a course of action is specifically tailored to the μ framework, it is important to keep in mind that when parametric errors are used in the structured

singular value framework the applicability and limitations of μ are similar to those of many of the other parameter uncertainty methods. Hence the insights gained in constructing a P–Δ description for the beam are generic to any parametric uncertainty model for structural systems. Furthermore, the task of casting the mismodeled dynamics of the beam model into the P–Δ system description serves as a parallel development to the work on defining an appropriate bound for the multiplicative error at the beam output that will highlight the differences in using a structured or unstructured uncertainty description of the errors in a model. The resulting error model will also be used in Chapter 5 to study the robustness of specific controllers based on the uncertain beam model and implemented on the actual truss system.

To begin the process, it is necessary to decide which parameters in the beam model will be considered uncertain and to define a realistic amount of uncertainty in them. Recall that in structural systems, describing the mismodeled dynamics as parametric bounds on the frequency, damping, and residue of the modes in the region of mismodeled dynamics is an appropriate description of the uncertainty in a model. In the beam model, the first two structural modes, that is the predominant dynamics below 700 rad/sec, can be classified as mismodeled dynamics. Drawing on the knowledge gained in the assessment of the uncertainty in the beam model, a realistic level of uncertainty in the frequency of the first two modes is a $\pm 5\%$ error in the value of the nominal frequency that is derived from the finite element model. Table 3.1, that shows the exact amount of uncertainty between the frequency of the mismodeled modes in the beam and truss, confirms that the $\pm 5\%$ level of error in the frequency is a sufficient level of uncertainty to consider. Recall that such information is realistically available from experimental transfer function measurements. Even though there is no damping uncertainty between the beam and truss models, it is still fruitful to consider uncertainty in the damping of the mismodeled beam modes to be consistent with reality. As in the academic example of Section 4.2.1, a $\pm .5\%$ variation in the nominal value of the percentage of damping ratio will be used to describe the damping uncertainty for the mismodeled beam modes in a realistic way. Since it is not clear how to measure and directly represent the residue uncertainty

	α	$\hat{\alpha}$	Error	$\underline{\alpha}$	$\overline{\alpha}$
Modal frequency	ω_1	46.13	$\pm 5\,\%$	43.8	48.4
Modal frequency	ω_2	287.64	$\pm 5\,\%$	273.3	302.0
Damping ratio	$\xi_{1,2}$	.01	$\pm 50\,\%$	.005	.015

Table 4.2: Realistic mismodeled uncertainty description of the beam model. Frequencies are in *rad/sec*.

in a multivariable model, the residues of the mismodeled beam modes will not be considered uncertain here. A table summarizing the above parametric uncertainty in the frequency and damping of the first two structural modes is shown in Table 4.2.

Notice from (2.10) and (2.5) that these parameters only appear in the A matrix of the state space representation of the beam model. In line with the notation used for parameter errors in Section 4.2.1, this uncertain matrix will be denoted as $A(\alpha)$ where α is the vector of uncertain parameters that can be defined as follows for the beam model

$$\alpha = \begin{pmatrix} \omega_1 \\ \omega_2 \\ \xi_1 \\ \xi_2 \end{pmatrix}. \tag{4.47}$$

In order to arrive at a P–Δ system description of a model with a $\Delta \in \mathbf{B}X_{\mathcal{K}}$, it becomes necessary to introduce some new notation. Rather than letting α_i be the uncertain variable that is bounded from above and below, $\delta_i \in \mathbf{R}$ will now denote an uncertain variable in the nominal model that can take on any value between $+1$ and -1, that is

$$|\delta_i| < 1. \tag{4.48}$$

There is no loss in generality in switching the uncertain variables in the model, as it is simply a matter of notation to consider the δ_i as the uncertain variables rather than the actual physical variables. Specifically, each uncertain variable will be represented as

$$\alpha_i = \hat{\alpha}_i + \delta_i q_i \qquad \text{with} \qquad |\delta_i| < 1 \tag{4.49}$$

where $\hat{\alpha}_i$ is the nominal value of the uncertain parameter and q_i is a scalar variable that quantifies the amount of error in α_i. By letting δ_i take on its maximum or minimum possible value, it is simple to evaluate q_i from (4.49) and the upper and lower bounds of the uncertain parameter α_i

$$q_i = \overline{\alpha}_i - \hat{\alpha}_i \quad \text{or} \quad q_i = \hat{\alpha}_i - \underline{\alpha}_i \tag{4.50}$$

In this way, the level of error in an uncertain variable is now directly reflected to q_i.

In using this kind of description of the uncertainty, the goal of obtaining a P–Δ system description boils down to defining fictitious inputs, v_i, and outputs, z_i, for the state space model of the beam

$$\begin{aligned} \dot{x}(t) &= A(\alpha)x(t) + B_2u(t) + B_1d(t) \\ y(t) &= Cx(t) + D_2u(t) \end{aligned} \tag{4.51}$$

for the m uncertain variables so that

$$v_i = \delta_i z_i \qquad i = 1, \ldots, m. \tag{4.52}$$

Realize that doing so will produce a block diagonal Δ matrix that will belong to the bounded set

$$\mathbf{B}X_{\mathcal{K}} = \{\Delta = \text{diag}\,(\delta_1, \delta_2, \ldots, \delta_m) \;:\; \delta_i \in \mathbf{R},\ \overline{\sigma}(\Delta) < 1\}\,. \tag{4.53}$$

where $\overline{\sigma}(\Delta) < 1$ because each element of Δ is similarly bounded by definition (4.49). Since this form of the uncertainty is directly applicable to the structured singular value framework presented in the previous section, the motivation for letting δ_i denote the uncertain variables rather than the true uncertain parameters, α_i, through (4.49) should now be apparent.

To see how the fictitious inputs and outputs can actually be defined, consider for the moment the canonical form of the $A(\alpha)$ matrix associated with the uncertain, scalar system, (4.32), used to generate the region of mismodeled dynamics in the Nyquist domain

$$A(\alpha) = \begin{bmatrix} 0 & 1 \\ -\omega_n^2 & -2\xi\omega_n \end{bmatrix}. \tag{4.54}$$

While the form of this example is very similar to the actual, uncertain $A(\alpha)$ matrix of the beam model, it is much simpler to work with in understanding how to define the v_i and z_i. By neglecting the residue uncertainty in this example the uncertain variables for (4.32) become

$$\alpha = \begin{pmatrix} \omega_n \\ \xi \end{pmatrix} \tag{4.55}$$

which is akin to the uncertainty description of the beam model. Before defining the fictitious inputs and outputs, it is necessary to switch to the δ_i notation for the uncertain variables. This can be done by substituting the δ_i uncertainty description of (4.49) for α_i into (4.54). Doing so decomposes $A(\alpha)$ into the nominal A matrix, denoted as $\hat{A}$, and a perturbation matrix, ΔA, that depends on the uncertain δ_i

$$A(\alpha) = \begin{bmatrix} 0 & 1 \\ -(\hat{\omega}_n + \delta_1 q_1)^2 & -2(\hat{\xi} + \delta_2 q_2)(\hat{\omega}_n + \delta_1 q_1) \end{bmatrix} = \hat{A} + \Delta\mathrm{A} \tag{4.56}$$

where

$$\hat{A} = \begin{bmatrix} 0 & 1 \\ -\hat{\omega}_n^2 & -2\hat{\xi}\hat{\omega}_n \end{bmatrix} \tag{4.57}$$

and

$$\Delta\mathrm{A} = \begin{bmatrix} 0 & 0 \\ -2\hat{\omega}_n q_1 \delta_1 - q_1^2 \delta_1^2 & -2\hat{\xi} q_1 \delta_1 - 2\hat{\omega}_n q_2 \delta_2 - 2 q_1 q_2 \delta_1 \delta_2 \end{bmatrix}. \tag{4.58}$$

Notice from this description that the uncertain δ_i parameters do not appear in a linear fashion in ΔA. Hence there is no way to define fictitious inputs and outputs to arrive at the linear relation of (4.52), which is a necessary step in reflecting the uncertainty into a form that can be handled in the μ framework. This inability to directly represent the uncertainty as bounds on any variable in a model of a system is a limitation of using parametric error descriptions in the linear P–Δ interconnection structure. As seen in this simple canonical example, this problem is especially relevant for structural systems in which it is simple to evaluate realistic levels of uncertainty in the frequency and damping of the structural modes, but for which it is not feasible to directly use this information in a technique that guarantees stability robustness for the mismodeled dynamics.

There are a few techniques that can be used to arrive at a linear combination of the uncertain parameters in a system. For example, one might try to linearize the non-linear relation amongst the uncertainties as proposed in [45]. However, the approach that will be applied here, which is used in many other parameter uncertainty methods [44, 20], is more conventional. Basically, the non-linear structure of the actual uncertain variables that may appear in ΔA is avoided by considering the individual elements in the state space matrices to be the parametrically uncertain variables. As long as the bounds on the uncertain elements in the state space matrices over bound the original uncertainty description in the model, this method, while slightly more conservative than the realistically defined error model, is safe to use. By further assuming that there is no dependence among these uncertain variables, a quite simple procedure for casting such parametric errors into the P–Δ system description is available [50]. In terms of the canonical example, this means that (4.55) will no longer be considered the uncertain parameters. Instead

$$\alpha = \begin{pmatrix} \omega_n^2 \\ 2\xi\omega_n \end{pmatrix} \tag{4.59}$$

will be defined as the uncertain variables in that model to get a linear relation amongst the uncertainty. To show that this is the case, notice that when the δ_i uncertainty description of (4.49) is substituted into (4.54) as above $A(\alpha)$ now decomposes as

$$A(\alpha) = \begin{bmatrix} 0 & 1 \\ -(\hat{\omega}_n^2 + \delta_1 q_1) & -(2\hat{\xi}\hat{\omega}_n + q_2\delta_2) \end{bmatrix} = \hat{A} + \Delta\mathrm{A} \tag{4.60}$$

where $\hat{A}$ is the same as in (4.57) and

$$\Delta\mathrm{A} = \begin{bmatrix} 0 & 0 \\ -q_1\delta_1 & -q_2\delta_2 \end{bmatrix} = \delta_1 \begin{bmatrix} 0 & 0 \\ -q_1 & 0 \end{bmatrix} + \delta_2 \begin{bmatrix} 0 & 0 \\ 0 & -q_2 \end{bmatrix}. \tag{4.61}$$

In essence to get a linear relation amongst the uncertain parameters of a structural system in order to form a linear feedback interconnection structure, the actual elements of the state space matrices of the model rather than the true uncertain parameters need to be considered the mismodeled variables.

Before returning to the uncertainty description of the beam and the process of defining the fictitious inputs and outputs of (4.52), there is some more notation and concepts which need to be discussed that are easily visualized from the canonical example. Notice that the independent and linear relation amongst the δ_i in ΔA from (4.61), that was arrived at by considering the elements of the A matrix be the uncertain parameters, leads to a further decomposition of ΔA into the sum of rank one perturbations matrices, to be denoted as A_k in general, weighted by the δ_k

$$\Delta \mathrm{A} = \sum_{k=1}^{m} \delta_k A_k. \tag{4.62}$$

As will be shown, writing the rank one A_k as the outer product of two vectors,

$$A_k = a_k b_k^T, \tag{4.63}$$

is instrumental in forming the P–Δ system when there are real parameter errors in a model. Also notice from (4.61) that for $A(\alpha) \in \mathbf{R}^{n \times n}$ with an uncertain element in the (i, j^{th}) location of $A(\alpha)$, a possible choice for a_k and b_k are n length vectors of zeros except for a q_k in the i^{th} row of a_k and a -1 in the j^{th} row of b_k. Finally realize that all these concepts and notation are directly applicable to the sample problem since the uncertain variables appear in (4.54) and (2.10, 2.5) in exactly the same way except for their location in the matrix.

Even though a realistic, parametric uncertainty model for the sample problem was laid out at the beginning of this section, the subsequent investigation has shown that a less realistic, yet useful, uncertainty model must be defined to arrive at a P–Δ system description. As in the case with the canonical example, the uncertainty description needs to be expressed as parametric bounds on the individual elements of the state space matrices to arrive at a linear representation of the errors. Hence the vector of uncertain variables that will be used to cast the knowledge of the mismodeled dynamics in the beam model into the P–Δ system description is

$$\alpha = \begin{pmatrix} \omega_1^2 \\ \omega_2^2 \\ 2\xi_1\omega_1 \\ 2\xi_2\omega_2 \end{pmatrix}. \tag{4.64}$$

Realize that admitting such an uncertainty model is somewhat unrealistic because it considers ω_1 and $2\xi_1\omega_1$ to be two independent, uncertain variables when they are not since the true independent, uncertain variables are ω_1 and ξ_1. The implication of doing this is, of course, a more conservative error model, but an error model that is still far less conservative than any unstructured error model. Further realize that at this point there has been a sufficient enough level of ad hoc engineering in defining the mismodeled dynamics model that a slight bit more should not make a drastic difference. In any case, the realistic uncertainty description that was previously defined will not be ignored. Rather it will be used to define the uncertainty model based on the uncertainty vector (4.64).

Acknowledging that (4.64) is the vector of uncertain parameters in the beam model that will be used in deriving the P–Δ system, it is necessary to evaluate the q_i to arrive at a model of the uncertainty in terms of the δ_i. To this end, the realistically evaluated upper and lower bounds on the ω_i and ξ_i for the first two bending modes of the beam, that are summarized in Table 4.2, were used to approximate the upper and lower bounds on the α_i of (4.64). Using over-bars and under-bars to respectively denote the upper and lower limits of the parametrically uncertain variables, an estimate for the set of bounds on (4.64) is

$$\underline{\alpha} = \begin{pmatrix} \underline{\omega}_1^2 \\ \underline{\omega}_2^2 \\ 2\underline{\xi}_1\underline{\omega}_1 \\ 2\underline{\xi}_2\underline{\omega}_2 \end{pmatrix} \quad \text{and} \quad \overline{\alpha} = \begin{pmatrix} \overline{\omega}_1^2 \\ \overline{\omega}_2^2 \\ 2\overline{\xi}_1\overline{\omega}_1 \\ 2\overline{\xi}_2\overline{\omega}_2 \end{pmatrix}. \tag{4.65}$$

Table 4.3 shows the values of these bounds and the percentage of error between the nominal values of the α in (4.64) and the upper and lower bounds defined in (4.65). Notice from this table that the amount of error between the upper and lower bounds and the nominal value of the variables is different. Since the level of error between the nominal value and its bounds for all the uncertain variables is greatest for the upper bound, the values of the q_i, which are shown in Table 4.3, were evaluated from (4.50) using $\overline{\alpha}_i$ in order to cover all the possible values of the parameters defined by the bounds in (4.65). Realize that there is really no loss of fidelity in the uncertainty

α	$\hat{\alpha}$	$\underline{\alpha}$	$\overline{\alpha}$	Error ($\underline{\alpha}$)	Error ($\overline{\alpha}$)	q
ω_1^2	2127.98	1920.2	2345.5	9.8 %	10.2 %	234.1
ω_2^2	82,736.77	74,665.6	91,216.1	9.8 %	10.2 %	9101.1
$2\xi_1\omega_1$	.922	.438	1.45	52.5 %	57.5 %	.536
$2\xi_2\omega_2$	5.74	2.74	9.06	52.5 %	57.5 %	3.32

Table 4.3: Parametric uncertainty description for a linear representation of the errors in the beam model. Frequencies are in *rad/sec*.

model by choosing the q_i in this fashion, as the uncertainty model is already ad hoc at this point from choosing to use a description that bounds the elements in the state space matrices rather than the truly uncertain variables.

Given this uncertainty description and the previously defined notation, it is now possible to construct the P–Δ system for the beam model with parametric uncertainty in the values of its A matrix. Without a loss of generality, the external inputs, w, and the performance variables, e, will be ignored for simplicity in forming the P–Δ system description so that

$$\begin{pmatrix} \dot{x} \\ z \\ y \end{pmatrix} = \left[\begin{array}{c|cc} A_P & B_{P_1} & B_{P_2} \\ \hline C_{P_1} & D_{P_{11}} & D_{P_{12}} \\ C_{P_2} & D_{P_{21}} & D_{P_{22}} \end{array}\right] \begin{pmatrix} x \\ v \\ u \end{pmatrix} \tag{4.66}$$

is the model that needs to be created. As was the case with the canonical model, using the δ_i uncertainty description of (4.49) for $A(\alpha)$ in (4.51) decomposes $A(\alpha)$ into a nominal matrix and a perturbed matrix that is linear in the uncertain δ_i parameters. Since the uncertain variables in (4.54) are exactly the same as those in (2.10, 2.5) except for their location in the matrix, the further decomposition of ΔA into (4.62) with (4.63) also applies to the beam model so that $A(\alpha)$ in (4.51) can be also be written as

$$A(\alpha) = \hat{A} + \sum_{k=1}^{m} \delta_k a_k b_k^T \tag{4.67}$$

As described in the case of the canonical example, the a_k and b_k vectors can be defined simply from the q_k and knowledge of the specific location of the k^{th} uncertain variable

in the uncertain A matrix. Now defining the fictitious output of the system to be

$$z_k(t) = b_k^T x(t) \qquad k = 1, \ldots, m, \tag{4.68}$$

recalling that the desired fictitious inputs needed to arrive at $\Delta \in \mathbf{B}X_{\mathcal{K}}$ in (4.53) are

$$v_k(t) = \delta_k z_k(t) \qquad k = 1, \ldots, m, \tag{4.69}$$

and using this information in (4.67) produces the state dynamics in terms of the inputs and outputs of (4.66)

$$\dot{x}(t) = \hat{A}x(t) + \sum_{k=1}^{m} a_k v_k(t) + B_2 u(t). \tag{4.70}$$

Further stacking the a_k and b_k vectors for the $m = 4$ uncertain elements in the beam model into matrices

$$v(t) = \begin{pmatrix} v_1 \\ \vdots \\ v_4 \end{pmatrix} \qquad \text{and} \qquad z(t) = \begin{pmatrix} z_1 \\ \vdots \\ z_4 \end{pmatrix} \tag{4.71}$$

produces the fictitious inputs and outputs of (4.66). Augmenting (4.71) to the inputs and outputs of (4.70) then provides the values of the matrices for the P–Δ system description of the beam model with parametric uncertainty in its A matrix, (4.66),

$$A_P = \hat{A} \qquad B_{P_2} = [a_1 \;\; a_2 \;\; a_3 \;\; a_4] \qquad B_{P_2} = B_2 \tag{4.72}$$

$$C_{P_1} = \begin{bmatrix} b_1^T & b_2^T & b_3^T & b_4^T \end{bmatrix}^T \qquad C_{P_2} = C \tag{4.73}$$

$$D_{P_{11}} = D_{P_{12}} = D_{P_{21}} = 0 \qquad D_{P_{22}} = D_2 \tag{4.74}$$

This is the desired model that could be used in the μ, as well as many other parametric uncertainty frameworks, to deal with the mismodeled dynamics in the beam model.

Having completed the mismodeled dynamics uncertainty model for the beam, a few comments are now in order. First of all realize that even though no residue uncertainty was considered in the beam model, mismodeled dynamics resulting from residue uncertainties could have been accounted for by letting elements in the B_2 and C matrices of (4.51) be parametrically uncertain and applying the same decomposition

tricks to them that were used on the $A(\alpha)$ matrix. The process of forming a P–Δ system for this more general case is described in [50].

Another item to consider here is that the added information available about the mismodeled dynamics was extensively utilized to create a very structured description of the uncertainty. While the description was limited to a linear form, it still directly represented parametric errors in the real values of the state space matrices. Unfortunately as a result of the very structured nature of the uncertainty model, there are no feasible design methodologies that can be employed to design compensators that are robust to such errors; as there are for unstructured error descriptions. Even though this is the case, the uncertainty description outlined above is still useful in evaluating the robustness of a given compensator to the mismodeled dynamics in the beam model. A possible, yet numerically intensive, method for checking the robustness of a compensator to a parametrically structured uncertainty model was already outline in Section 4.2.1. Recall that this involves evaluating $\tilde{\mathcal{N}}(j\omega)$ in (4.1) over all the possible values of the uncertain variables, which are the δ_i in this case, and checking whether or not the critical point lies in the resulting region. Given a mathematical model of the truss system, the fidelity of the mismodeled dynamics model for the beam outlined in this section could also be evaluated by constructing the $\tilde{\mathcal{N}}(j\omega)$ region and checking whether or not the Nyquist contour for the truss lies within it. Realize that these numerically extensive tests do not lead to any simple procedures that can be used to design compensators which are robust to parametric uncertainties, and they are thus of limited interest in general.

At this point the assessment of the uncertainty in model of a system along with a thorough overview of how to deal with the uncertainties in a model has been presented. In the following section, compensators will be derived based on the beam model and applied to the actual truss model to see to what extent a realistic assessment of the uncertainty and the robustness techniques discussed can be used to ensure stably robust compensators. Also given a specific compensator, some of the mismodeled dynamics visualizations for multivariable systems that require compensators will be presented using the parametric uncertainty model of the beam derived in this section.

Chapter 5

$\mathcal{H}_2$ Control Designs

Given a quantifiable description of the uncertainty in a model, one can incorporate stability constraints in their controller designs to ensure robustness. However as seen in the previous chapter, not all classes of modeling errors can be accounted for in simple and useful ways. In this chapter, the framework of the sample problem will be used to investigate to what extent stability robustness can be guaranteed for unmodeled dynamics and what the ramifications of not having any simple and useful ways to handle mismodeled dynamics in a model are on the stability properties of the actual closed loop system. Developing compensators based on the beam design model, derived in Chapter 2 and analyzed in Chapter 3, and applying them to the actual truss system not only allows for such an investigation but also provides an indication of the level of performance that can be achieved given a typical structural model with mismodeled and unmodeled dynamics. In essence, the methods, or lack there of, for dealing with the uncertainty in a model that were discussed in Chapter 4 will be tested in the framework of the sample problem by deriving compensators based on the beam model and applying them to the actual truss system. If it is possible to synthesize multivariable controllers based on the uncertain beam model that achieve a decent level of performance and are stably robust given the modeling errors, it should be possible to achieve similar results for realistic systems like the Interferometer testbed that the sample problem mimics.

Before facilitating a discussion on the effects of modeling uncertainty in the closed

loop, the process that was used to design compensators for the sample problem must be described. To this end, the specific design requirements and evaluation criterion which were used in designing compensators for the sample problem are outlined in the following section. Once the design specifications are laid out, the details of the frequency weighted $\mathcal{H}_2$ synthesis method used to design the compensators will be presented along with a discussion of the heuristics of how to choose the frequency weights to meet the design specifications. Since the intent intent here is not to evaluate which synthesis procedure provides the best compensators, only a few designs will be discussed in the final section to illustrate the insights and results of the previous work on assessing and dealing with the uncertainty in a model of a structural system.

5.1 Design Specifications

The majority of structural control problems in one way or another are intended to quiet the motion at particular locations on a structure resulting from some sort of external or internal disturbance. Hence, a disturbance rejection control problem to quiet the motion of the truss' outputs, y_i, in the presence of the internal disturbances, d_i, will be considered for the sample problem. In doing so, it is vital to realize that the primary motivation in designing such a control system is to achieve a high level of performance, that is disturbance rejection, since the open loop dynamics are stable. However since the truss is a lightly damped structure that is difficult to model precisely, which is accounted for by basing the control designs on the beam model, it becomes important to ensure that control systems developed for performance are robust to the uncertainties in the model used to design them so that they do not cause a closed loop instability. These remarks allude to a simple and concise set of specifications for the sample problem that will provide the basis for designing compensators for the truss system based on the beam model. Specifically any compensator, $K(s)$, should

1. Provide the greatest amount of disturbance rejection at the outputs possible and

2. be robust to the uncertainties in the nominal model used to design $K(s)$ so that it will not cause a closed loop instability when applied to the actual truss system.

As is usually the case, both criterion can not be met simultaneously and there will be an inherent trade off between the achievable performance and amount of robustness in any one design.

Before proceeding onto a description of the synthesis method that will be used to achieve the outlined design goals, it is useful to outline how the design specifications will be evaluated for a given compensator design. As far as evaluating the performance is concerned, it is necessary to classify a model for the expected disturbances to evaluate how well a given controller minimizes their affect on the outputs of the truss. In defining the disturbances, it is useful to recall that the nominal design model of the beam derived in Chapter 2

$$\dot{x}(t) = Ax(t) + B_2u(t) + B_1d(t) \tag{5.1}$$

$$y(t) = Cx(t) + D_2u(t) + \theta(t) \tag{5.2}$$

is driven by truss disturbances, d_i, and inputs, u_i, and produces truss outputs, y_i. To account for the fact that perfect sensors do not exist in reality, the sensor noise, $\theta(t)$, is now included in the model of the truss outputs. Letting the sensor noise and disturbances be independent, zero mean, Gaussian, white noise processes with covariances

$$\Sigma_{ww}(t,\tau) \triangleq \mathrm{E}\left\{ \begin{bmatrix} d(t) \\ \theta(t) \end{bmatrix} \begin{bmatrix} d^T(\tau) & \theta^T(\tau) \end{bmatrix} \right\} = \begin{bmatrix} \Xi & 0 \\ 0 & \Theta \end{bmatrix} \delta(t-\tau) \tag{5.3}$$

allows for a realistic and simple stochastic framework in which to work in. Realize that there is no loss in generality in allowing the disturbances to be white, as any non-white disturbance could be modeled as the output of a shaping filter driven by white noise. The intensity of the disturbances, Ξ,

$$\Xi = \begin{bmatrix} 1 \times 10^{-6} N^2 s & 0 \\ 0 & 1 \times 10^{-6} N^2 m^2 s \end{bmatrix} \tag{5.4}$$

was chosen to produce reasonable levels of open loop motion at the outputs of the truss. On the other hand, the sensor noise intensity, Θ, was chosen to reflect the accuracy in the measurement system. For the sample problem, a nanometer level of RMS, root mean square, accuracy was assumed for the true sensors so that the actual sensor noise intensity, Θ_{true}, was set at

$$\Theta_{\text{true}} = \begin{bmatrix} 1 \times 10^{-18} m^2 s & 0 \\ 0 & 1 \times 10^{-18} m^2 s \end{bmatrix}. \tag{5.5}$$

However, the outputs in (5.2) are scaled by (2.32), and thus the true sensor noise intensity needed to be scaled appropriately by (2.32) as well.

$$\Theta = Q_y \Theta_{\text{true}} Q_y^T = \begin{bmatrix} 8.1 \times 10^{-8} s & 0 \\ 0 & 2.6 \times 10^{-5} s \end{bmatrix}. \tag{5.6}$$

With this model of the truss, the steady state frequency domain representation of (5.1,5.2) becomes

$$y(s) = G_2(s)u(s) + G_1(s)d(s) \tag{5.7}$$

$$G_2(s) = C(sI - A)^{-1}B_2 + D_2 \qquad G_1(s) = C(sI - A)^{-1}B_1 \tag{5.8}$$

where $G_2(s)$ and $G_1(s)$ will be respectively referred to as the control and disturbance, open loop, transfer function matrices.

Given the disturbance model defined above, the statistics of the outputs can be used to evaluate the extent to which a specific compensator meets the performance metric for the sample problem. Specifically, the amount of corruption at the outputs of the truss can be evaluated from the RMS values of the beam outputs in (5.2) as well as the magnitude of the disturbance to output transfer function, $\overline{\sigma} G_1(j\omega)$, of the beam model. Both these measures of the output degradation for the open loop system are shown in Figure 5.1. Using this portrayal of the open loop performance, the performance of specific compensators will be evaluated by comparing the open and closed loop RMS values of the beam outputs as well as the magnitude of the open loop and closed loop, disturbance to output transfer function matrix of the beam system. Using this visualization of the performance of a compensator, the desire to provide as

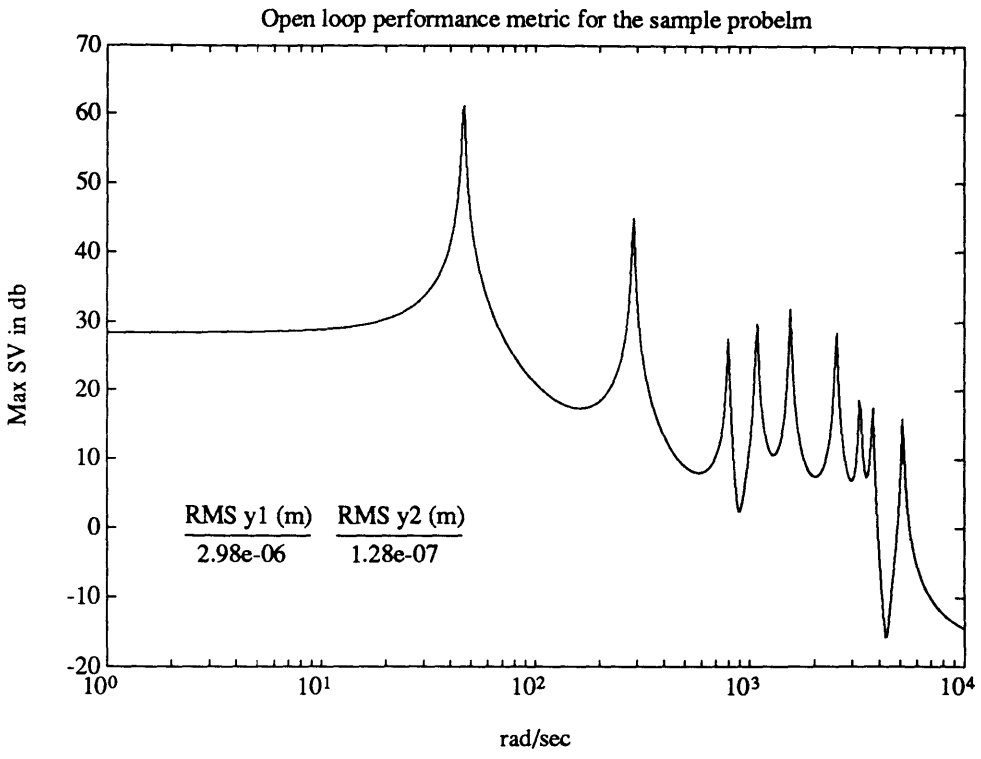

Figure 5.1: Open loop performance metric for the sample problem: $\overline{\sigma}G_1(j\omega)$ and the open loop RMS values of $y(t)$.

much disturbance rejection as possible at the outputs of the truss will be measured by the ability to reduce the RMS values of the outputs as much as possible; which is also analogous to reducing the magnitude of the disturbance to output transfer function as much as possible.

The robustness specification for the controller will be analyzed in two ways. First, for a given $K(s)$ the analysis methods for dealing with the uncertainty from Chapter 4 will be used to check that the compensator is robust to the unmodeled dynamics in the beam model. Specifically, Theorem 4.3 will be used via (4.21) with the $w_m(s)$ defined in Section 4.1.3 to verify if a given compensator is robust to the unmodeled dynamics in the beam model. While no analogous test exists to easily check the robustness of a compensator to the mismodeled dynamics in the beam model, the robustness of some of the compensators derived for the truss to the mismodeled dynamics will be discussed in terms of the mismodeled dynamics region in the Nyquist domain; as was done for the scalar example (4.32) in Section 4.2.1. The second way in

which compensators will be analyzed for their robustness to the modeling errors is by evaluating the poles of the actual closed loop system that can be calculated by directly applying the beam based compensator to the analytical model of the truss. This step is akin to applying a compensator designed based on a model of a system directly to the actual system. If doing so drives the actual closed loop system unstable, the compensator will obviously not satisfy the robustness specification.

Realize that both the performance and robustness specifications for the control system have frequency domain interpretations. The performance metric can be visualized as minimizing the magnitude of the disturbance to output transfer function matrix, and the robustness specification for unmodeled dynamics can be evaluated by comparing the size of the multiplicative error at the output of the beam model to the size of the closed loop transfer function matrix. As a result of these frequency domain specifications, a loop shaping approach to designing the compensators to achieve the desired performance and robustness was pursued.

5.2 Frequency Weighted $\mathcal{H}_2$ Synthesis

The performance specifications in the previous section can be readily met by considering a $\mathcal{H}_2$ controller synthesis. For the standard feedback system interconnection the objective of a $\mathcal{H}_2$ controller is to find a stable compensator, $K(s)$, that minimizes

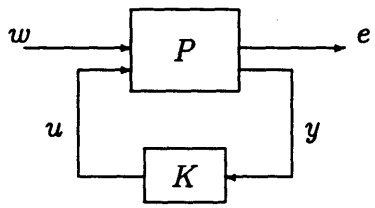

Figure 5.2: The general feedback system description.

$\|T_{ew}\|_2$, the $\mathcal{H}_2$ norm of the closed loop transfer function matrix from the exogenous signals, w, to the performance variables, e. A $\mathcal{H}_2$ cost criterion is preferable given the RMS output performance metric since it seeks to minimize the average energy over all frequencies captured by the disturbance to output transfer function. Furthermore,

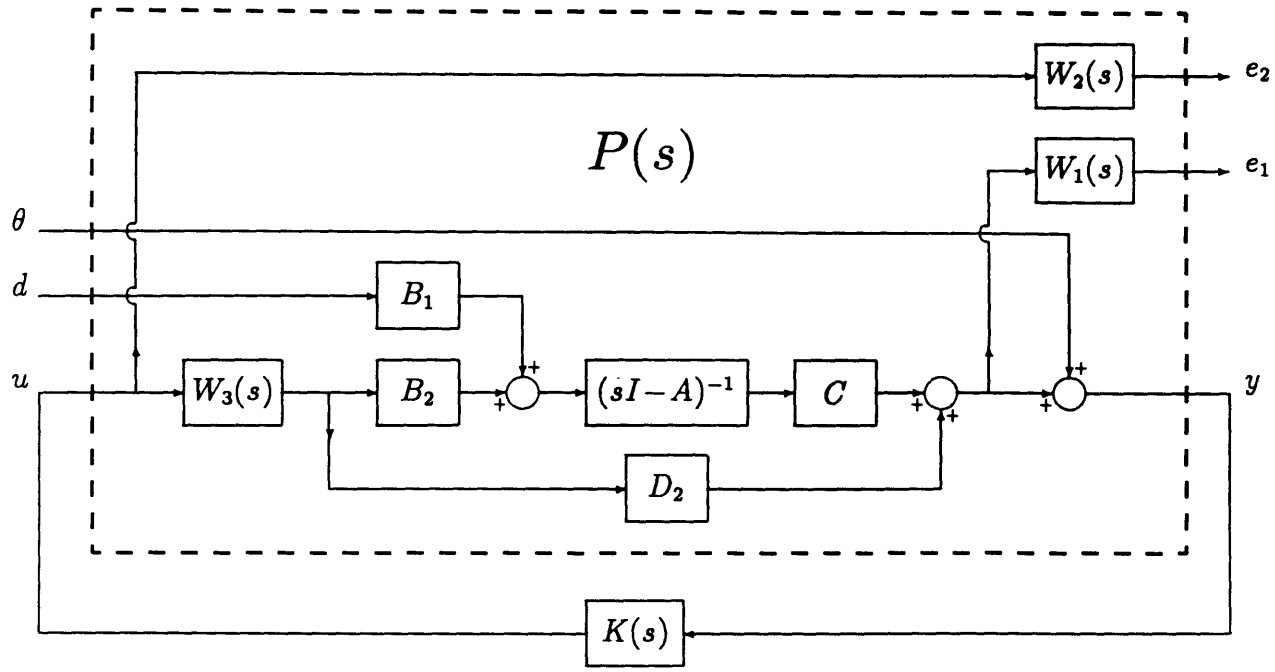

Figure 5.3: Block diagram of the beam model with frequency weights.

the robustness specification for the unmodeled dynamics can be easily satisfied in the $\mathcal{H}_2$ framework by including frequency weights in the design, which simply amounts to augmenting the desired weights to the general system, $P(s)$. Both these features of $\mathcal{H}_2$ optimal control, as well as the ease of synthesizing compensators, make it an appropriate method to use in developing compensators for the sample problem given the design specifications laid out in the previous section.

In using a $\mathcal{H}_2$ synthesis procedure to develop controllers for the sample problem, it is useful to cast the beam model into the general feedback form of Figure 5.2. To this end, the block diagram representation of the beam dynamics (5.1,5.2) in the general system description form along with some weighting functions is shown in Figure 5.3. Since the design specification call for a reduction of the motion of the outputs while maintaining stability in the presence of the modeling uncertainties, the performance variables for the sample problem

$$e = \begin{pmatrix} e_1 \\ e_2 \end{pmatrix} \tag{5.9}$$

and their respective weights, $W_1(s)$ and $W_2(s)$ in Figure 5.3, were defined to penalize the noiseless outputs and the control inputs of the system. The third weight shown in Figure 5.3, $W_3(s)$, can be used as an additional degree of freedom in the controller design, or it can alternatively be viewed as as a means to model the actuator dynamics. For now it is sufficient to realize that the weights will be used to shape specific loops to meet the design specifications. The actual heuristics of how to choose the weights to do so will be discussed in the sequel.

In synthesizing $\mathcal{H}_2$ compensators, it is also useful to work with a state space model that captures the inputs and outputs of the general system shown in Figure 5.2. Namely the state space representation

$$\left(\begin{array}{c} \dot{x}_p \\ \hline e \\ y \end{array}\right) = \left[\begin{array}{c|cc} A_P & B_{P_1} & B_{P_2} \\ \hline C_{P_1} & D_{P_{11}} & D_{P_{12}} \\ C_{P_2} & D_{P_{21}} & D_{P_{22}} \end{array}\right] \left(\begin{array}{c} x_p \\ \hline w \\ u \end{array}\right) \tag{5.10}$$

will be now used to classify the dynamics of the design model for the sample problem used to synthesize $\mathcal{H}_2$ optimal controllers. In this representation for the sample problem, the exogenous signals

$$w = \begin{pmatrix} d \\ \theta \end{pmatrix} \tag{5.11}$$

are the independent, zero mean, Gaussian, white noise disturbances with the covariance defined by (5.3), (5.4), and (5.6). The specific values of the matrices in (5.10) are simply arrived at by augmenting the appropriate weight dynamics to the design plant model dynamics, (5.1, 5.2), and playing with the signal interconnection structure to arrive at the inputs and outputs needed to form (5.10). In fact, the real advantage of using this general system description is that the frequency domain weights, shown in Figure 5.3 that are used to shape certain loops to meet the design specifications, are simply included in the controller synthesis by forming the state space representation of (5.10). Specific values of the state matrices in (5.10) along with a more detailed description of how they were obtained for various combinations of the weights that were used in the sample problem designs are included in Appendix C for reference.

Given the general description of the sample problem in (5.10), it is now possible

to derive the form of the $\mathcal{H}_2$ optimal compensators, $K(s)$ that will be used to control the truss. In the stochastic framework at hand, the well known solution to the LQG, Linear Quadratic Gaussian, controller synthesis problem can be used to find the form of the optimal $\mathcal{H}_2$ compensator since the $\mathcal{H}_2$ cost is equivalent to a quadratic cost criterion

$$J = \mathrm{E}\left\{ \lim_{T\to\infty} \left(\frac{1}{T} \int_0^T e^T(t) e(t) \mathrm{d}t \right) \right\} \tag{5.12}$$

in this situation. If $D_{P_{11}} = 0$ and both $D_{P_{12}}$ and $D_{P_{21}}^T$ have full column rank, the separation principal applies and allows the optimal $\mathcal{H}_2$ compensator to be constructed by designing a Kalman Filter to estimate the states in (5.10) and designing a full state feedback control law that minimizes the cost in (5.12) to regulate the estimated states [21]. Since the solution to the $\mathcal{H}_2$ problem is well known and appears in [22], only the key aspects of the procedure involved in forming the optimal compensator will now be presented.

The first part of the solution involves the construction of a Kalman Filter to estimate the state of the model. With the model now in the general system description of (5.10), the estimated state, $\hat{x}_p(t)$, must be determined form the statistical model for $w(t)$, the dynamical model for $x_p(t)$ from (5.10), and the measurement model for $y(t)$ from (5.10)

$$\dot{x}_p(t) = A_P x_p(t) + B_{P_2} u(t) + B_{P1} w(t) \tag{5.13}$$

$$y(t) = C_{P_2} x_p(t) + D_{P_{22}} u(t) + D_{P_{21}} w(t). \tag{5.14}$$

This estimation problem can be simplified to a more standard one by realizing that the statistical model for $w(t)$ will not change from design to design since it has already been specified, and that the measurement model for $y(t)$ will not change from design to design since the performance variables and the design degrees of freedom are represented in terms of $e(t)$ rather than $y(t)$ in this framework. As a result, the B_{P1} and $D_{P_{21}}$ matrices will always be of the form

$$B_{P1} = \begin{bmatrix} B_1 & 0 \\ 0 & 0 \end{bmatrix} \qquad \text{and} \qquad D_{P_{21}} = \begin{bmatrix} 0 & I \end{bmatrix} \tag{5.15}$$

for the beam design model (5.1, 5.2) [1]. Using this information and the definition of w in (5.11), the estimation problem for (5.13, 5.14) reduces to a more standard estimation problem for

$$\dot{x}_p(t) = A_P x_p(t) + B_{P_2} u(t) + \mathcal{B}_1 d(t) \tag{5.16}$$

$$y(t) = C_{P_2} x_p(t) + D_{P_{22}} u(t) + \theta(t) \tag{5.17}$$

where

$$\mathcal{B}_1 = \begin{bmatrix} B_1 \\ 0 \end{bmatrix}. \tag{5.18}$$

For these dynamics and the noise models for $d(t)$ and $\theta(t)$ defined by (5.3), (5.4), and (5.6), the dynamics of the Kalman filter for the estimated states, $\hat{x}_p(t)$, are

$$\dot{\hat{x}}_p(t) = A_P \hat{x}_p(t) + B_{P_2} u(t) + K_e \left[y(t) - \hat{y}(t) \right] \tag{5.19}$$

$$\hat{y}(t) = C_{P_2} \hat{x}_p(t) + D_{P_{22}} u(t) \tag{5.20}$$

In the state equation for $\hat{x}_p(t)$

$$K_e = \Sigma_{xx} C_{P_2}^T \Theta^{-1} \tag{5.21}$$

is the filter gain, and Σ_{xx}, the estimation error covariance, is the unique positive definite solution of the estimator Riccati equation

$$0 = \Sigma_{xx} A_P^T + A_P \Sigma_{xx} + \mathcal{B}_1 \Xi \mathcal{B}_1^T - \Sigma_{xx} C_{P_2}^T \Theta^{-1} C_{P_2} \Sigma_{xx}. \tag{5.22}$$

The second part of the optimal compensator solution involves finding a regulator gain, K_r, that produces a linear control based on the estimated dynamics

$$u(t) = -K_r \hat{x}_p(t) \tag{5.23}$$

The value of the gain K_r is determined by minimizing the quadratic cost in (5.12) subject to the constraint that

$$\dot{x}_p(t) = A_P x_p(t) + B_{P_2} u(t) + B_1 d(t), \tag{5.24}$$

[1] This can be seen in Appendix C where specific values for the matrices in the state space descriptions of (5.10) for the sample problem are presented.

where $d(t)$ is a white noise process. Notice from (5.10), in which $D_{P_{11}} = 0$ by assumption, that

$$e(t) = C_{P_1} x_p(t) + D_{P_{12}} u(t), \tag{5.25}$$

$$e(t)^T e(t) = x_p^T(t) R_{xx} x_p(t) + 2u(t)^T R_{ux} x_p(t) + u(t)^T R_{uu} u(t) \tag{5.26}$$

$$R_{xx} \triangleq C_{P_1}^T C_{P_1} \qquad R_{ux} \triangleq D_{P_{12}}^T C_{P_1} \qquad R_{uu} \triangleq D_{P_{12}}^T D_{P_{12}}, \tag{5.27}$$

and the cost in (5.12) is nothing more than the standard stochastic version of the cost for a LQR, Linear Quadratic Regulator, problem. Thus, the optimal choice for the desired gain K_r is given by the solution of the well known LQR problem for which

$$K_r = R_{uu}^{-1} \left[B_{P_2}^T S + R_{ux} \right]. \tag{5.28}$$

In the expression for K_r, S is the unique positive definite solution of the regulator Riccati equation

$$0 = S\bar{A} + \bar{A}^T S - S B_{P_2} R_{uu}^{-1} B_{P_2}^T S - R_{ux}^T R_{uu}^{-1} R_{ux} + R_{xx} \tag{5.29}$$

where

$$\bar{A} \triangleq A_P - B_{P_2} R_{uu}^{-1} R_{ux}. \tag{5.30}$$

Once the estimator and regulator gains are evaluated, the optimal $\mathcal{H}_2$ controller can be realized through a model based compensator that uses the inputs and measured outputs to drive the Kalman Filter (5.19, 5.20) which in turn provides the estimated states used to compute the actual control in (5.23). Assuming a negative feedback interconnection structure for the compensator and letting $x_c(t)$ denote the states of the compensator, the dynamics of the optimal $\mathcal{H}_2$ compensator that minimizes the cost in (5.12) are

$$\dot{x}_c(t) = A_c x_c(t) + K_e y(t) \tag{5.31}$$

$$u(t) = -K_r x_c(t) \tag{5.32}$$

where

$$A_c \triangleq A_P - B_{P_2} K_r - K_e C_{P_2} + K_e D_{P_{22}} K_r. \tag{5.33}$$

Given this notation, the frequency domain representation of the compensator is

$$K(s) = -K_r(sI - A_c)^{-1}K_e. \tag{5.34}$$

This completes the description of the form of the optimal $\mathcal{H}_2$ compensator that will be used to control the truss.

Notice that the order of the optimal $\mathcal{H}_2$ compensator has the same number of states as the general system in (5.10). That is

$$\dim(A_c) = \dim(A_P) = n + n_1 + n_2 + n_3 \tag{5.35}$$

where n is the number of states in the original design model of (5.1) and n_i is the number of states needed to represent weight $W_i(s)$. Obviously then the use of frequency dependent weights directly increases the order of the optimal compensator. Hence, the order of the frequency weights is an issue to consider when designing a control system, as the compensator must ultimately be implemented.

At this point the method for synthesizing compensators for the sample problem has been outlined, and it is worthwhile to notice how the feed–forward $D_{P_{22}}$ term in the measurements, that arises from including the static correction of the truncated dynamics in the reduced order model, enters into the synthesis process; as it is not standard practice to include such a term in a model. First of all, realize that the inclusion of the $D_{P_{22}}u(t)$ term in the measurements simply gets carried along for the ride in the Kalman Filter portion of the solution just like the contribution of the controls, $B_{P_2}u(t)$, since it is a deterministic quantity. Then in the regulator calculation, the $D_{P_{22}}$ term simply leads to a cost with a cross weighting which is nothing out of the ordinary. Finally, there is an extra term in the A_c matrix of the model based compensator that arises from the portion of the Kalman Filter that mimics the noise free dynamics of the design model. All in all, the inclusion of the feed–forward $D_{P_{22}}$ term does not have any drastic effect on the controller synthesis.

It is also useful at this point to present the form of the closed loop dynamics that will be used to evaluate the performance and stability characteristics of a given compensator $K(s)$. Recall that the performance will be evaluated by calculating the

RMS values of the outputs of the closed loop system and computing the magnitude of the output to disturbance closed loop transfer function. Both computations require the formation of the closed loop system dynamics. Augmenting the compensator dynamics, (5.31, 5.32), to the open loop dynamics, (5.10), and letting the augmented state be

$$\mathrm{x}(t) = \begin{pmatrix} x_p(t) \\ x_c(t) \end{pmatrix}, \tag{5.36}$$

the closed loop dynamics of the sample problem for a given compensator are

$$\dot{\mathrm{x}}(t) = A_{cl}\mathrm{x}(t) + B_{cl}w(t) \tag{5.37}$$

$$y(t) = C_{cl}\mathrm{x}(t) + \theta(t) \tag{5.38}$$

where

$$A_{cl} \triangleq \begin{bmatrix} A_P & -B_{P_2}K_r \\ K_eC_{P_2} & A_c - K_eD_{P_{22}}K_r \end{bmatrix} \qquad B_{cl} \triangleq \begin{bmatrix} B_{P_1} & 0 \\ 0 & K_e \end{bmatrix} \tag{5.39}$$

$$C_{cl} \triangleq \begin{bmatrix} C_{P_2} & -D_{P_{22}}K_r \end{bmatrix} \tag{5.40}$$

With this representation, the RMS values of the outputs in the closed loop can be readily evaluated since $w(t)$ is a white noise process driving a linear system. Taking (5.37, 5.38) into the frequency domain,

$$y(s) = G_{cl}(s)w(s) \qquad \text{with} \qquad G_{cl}(s) = C_{cl}(sI - A_{cl})^{-1}B_{cl}, \tag{5.41}$$

yields the expression for the closed loop disturbance to output transfer function, $G_{cl}(s)$, whose magnitude, $\overline{\sigma}G_{cl}(\jmath\omega)$, will compared to $\overline{\sigma}G_1(\jmath\omega)$ to provide a picture of the performance achieved by a given compensator.

As far as the stability analysis of a compensator is concerned, realize that the process of applying the beam based compensator, $K(s)$, to the truss model and checking if the actual closed loop will be stable can be carried out by replacing the A, B_1, B_2, C, and D_2 terms of the beam model in A_{cl} with the corresponding terms of the truss model and checking whether or not the real parts of the eigenvalues of the resulting A_{cl} are all negative. While this provides an absolute measure of the stability

of the actual closed loop system, recall that the robustness of a given compensator to the unmodeled dynamics in the model will be carried out by checking that (4.21) is satisfied for the error bounds defined in Section 4.1.3. To do so, realize that the $C(s)$ term in (4.21) was derived specifically from the feedback interconnection structure shown in Figure 4.4, and as a result the stability robustness condition in (4.21) only applies to systems in the feedback interconnection structure of Figure 4.4. Obviously, the feedback interconnection of Figure 5.3 used to derive the $\mathcal{H}_2$ optimal compensator is not in the form needed to test for stability robustness through (4.21). To get the proper expression for $C(s)$ to check a given compensator's robustness to unmodeled dynamics, the system description of Figure 5.3 used to derive $K(s)$ in (5.34) can be reduced to the simple structure of Figure 4.4. This is done by neglecting the disturbances in the system, that is setting $w(t) = 0$; adding a fictitious reference signal, r, to the loop after y and before $K(s)$ in Figure 5.3; augmenting the the actuator dynamics, $W_3(s)$ to the control loop dynamics, $G_2(s)$, so that $G(s)$ in Figure 4.4 is now given by $G(s) = G_2(s)W_3(s)$; and realizing that the bounds on the multiplicative error developed in Section 4.1.3 are for a multiplicative error at the output of the control loop which, with $w(t) = 0$, is before y in Figure 5.3. Doing so, the proper test to check the stability robustness of a given $\mathcal{H}_2$ compensator to the unmodeled dynamics in the beam model of (5.1, 5.2) is

$$\overline{\sigma} C_{sr}(j\omega) < \frac{1}{|w_m(j\omega)|} \qquad \forall \omega \tag{5.42}$$

where

$$C_{sr}(s) \triangleq -\left[I - G_2(s)W_3(s)K(s)\right]^{-1} G_2(s)W_3(s)K(s). \tag{5.43}$$

Since the $\mathcal{H}_2$ framework is hands on in the sense that a given compensator design is arrived at by iterating on choices of the weights to achieve the desired design requirements, the hands on weight for $w_m(s)$ defined by (4.25) will be used as the bound on the multiplicative error at the output in the beam model to check the robustness properties of compensators derived based on the beam model.

In essence, this section has been very notational so that the actual compensators and the performance and robustness measures that will be used to evaluate them are

clearly understood. In the next section, the heuristics of how to actually choose the design weights will be described.

5.3 Frequency Weight Selection

Weights in any optimal control design framework act as knobs that the control system designer can tune to arrive at a design that meets the desired specifications. Typically, constant weighting values provide a sufficient enough level of freedom to meet the design requirements. However, there are cases in which constant weights do not provide enough freedom in designing compensators to meet the specifications. The sample problem is one such case as will be seen in the next section when a standard LQG design for the sample problem in which

$$W_1(s) = W_3(s) = I \qquad \text{and} \qquad W_2(s) = \rho^{\frac{1}{2}} \cdot I \tag{5.44}$$

is presented. In cases where the performance and robustness criterion are stringent, frequency dependent weights can be used to provide the extra degrees of freedom needed in the design process to meet the outlined specifications. In the case of the sample problem, a sufficient enough level of design freedom was arrived at by using frequency dependent weights that influenced each component of the signal past through them equally. That is

$$W_1(s) = w_1(s) \cdot I, \quad W_2(s) = w_2(s) \cdot I, \quad \text{and} \quad W_3(s) = w_3(s) \cdot I \tag{5.45}$$

where the $w_i(s)$ for $i = 1, 2, 3$ are the scalar transfer function weights that were specified in each design to attempt to satisfy the desired specifications.

To see how the choice of the weights influence the controller characteristics, consider first $W_1(s)$ and $W_2(s)$ that directly weight the performance variables in (5.10). These weights will obviously have a strong effect on the compensator since they directly influence the $\mathcal{H}_2$ cost, $\|T_{ew}\|_2$, that is minimized by $K(s)$ in (5.34). To explicitly see how the weights influence the control system design, a frequency domain extension of the the equivalent quadratic cost of (5.12) will be used [51]. Letting

$$y_n(t) = C_{P_2} x_p(t) + D_{P_{22}} u(t) \tag{5.46}$$

denote the noiseless output and using Parseval's theorem to express the cost (5.12) in the frequency domain roughly yields

$$J \approx \frac{1}{2\pi}\int_{-\infty}^{\infty}\left\{|w_1(\jmath\omega)|^2 y_n^H(\jmath\omega)y_n(\jmath\omega) + |w_2(\jmath\omega)|^2 u^H(\jmath\omega)u(\jmath\omega)\right\}\mathrm{d}\omega\,, \qquad (5.47)$$

which provides an explicit representation of how $W_1(s)$ and $W_2(s)$ influence the cost used in synthesizing controllers for the sample problem. From this approximate frequency domain expression for the cost and the design specifications, it becomes clear how to choose $w_1(s)$ and $w_2(s)$. To understand why this is so, recall that it is the objective of the control to minimize the cost in (5.47). Further, quantities with a large weighting in the cost are considered more detrimental to the minimization and are thus penalized heavier. Hence, a large weight should be applied to the variables in the cost that the controller needs to make small. With the frequency domain interpretation of the cost, these concepts can be applied on a frequency by frequency basis.

In the case of the sample problem, recall that the robustness specification calls for a small closed loop gain at high frequencies to satisfy (5.42). To meet this specification, $w_2(s)$ should be chosen so that its magnitude is large at high frequencies and small at low frequencies. In this way, $W_2(s)$ tells the cost that it wants each control to be small at high frequencies where the fidelity of the model is poor and large at the low frequencies to get a good level of performance where the fidelity of the model is good. As far as the output weight is concerned, realize that since the model of the truss is not accurate at high frequencies it would be foolish to try and achieve a high level of disturbance rejection at high frequencies. Hence $w_1(s)$ should be chosen to have a large magnitude at low frequencies to tell the cost that it should concentrate its efforts on making the outputs small where the model is well known. Indeed, these were the kinds of weights that were used to meet the design specifications of the sample problem as will be seen in the next section.

As far as the control signal filter, $W_3(s)$, is concerned, realize that even though its influence is not directly included in the cost used to derive the compensator it still directly influences the closed loop behavior since it directly filters the signals

produced by the compensator. The logic in placing $W_3(s)$ in the synthesis model of (5.10) is simple. In order to meet the unmodeled dynamics bound and still achieve a good amount of disturbance rejection over the first few structural modes, it will be necessary to force the compensator roll off hard. If it is not possible to do this by an appropriate choice of $W_1(s)$ and $W_2(s)$, the presence of $W_3(s)$ could provide an extra degree freedom to filter out the high frequency components of the control that could cause an instability in the range of the unmodeled dynamics. Typically, $w_3(s)$ was thus chosen to be a low pass filter to let the low frequency components of the control pass to the plant while diminishing the effect any undesirable high frequency contributions of the control may have on the closed loop system. Alternatively since $W_3(s)$ directly influences $C_{sr}(s)$ in (5.42), it could be chosen to shape $C_{sr}(s)$ to meet the stability robustness requirement for the unmodeled dynamics. In either case, it is important to realize that the dynamics of $W_3(s)$ become part of the compensator unlike the dynamics of $W_1(s)$ and $W_2(s)$ that only influence the the choice of the filter and regulator gains.

Notice at this point that the details of how to design controllers based on the beam model to achieve an improvement in the open loop performance while maintaining stability in the presence of unmodeled dynamics has been spelled out. It is by no means coincidental that there has been no mention of how to incorporate features into the synthesis that will produce controllers that are also robust to the mismodeled dynamics in the design model. Basically, the $\mathcal{H}_2$ methodology presented here ignores the fact that there are mismodeled dynamics in the design model since there are no simple and useful methods for dealing with them. The ramifications of ignoring these modeling errors on the stability properties of the actual closed loop system will be studied for a specific frequency weighted design in the sequel.

While these brief comments based on a frequency domain interpretation of the cost provide the heuristics of how to choose the design weights, it is worth noting that the selection of the appropriate weights to meet the design specifications is very iterative. For any given set of design specifications, it is unreasonable to expect to choose a sufficient set of weights a priori. In fact, the designs that will be presented for

the sample problem in the next section reflect the culmination of numerous iterations through various sets of weights.

5.4 Sample Problem Designs

Before presenting the designs, it is important to realize that the emphasis in doing so is not to elaborate on which combinations of weights produced the control system that best met some design specifications. Rather, the main focus of this section, and the chapter, is to investigate to what extent a detailed assessment of the uncertainty in a model along with the associated methods for dealing with the uncertainty can be applied in a practical design situation. In essence , the details presented thus far in the chapter have simply provided the necessary machinery to carry out such a study. To concisely discuss the implications a detailed robustness analysis has on the controller synthesis, only two designs will be discussed here. The first, a typical LQG design, is included to motivate why it was necessary to use the frequency weights in the synthesis procedure. The second design, which will be discussed in great detail, is a typical frequency weighted $\mathcal{H}_2$ design that sufficiently satisfied the design specifications. It is entirely possible that better designs than those presented exist. However, the goals of this chapter can be readily satisfied with those presented.

5.4.1 Design # 1: Standard LQG

In a standard LQG design, constant weights are used to penalize the performance variables in the cost. In terms of the sample problem, this means that

$$W_1(s) = W_3(s) = I \qquad \text{and} \qquad W_2(s) = \rho^{\frac{1}{2}} \cdot I, \tag{5.48}$$

and the only degree of freedom in designing a controller becomes the choice of the control weight ρ. In keeping with the design specifications, a value of $\rho = 1.5$ was found to be the smallest possible value of ρ that did not cause an instability in the closed loop truss system. Recall that the controllers are developed based on the beam model and that their performance is evaluated in terms of the RMS values of the beam

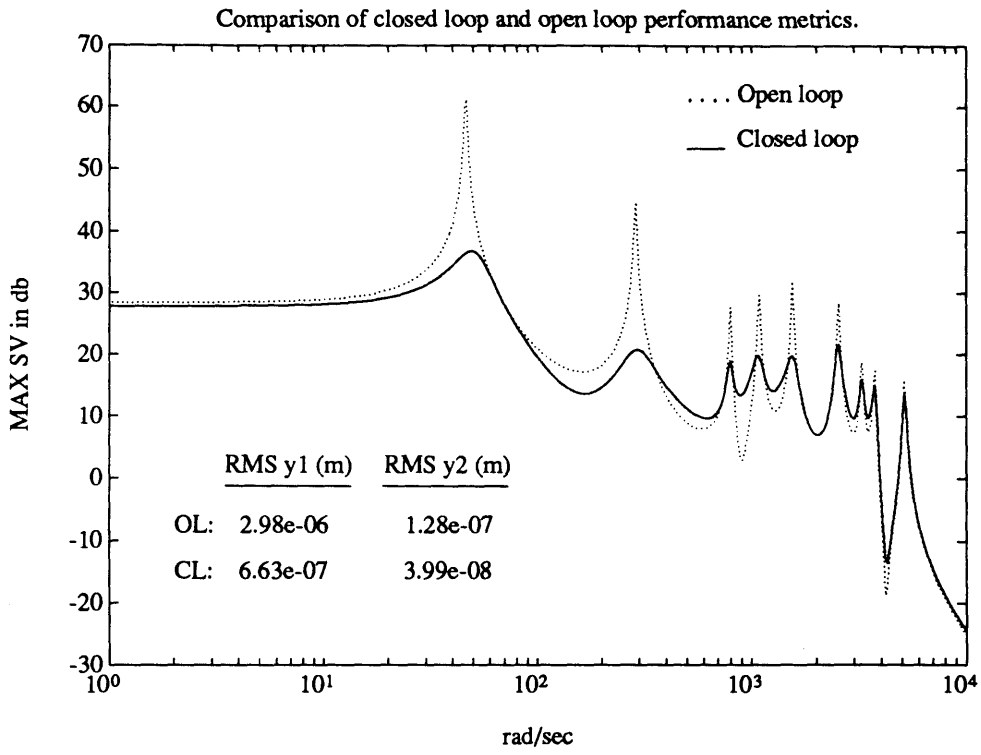

Figure 5.4: Nominal performance of the standard LQG design shown by a comparison of the magnitude of the open loop and closed loop output to disturbance transfer function matrices of the beam system: $\overline{\sigma}G_1(\jmath\omega)$ .vs. $\overline{\sigma}G_{cl}(\jmath\omega)$.

outputs and the magnitude of the output to disturbance transfer function matrix of the beam. Then the beam based controllers are applied to the truss to make sure that they do not destabilize the actual system that they are designed for. Hence, this value of ρ maximizes the achievable performance of the standard LQG design since it tells the cost to use as much control as it wants to minimize the degradation in the outputs caused by the disturbances as long as it does not cause a closed loop instability in the actual system. The optimal $\mathcal{H}_2$ compensator for these values of the weights was evaluated, and its performance and robustness characteristics are respectively shown in Figures 5.4 and 5.5.

From Figure 5.4 it is clear that this design achieves a decent level of performance. As expected of a $\mathcal{H}_2$ cost, the controller minimizes the average energy in the disturbance to output transfer function by adding damping to all the structural modes that appear in that transfer function. In terms of the RMS metric, realize that RMS

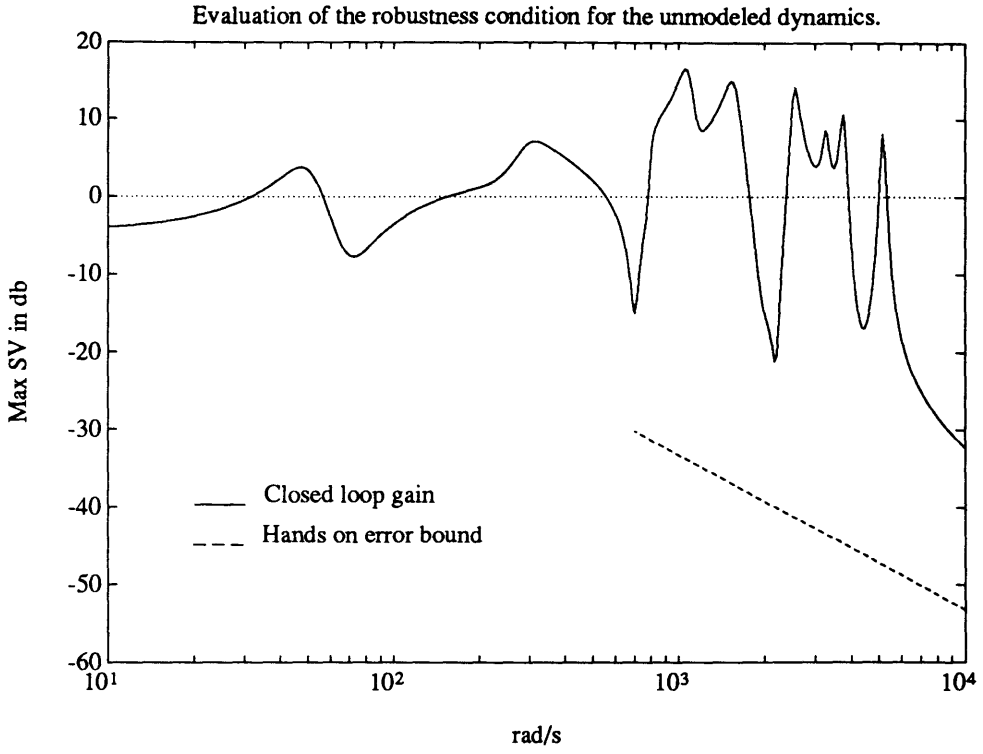

Figure 5.5: The robustness of the standard LQG design to the unmodeled dynamics evaluated by (5.42) for the closed loop gain, $\overline{\sigma}C_{sr}(j\omega)$, and hands on error bound, $|w_m(j\omega)|$, from (4.25).

values can be viewed as the area under the square of the disturbance to output transfer function, and on a linear scale such a plot would still have large spikes at the frequencies of the structural modes for the level of damping achieved by the LQG design. As a result, there is only a slight amount of improvement in the RMS values of the outputs in the closed loop. In general though, the damping behavior exhibited by the LQG design is the type of performance that the design specifications call for.

Inevitably, the ability of the compensator to damp all the modes in the performance metric is accomplished at the expense of a large bandwidth for the compensator. This is obviously seen in Figure 5.5 which shows the closed loop gain, $\overline{\sigma}C_{sr}(j\omega)$, of the system. The consequence of such a high bandwidth is that the LQG compensator does not even come close to satisfying the stability robustness condition of (5.42). In other words, the LQG compensator is not at all robust to the unmodeled dynamics in the beam model used to derive the compensator. On the other hand

since the actual truss system for this compensator is stable, this design simply confirms a limitation of Theorem 4.3 which does not guarantee anything about the actual stability of the true closed loop system if (5.42) is violated. Even though the actual truss closed loop system is stable, the LQG compensator can not be considered robust since it fails the multiplicative error stability robustness criterion. In fact, for any smaller value of the control weight ρ, the closed truss system is unstable. Further, the closed loop poles of the truss for the design with ρ slightly less than 1.5 that sit in the right half plane are those corresponding to the third bending mode of the beam, which were classified as unmodeled due to the large error in their modeled frequency of vibration. Hence, this result provides a case which shows that there could be a closed loop instability if the robustness condition of (5.42) is not met. In summary, the assessment of the uncertainty along with the unmodeled dynamics stability robustness condition were able to predict the instability for $\rho < 1.5$, and thus they are useful in dealing with the uncertainty.

At this point, it is not even worth it to talk about the robustness of this design to the mismodeled dynamics; since the LQG compensator is already not robust to the unmodeled dynamics and thus does not meet the design specification.

To achieve a similar level of performance while meeting the unmodeled dynamics stability robustness condition, it was obviously necessary to have more degrees of freedom available in designing a control system. Here in lies the primary reason for using frequency dependent weights in the controller synthesis.

5.4.2 Design # 2: Typical frequency Weighted $\mathcal{H}_2$

Acknowledging that it would be necessary to use frequency dependent weights in the controller synthesis to meet the design specifications led to the $\mathcal{H}_2$ design framework already described. In trying to meet the design specifications, many iterations through various choices for the three weights shown in Figure 5.3 were performed. In the iterations, the ability of the compensator to meet the outlined design goals as well as the order of the resulting compensator were considered in evaluating each set of weights. After numerous simulations, the following set of weights were chosen to

synthesize a $\mathcal{H}_2$ optimal compensator to use in discussing the the desired robustness aspects of the design.

$$W_1(s) = w_1(s)\cdot I, \qquad w_1(s) = \frac{17.78}{(s/900+1)^2} \tag{5.49}$$

$$W_2(s) = w_2(s)\cdot I, \qquad w_2(s) = .178\frac{(s/100+1)^2}{(s/1000+1)^2} \tag{5.50}$$

$$W_3(s) = w_3(s)\cdot I, \qquad w_3(s) = \frac{1}{(s/45+1)^2}. \tag{5.51}$$

Figures 5.6, 5.8, and 5.7 respectively show the performance achieved by this selection of weights, the unmodeled dynamics robustness test for the design, and the magnitude of the weights used in the design.

It is immediately apparent from Figures 5.6 and 5.8 that the frequency weighted $\mathcal{H}_2$ design achieves a decent level of performance, however unlike the LQG design it does satisfy the stability robustness condition. Furthermore, the closed loop truss system under the control of the beam based compensator is stable. As a result, the $\mathcal{H}_2$ design derived using the weights in (5.49-5.51) meets the outlined design specifications for the sample problem. Realize that the performance attained by the frequency weighted $\mathcal{H}_2$ design is about as good as one can expect given the fidelity of the model. That is, a reasonable improvement in the open loop performance was obtained where the model is well known, and stability robustness to unstructured errors is guaranteed over the frequency range where the dynamics are not well known.

To get a feeling for the process of selecting an appropriate set of weights, consider the logic that went into choosing (5.49-5.51). Since the control signal filter, $W_3(s)$, directly influences the closed loop gain, $C_{sr}(s)$, as seen in (5.43), it was used as the primary design knob to shape $C_{sr}(s)$ to satisfy the robustness condition of (5.42) and thus provide a controller that was robust to the unmodeled dynamics in the beam model. On the other hand, the values of $W_1(s)$ and $W_2(s)$ were used to squeeze out as much performance as possible from the controller while not violating (5.42). In line with the discussion in Section 5.3 on how to select the weights, the magnitude of the output weight, $|w_1(j\omega)|$, was chosen to be large in the low frequency region where the model is well known so that the controller would exert most of its effort

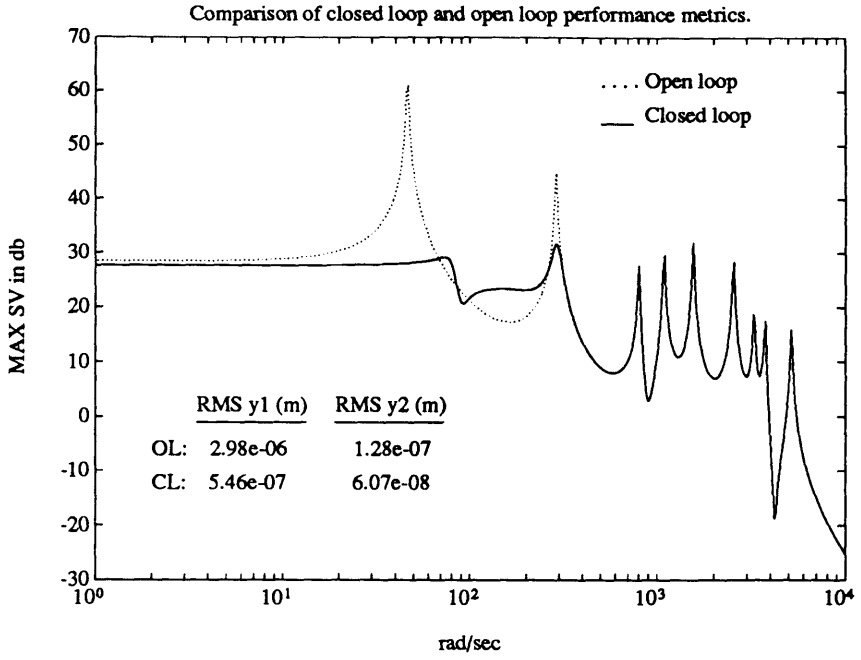

Figure 5.6: Nominal performance of the frequency weighted $\mathcal{H}_2$ design shown by a comparison of the magnitude of the open loop and closed loop output to disturbance transfer function matrices of the beam system: $\overline{\sigma}G_1(j\omega)$ .vs. $\overline{\sigma}G_{cl}(j\omega)$.

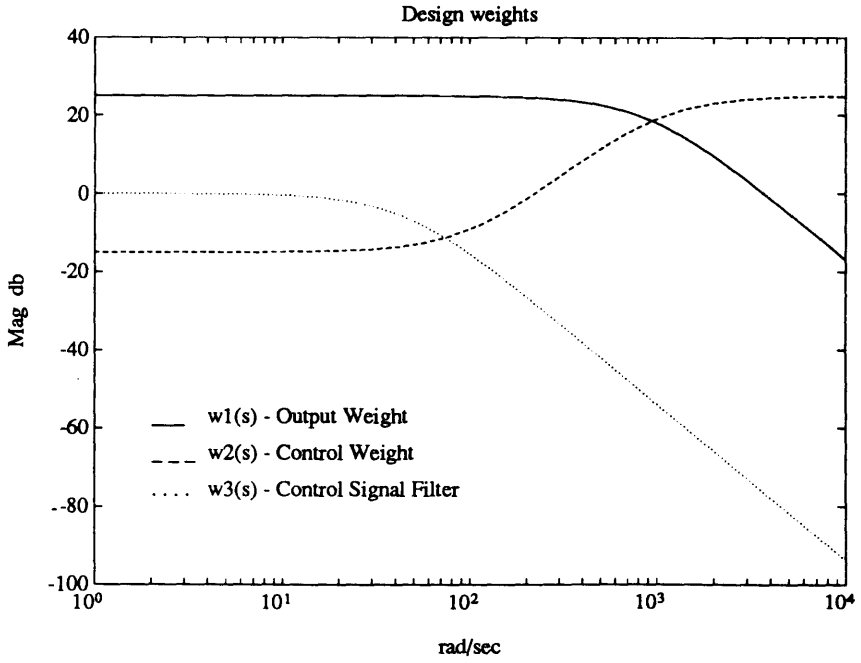

Figure 5.7: The Magnitude of the weights (5.49, 5.50, 5.51) used in the frequency weighted $\mathcal{H}_2$ design.

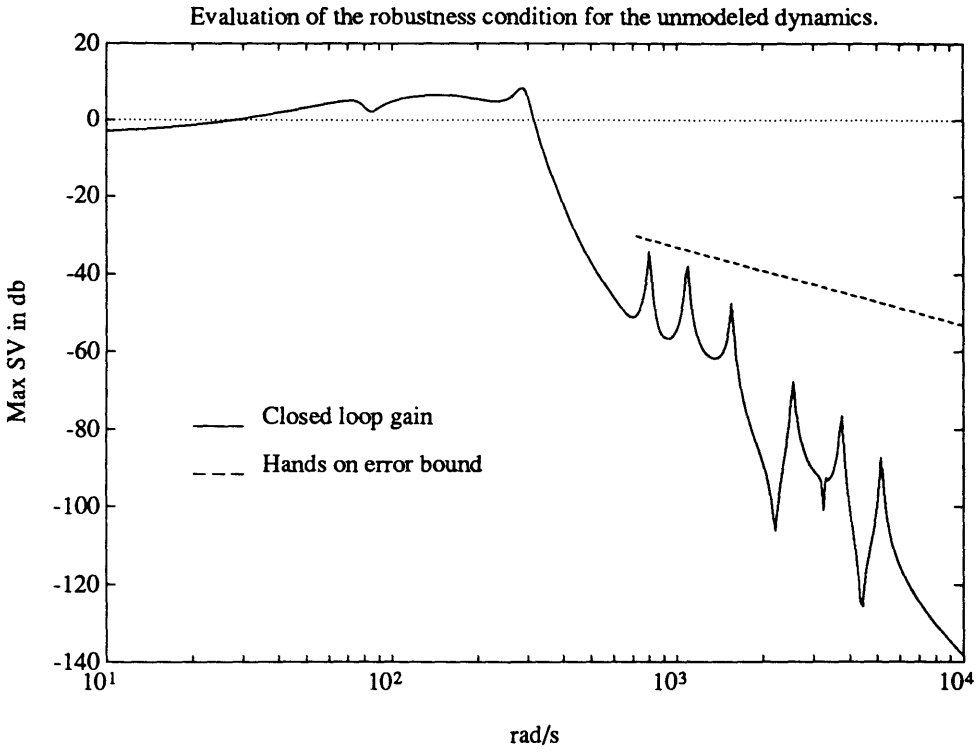

Figure 5.8: The robustness of the frequency weighted $\mathcal{H}_2$ design to the unmodeled dynamics evaluated by (5.42) for the closed loop gain, $\overline{\sigma}C_{er}(j\omega)$, and hands on error bound, $|w_m(j\omega)|$, from (4.25).

there. In a symbiotic manner, the magnitude of the control weight, $|w_2(j\omega)|$, was chosen to be small at low frequencies to let the control exert most of its effort where the dynamics were well known and to be large at high frequencies to tell the cost to keep the size of the controls small in the range of unmodeled dynamics. Realize that even though the weights of (5.49-5.51) were able to shape the appropriate loops to get a decent level of performance and robustness, they directly added 12 states to the dynamic compensator. As a result, the optimal $\mathcal{H}_2$ controller being discussed here had 30 states where as the standard LQG controller of the previous section only had 18 states.

A notable feature of the frequency weighted $\mathcal{H}_2$ design, as seen by the achieved closed loop performance shown in Figure 5.6, is that it captures the performance/robustness trade off inherent to robust controller synthesis. Recall from the assessment of the uncertainty presented in Chapter 3 that the beam model used to derive the controller

for the truss is known to be accurate up to about 700 rad/sec. Beyond 700 rad/sec are the unmodeled dynamics that are represented by a multiplicative error at the output of the beam control loop. In order guarantee stability robustness for these uncertainties, it becomes necessary to constrain the bandwidth of the controller to satisfy the robustness criterion of (5.42). In turn, the bandwidth constraint limits the range over which it is possible to achieve a good level of performance. As a result, the desire to guarantee stability robustness to the unmodeled dynamics in the beam model limits the achievable performance of the controller, which is the crux of the performance/robustness trade off. In terms of the $\mathcal{H}_2$ design, this is evident in Figure 5.6 that shows how the design only achieves a reasonable level of performance up to 300 rad/sec. It would be unrealistic to expect a better level of performance over a larger bandwidth given the knowledge that the model is poor at high frequencies. To achieve a better level of performance, it would be necessary to obtain an accurate model over a larger bandwidth to push up the frequency range where the unmodeled dynamics begin. In essence then, the unstructured error robustness condition provides a logical way of telling the controller synthesis that it should produce a controller that improves the open loop performance only where the model is well known.

The frequency weighted $\mathcal{H}_2$ design also exemplifies that it is possible to design controllers that are robust to the high frequency unmodeled dynamics. This is evident since the $\mathcal{H}_2$ controller satisfies the stability robustness condition of (5:42), and since the $\mathcal{H}_2$ controller does not destabilize the actual truss system when applied to it. Furthermore, realize that the process of getting a design to meet the robustness specification was as simple as choosing the appropriate weights to shape the closed loop gain, $\overline{\sigma}C_{sr}(j\omega)$. If a $K(s)$ was found that didn't satisfy the robustness condition of (5.42), it was relatively easy to infer how to choose a new set of weights, given the insight of their influence on the design from Section 5.3, to find a $K(s)$ that did satisfy (5.42). Also it should be noted that out of all the designs that were evaluated, none of the controllers that satisfied the stability robustness condition of (5.42) caused a closed loop instability when they were applied to the truss. This further emphasizes

the fact that it is possible to design controllers which are robust to the unmodeled dynamics in the design model.

Even though it is possible to guarantee robustness to the unmodeled dynamics while achieving an improvement in performance, the ability to do so is done at the expense of the compensator order. In the design presented here, the weights added nearly as many states, 12, to the compensator as the number of states in the original design model of (5.1, 5.2) that had 18 states. In the context of this mathematical sample problem, this may not seem like an issue. However in the real world where such compensators must ultimately be implemented, the order of the compensator is an issue. Hence, the extent to which robustness can be guaranteed for unmodeled dynamics in the class of systems that the sample problem mimics is the extent to which a large order dynamic compensator can be implemented.

Given the decent level of performance achieved by the frequency weighted $\mathcal{H}_2$ design and its guaranteed robustness to the unmodeled dynamics, the $\mathcal{H}_2$ design would truly be complete if there was a simple way to show that it is also guaranteed to be robust to the low frequency mismodeled dynamics in the design model. Unfortunately as seen in Section 4.2, the process of doing so is not at all as simple as comparing the size of the closed loop gain with the size of a bound on the error, as was the case with the unmodeled dynamics. None the less, it is still possible to investigate if the frequency weighted $\mathcal{H}_2$ controller is stably robust to the mismodeled dynamics by using the Nyquist domain analysis concepts that were exploited to visualize why it is difficult to guarantee robustness for mismodeled dynamics.

Robustness of the Frequency Weighted $\mathcal{H}_2$ Design to the Mismodeled Dynamics

In analyzing the robustness of the frequency weighted $\mathcal{H}_2$ compensator to the mismodeled dynamics, realize that at the simplest level the mismodeled dynamics do not interfere with the stability of the actual closed loop system; as the truss closed loop is stable when the beam based compensator is applied to it. While this shows the absolute stability of the design, it unfortunately says nothing about the stability

robustness of the control system to the mismodeled dynamics. However given the parametric error uncertainty description of the mismodeled dynamics in the beam model presented in Section 4.2.3, the computationally intensive, brute force analysis technique used to visualize the mismodeled dynamics in the Nyquist domain, from Section 4.2.1, could be used to analyze the robustness of the frequency weighted $\mathcal{H}_2$ compensator to the mismodeled dynamics in the beam model.

Recall that the stability robustness of a system with a parametric uncertainty description can be evaluated by constructing the region in the Nyquist domain in which the nominal model with its mismodeled dynamics may lie. That is computing

$$\tilde{\mathcal{N}}(s) = -1 + \det[I + \tilde{G}(s)K(s)] \tag{5.52}$$

for $s \in D_r$ and all the possible values of the uncertain variables, α, in

$$\tilde{G}(s) = \{G(\alpha, s) \; : \; \underline{\alpha_i} \leq \alpha_i \leq \overline{\alpha_i} \quad \forall \alpha_i\}. \tag{5.53}$$

Then if the critical point does not lie in the resulting region there will not be a change in the number of encirclements of the critical point, and the closed loop system will be robustly stable to the mismodeled dynamics represented by α. Realize that such a test is computationally intensive since it involves the evaluation of $\tilde{\mathcal{N}}(j\omega)$ over all the possible values of the α_i at each frequency. None the less, given a compensator, $K(s)$, this test does provide a way to investigate the stability robustness of a control system to mismodeled dynamics.

To make use of these concepts, it is first necessary to come up with the appropriate $\tilde{\mathcal{N}}(s)$ and $\tilde{G}(s)$ for the frequency weighted $\mathcal{H}_2$ design based on the beam model. Realize that $\mathcal{N}(s)$ defined in Theorem 4.1 is specific to the feedback interconnection structure of Figure 4.1. Realize also that the interconnection structure of Figure 4.1 is very similar to that of Figure 4.4 which was used to derive Theorem 4.3. Hence the same arguments that led to $C_{sr}(s)$ in (5.43) were used to arrive at the proper forms of $\mathcal{N}(s)$ and $\tilde{\mathcal{N}}_{sr}(s)$,

$$\mathcal{N}_{sr}(s) = -1 + \det[I + G_2(s)W_3(s)K(s)] \tag{5.54}$$

$$\tilde{\mathcal{N}}_{sr}(s) = -1 + \det[I + \tilde{G}_2(s)W_3(s)K(s)], \tag{5.55}$$

that can be used to analyze the robustness of the $\mathcal{H}_2$ compensator to the mismodeled dynamics in the beam model. In these expressions, $K(s)$ is the frequency domain representation of the optimal $\mathcal{H}_2$ compensator from (5.34), and $G_2(s)$ is the control loop transfer function matrix of (5.8) that contains mismodeled dynamics which are approximated by $\tilde{G}_2(s)$.

As far as the description of the mismodeled dynamics are concerned, the parametric error model of the mismodeled dynamics for the sample problem developed in Section 4.2.3 can be used to define $\tilde{G}_2(s)$. Recall that only the frequency and damping values of the first two structural modes were considered to be in error in defining the mismodeled dynamics uncertainty model. Hence the the only mismodeled uncertainty in $G_2(s)$ is in its A matrix. Further recall that $A(\alpha)$ was defined by (4.67) so that the possible values that $A(\alpha)$, given the definition of the uncertain parameters in (4.64) with their nominal values and bounds shown in Table 4.3, could be evaluated by ranging the δ_i over -1 to $+1$ in (4.67). Thus $\tilde{G}_2(s)$ for the beam model was defined to be

$$\tilde{G}_2(s) = \left\{ G_2(\alpha, s) = C\left[sI - A(\alpha)\right]^{-1} B_2 + D_2 \;:\; -1 \leq \delta_i \leq +1 \quad \forall \delta_i \right\} \tag{5.56}$$

with $A(\alpha)$ given by (4.67).

Evaluating (5.55) over all the possible values of the δ_i at each frequency produces the region of mismodeled dynamics in the Nyquist domain for the frequency weighted $\mathcal{H}_2$ design. If the critical point, $(-1, 0)$, does not lie in this region, the $\mathcal{H}_2$ design will be robust to the defined mismodeled dynamics. Unfortunately, the creation of the mismodeled dynamics region is a very computationally intense process. Therefore, only carefully chosen pieces of the region along with some engineering insight will be used to investigate the robustness of the frequency weighted $\mathcal{H}_2$ design to the mismodeled dynamics in the beam model.

As mentioned, the computational burden of evaluating the entire mismodeled dynamics region is overwhelming. However by computing the mismodeled dynamics region at a few wisely chosen frequencies, it should be possible to get a clear picture of whether or not the mismodeled dynamics pose a stability problem. Obviously, it

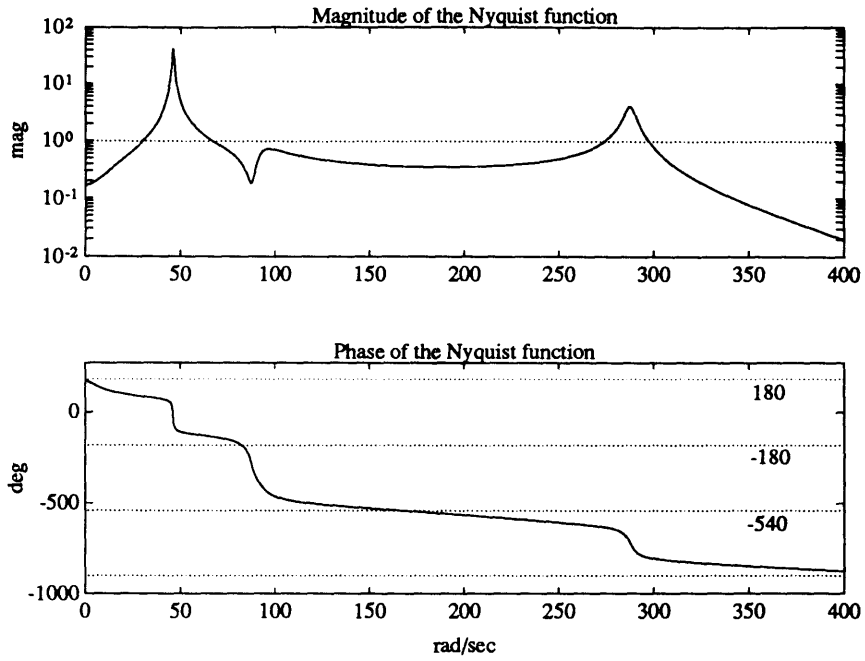

Figure 5.9: Bode type plots of $|\mathcal{N}_{sr}(j\omega)|$ and the $\angle\mathcal{N}_{sr}(j\omega)$ for $\mathcal{N}_{sr}(j\omega)$ from (5.54). Note the linear frequency scale.

would be beneficial to know what the region of mismodeled dynamics looks like near the critical point since the robustness to the mismodeled dynamics is contingent on the critical point not being in that region. The frequencies at which the Nyquist plot is near the critical point can be readily determined from a Bode type plot of the $|\mathcal{N}_{sr}(j\omega)|$ and the $\angle\mathcal{N}_{sr}(j\omega)$ as a function of ω. Such a plot is shown in Figure 5.9 for $\mathcal{N}_{sr}(j\omega)$ from (5.54). From this plot, the values of ω where the

$$|\mathcal{N}_{sr}(j\omega)| \approx 1 \quad \text{and} \quad \angle\mathcal{N}_{sr}(j\omega) \approx -180°(2n+1),\ n = 0, 1, \ldots$$

are the values of ω where the nominal Nyquist plot of the frequency weighted $\mathcal{H}_2$ design is near the critical point. Using this insight, the following values of ω

$$\omega = \{67,\ 76,\ 95,\ 130,\ 213\}\ rad/sec \tag{5.57}$$

were chosen as a candidate set of frequencies to evaluate $\tilde{\mathcal{N}}_{sr}(j\omega)$ at to create regions of mismodeled dynamics, which allows for an investigation of the robustness of the $\mathcal{H}_2$ frequency weighted design to the mismodeled dynamics in the beam model.

There is another set of frequencies for which it is useful and insightful to construct

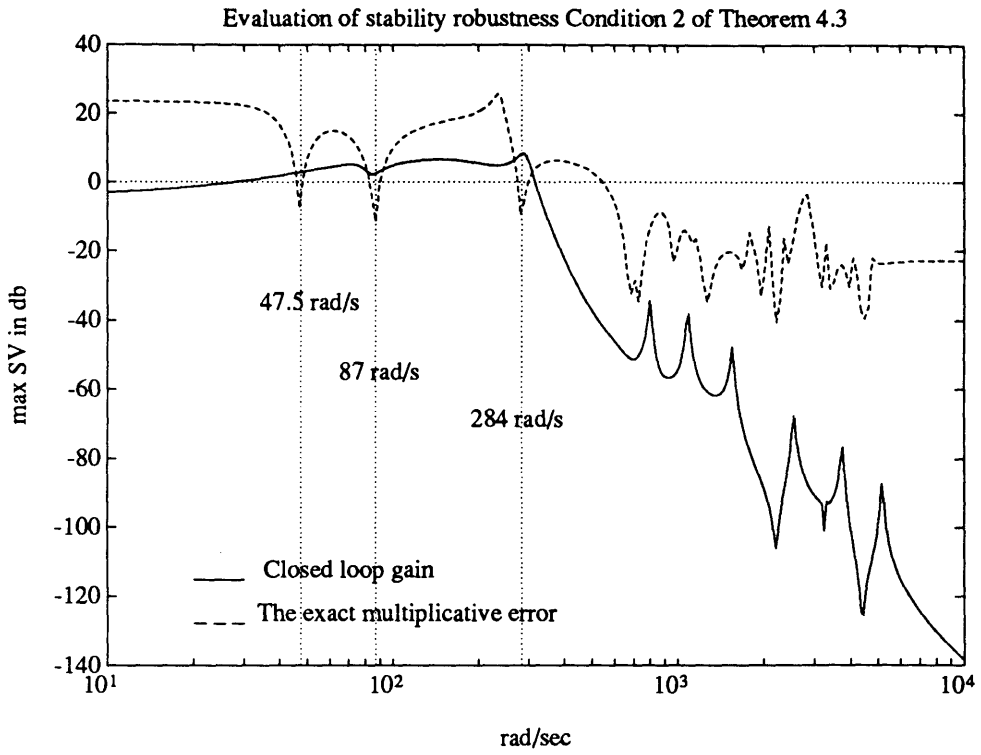

Figure 5.10: A graphical comparison of stability robustness Condition *2* from Theorem 4.3 for the frequency weighted $\mathcal{H}_2$ design: $\overline{\sigma}C_{sr}(j\omega)$ .vs. $1/\overline{\sigma}[\Delta_m(j\omega)]$. Here $\Delta_m(s)$ is the exact multiplicative error between the beam and truss from (4.29).

regions of mismodeled dynamics. To see this consider Figure 5.10 that graphically represents the stability robustness test of Theorem 4.3 using the exact multiplicative error between the beam and truss models from (4.29) and the closed loop gain of the frequency weighted $\mathcal{H}_2$ design, $\overline{\sigma}C_{sr}(j\omega)$. According to Theorem 4.3, the frequency weighted $\mathcal{H}_2$ design is not robust to the actual multiplicative error at the plant output since

$$\overline{\sigma}[C_{sr}(j\omega)] > \frac{1}{\overline{\sigma}[\Delta_m(j\omega)]} \tag{5.58}$$

at

$$\omega = \{47.5,\ 87.0,\ 284.0\}\ rad/sec. \tag{5.59}$$

In other words, the size of the unstructured multiplicative error perturbation at these frequencies is large enough to cause an instability or, in terms of the Nyquist domain picture, a change in the number of encirclements of the critical point. However as

already mentioned, the modeling errors below $700 rad/sec$ are not at all unstructured and considering them as such introduces conservatism into the robustness analysis. This conservatism is apparent due to the fact that the actual truss system is stable when the beam based, frequency weighted $\mathcal{H}_2$ controller is applied to it. For these reasons, it is very instructive to see what the regions of uncertainty look like at the frequencies in (5.59) for the more structured and accurate description of the uncertainty in the beam model. Hence, $\tilde{N}_{sr}(j\omega)$ was also evaluated at the frequencies in (5.59) to see if the actual system is in danger of an instability, as predicted by Theorem 4.3, and to further example of the conservatism of using unstructured error models to describe structured modeling errors.

Since the regions of mismodeled dynamics will be drawn around the Nyquist plot of the nominal system near the critical point, the multivariable Nyquist plot of the nominal system, $N_{sr}(j\omega)$ from (5.54), and a blow up of this plot near the critical point are respectively shown in Figures 5.11 and 5.12 to help visualize what the overall Nyquist plot of the frequency weighted $\mathcal{H}_2$ design looks like. With this understanding of the nominal Nyquist plot, the regions of mismodeled dynamics near the critical point evaluated from (5.54, 5.56) over the possible values of the δ_i at the frequencies in (5.57) and (5.59) are shown in Figures 5.13–5.16. Unlike the situation in Section 4.2.1 where the mismodeled dynamics region at one frequency was simply used to illustrate the complex shape of the mismodeled dynamics region, the multiple regions of Figures 5.13–5.16 are shown to help visualize what the entire region of mismodeled dynamics looks like for the frequency weighted $\mathcal{H}_2$ controller. Given these figures, it is now appropriate to discuss the robustness of the frequency weighted $\mathcal{H}_2$ design to the mismodeled dynamics in the model used to formulate the controller.

It is immediately obvious from Figures 5.13–5.16 that the frequency weighted $\mathcal{H}_2$ design seems to be robust to the defined mismodeled dynamics in the beam model. This is the case since the critical point does not lie in any of the mismodeled dynamics regions, nor does it seem that it would if the region of mismodeled dynamics was evaluated at all the frequencies. Even though there were no conditions built into the

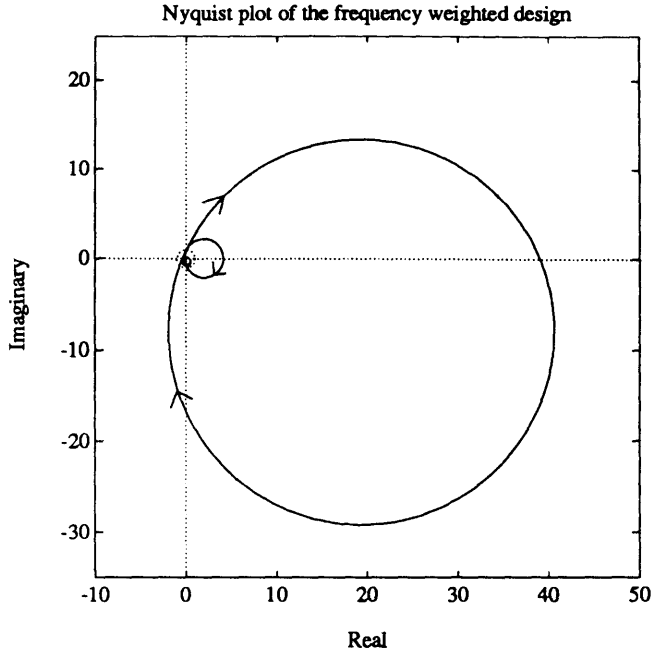

Figure 5.11: Nyquist plot of the frequency weighted $\mathcal{H}_2$ control system, $\mathcal{N}_{sr}(j\omega)$ from (5.54). Only the map of $\mathcal{N}_{sr}(j\omega)$ for $\omega \in (0, \infty)$ is shown to maintain clarity.

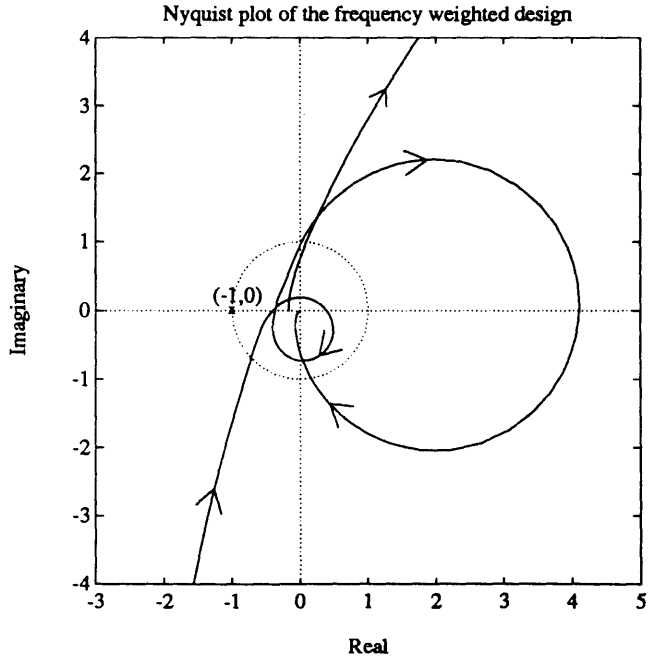

Figure 5.12: Blow up of the Nyquist plot of the frequency weighted $\mathcal{H}_2$ control system, $\mathcal{N}_{sr}(j\omega)$ from (5.54), near the critical point. Only the map of $\mathcal{N}_{sr}(j\omega)$ for $\omega \in (0, \infty)$ is shown to maintain clarity.

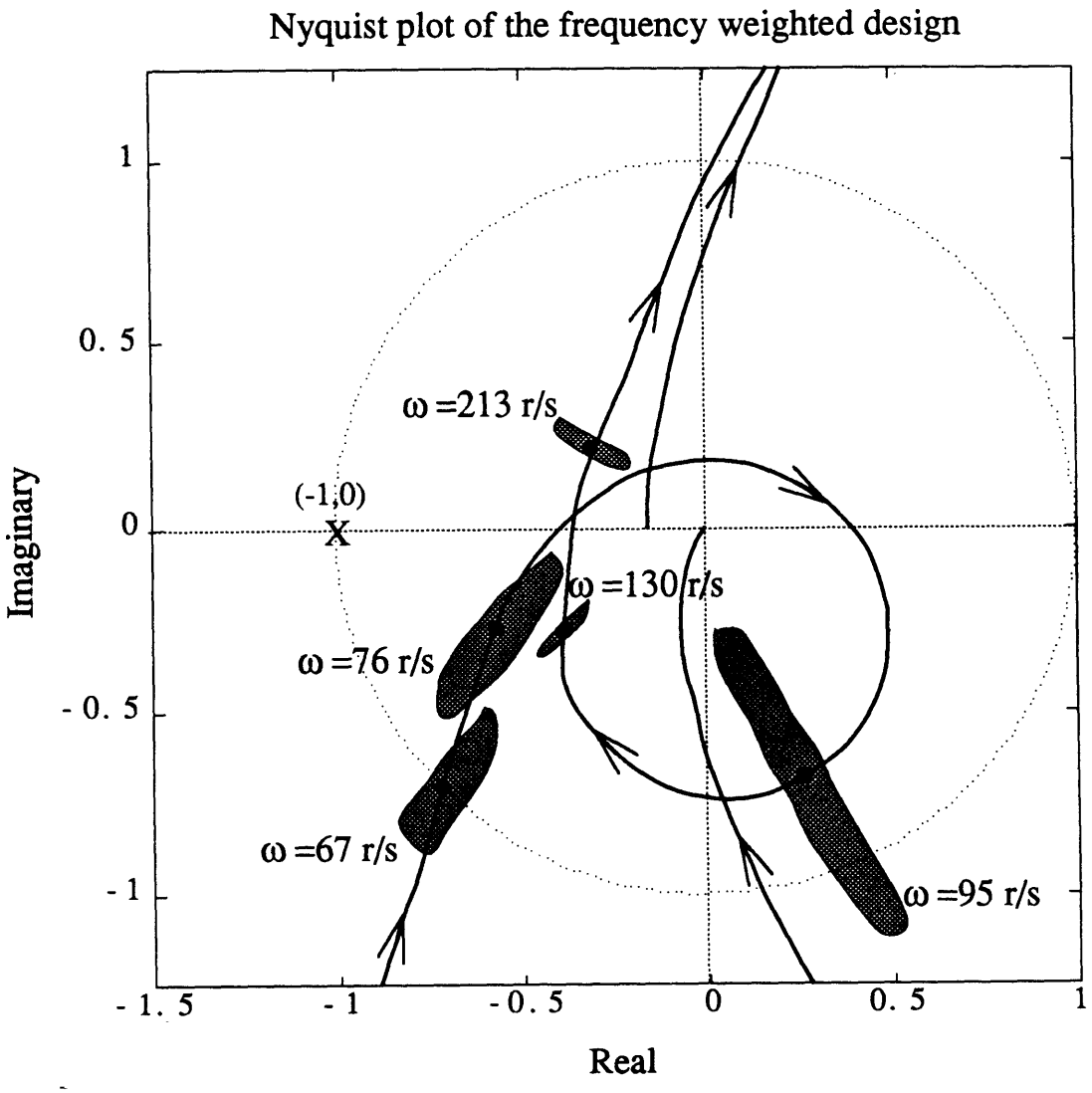

Figure 5.13: Blow up of the Nyquist plot of the frequency weighted $\mathcal{H}_2$ design, $\mathcal{N}_{sr}(j\omega)$, near the critical point. The shaded regions indicate the possible locations of the actual plant, $\tilde{\mathcal{N}}_{sr}(j\omega)$, based on the mismodeled dynamics description of (5.56) at the frequencies in (5.57).

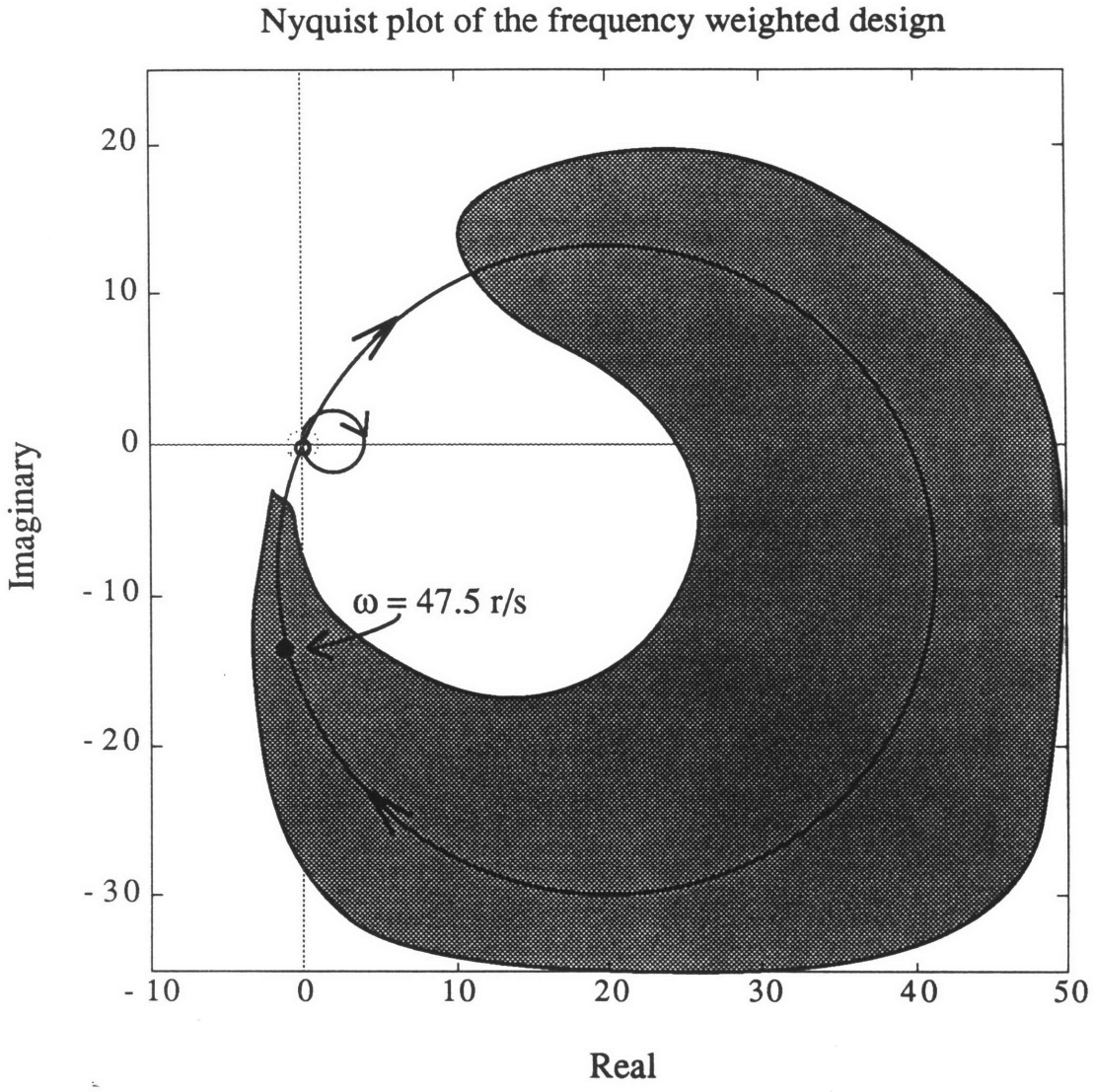

Figure 5.14: Nyquist plot of the frequency weighted $\mathcal{H}_2$ design, $\mathcal{N}_{sr}(j\omega)$. The shaded region indicates the possible locations of the actual plant, $\tilde{\mathcal{N}}_{sr}(j\omega)$, based on the mismodeled dynamics description of (5.56) at $\omega = 47.5\, rad/sec$.

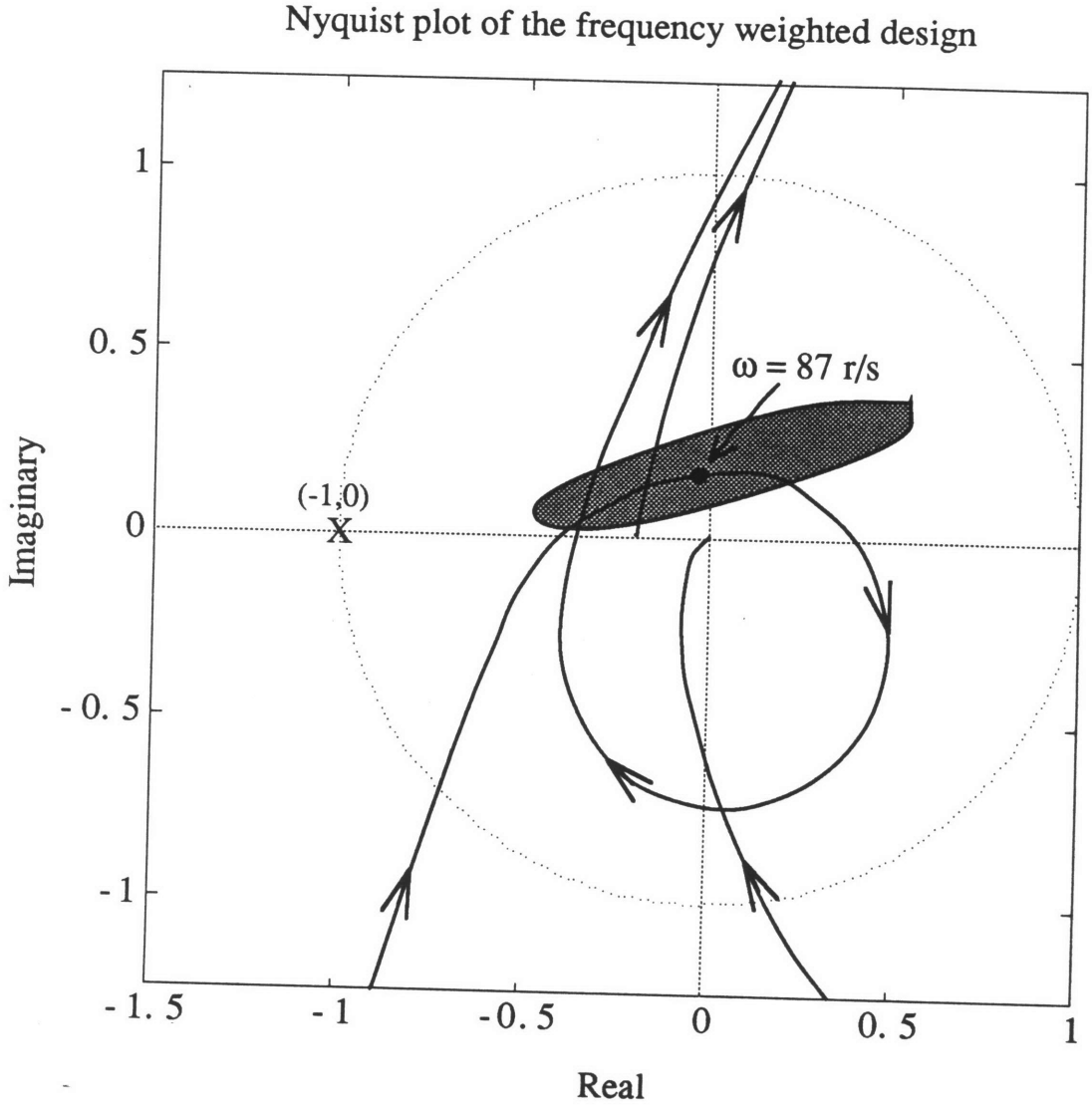

Figure 5.15: Blow up of the Nyquist plot of the frequency weighted $\mathcal{H}_2$ design, $\mathcal{N}_{sr}(j\omega)$, near the critical point. The shaded region indicates the possible locations of the actual plant, $\tilde{\mathcal{N}}_{sr}(j\omega)$, based on the mismodeled dynamics description of (5.56) at $\omega = 87\ rad/sec$.

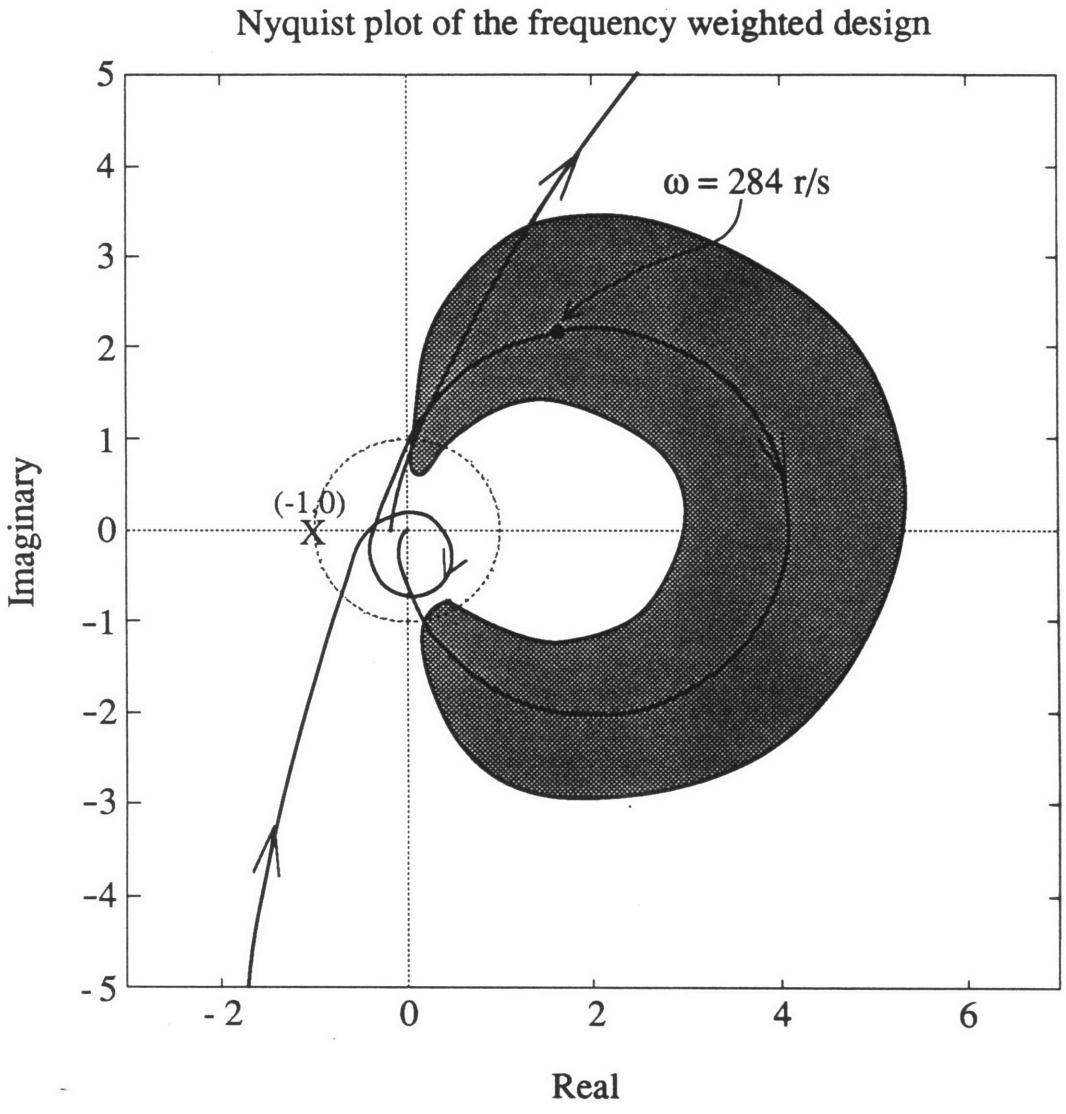

Figure 5.16: Blow up of the Nyquist plot of the frequency weighted $\mathcal{H}_2$ design, $\mathcal{N}_{sr}(j\omega)$, near the critical point. The shaded region indicates the possible locations of the actual plant, $\tilde{\mathcal{N}}_{sr}(j\omega)$, based on the mismodeled dynamics description of (5.56) at $\omega = 284\, rad/sec$.

controller synthesis to ensure that the controller would be robust to the mismodeled dynamics in the design model, Figures 5.13–5.16 clearly shows that the frequency weighted $\mathcal{H}_2$ controller should not destabilize the truss system for the level of uncertainty in the beam model. However, based on this analysis, it would be incorrect to say that the $\mathcal{H}_2$ controller was truly robust to the mismodeled dynamics in the beam model. This is the case since the region of mismodeled dynamics was only evaluated at a small set of frequencies and the uncertainties in the residues were not at all considered in the mismodeled dynamics model used to evaluate the regions of uncertainty. None the less, the results of creating the mismodeled dynamics regions for the frequency and damping errors are promising. They show that it is possible to design a multivariable controller that provides a decent level of performance over the range of mismodeled dynamics and at the same time is robust to typical levels of mismodeled dynamics.

For the frequency weighted $\mathcal{H}_2$ design and the mismodeled dynamics uncertainty model of the beam, there are really no ramifications of not having a useful and simple way to synthesize controllers that are robust to the the mismodeled dynamics in a model. The evidence of Figures 5.13–5.16, which shows that the critical point will most likely not lie in the region of mismodeled dynamics, supports this claim, but only to the extent that it applies to the specific compensator and model at hand. In general, this after the fact analysis method could be applied to any structural control design. However if the critical point were in the region of mismodeled dynamics for a given compensator and level of uncertainty, there is really no simple way to to know how to adjust the synthesis to arrive at a robust controller that still delivers a useful level of performance. Realize that this was not at all the case for the method of dealing with the unstructured errors in the model. If a controller did not satisfy (5.42), it was a simple manner to choose a different set of weights, which directly influenced both the performance and robustness of the controller, to arrive at a design that met the robustness conditions while providing a decent level of performance. Thus in general while it is possible to analyze a compensator for its robustness to mismodeled dynamics, it is not at all obvious how to influence the synthesis to arrive

at a compensator that is robust to the mismodeled dynamics.

Figures 5.13–5.16 also solidifies the conclusions drawn from the visualization of the mismodeled dynamics region of the scalar system, (4.32), presented in Section 4.2.1 regarding why it is difficult to deal with the mismodeled dynamics. Specifically, Figures 5.13–5.16 shows that in the multivariable case the region of mismodeled dynamics is also a quite complex shape at each frequency that is not easily described by a simple region like the unstructured error disk. Further, it is even more complicated to test whether or not the mismodeled dynamics region contains the critical point in the multivariable case due the presence of the determinant in the Nyquist function. Basically, Figures 5.13–5.16 reinforce the conclusion that it is difficult to guarantee robustness for mismodeled dynamics due to the highly structured nature of the errors that lead to complicated regions of uncertainty in the Nyquist domain whose distance from the critical point is quite difficult to calculate.

The conservatism of using an unstructured error description for the mismodeled dynamics is also seen in Figures 5.14–5.16. Each one of these figures is analogous to Figure 4.6 that compared a region of mismodeled dynamics to a disk of uncertainty associated with a multiplicative error for the scalar system of (4.32). In Figure 4.6 the error disk contained the critical point and provided evidence that unstructured error descriptions are conservative for describing mismodeled dynamics in scalar systems. Analogously, the violation of the stability robustness condition at the frequencies of (5.59), shown in Figure 5.10, and the fact that the actual regions of uncertainty shown in Figures 5.14–5.16 do not contain the critical point is proof in the multivariable case that representing mismodeled dynamics as unstructured errors introduces conservatism into the stability robustness analysis of a control system. This is not to say that the mismodeled dynamics in the beam model are trivial. As seen in Figures 5.13–5.16, the size of the mismodeled dynamics regions are quite large. However since the errors do not point in the unfavorable direction of the critical point, the mismodeled perturbations are not as drastic as the exact multiplicative error between the beam and truss predicts. In essence, these figures exemplify the need for less conservative and useful techniques to handle the more structured uncertainties

in models of lightly damped systems.

In conclusion, the frequency weighted $\mathcal{H}_2$ design for the sample problem has illustrated a major theme of this work. That is, given a detailed assessment of the uncertainty in a model it is possible to use this information to arrive at uncertainty models that are useful in guaranteeing the stability robustness of a controller designed from an uncertain model. This is seen for the unmodeled dynamics by the closed loop gain of the frequency weighted $\mathcal{H}_2$ controller, $\overline{\sigma}C_{sr}(j\omega)$, that satisfies the condition of (5.42) needed to guarantee stability robustness to the unmodeled dynamics in the beam model. Further, the mismodeled dynamics regions, shown in Figures 5.13–5.16, indicate that the $\mathcal{H}_2$ controller will most likely not destabilize the truss since the critical point is not near any of the regions. In terms of the actual synthesis procedure, it is clear that the $\mathcal{H}_2$ methodology can be used to arrive at compensators that deliver useful performance and are guaranteed to be robust to the unmodeled dynamics in the design model. However, there was no simple way in the $\mathcal{H}_2$ framework to specify conditions that lead to controllers which are robust to the mismodeled dynamics. Since the sample problem framework strongly mimics a broad class of structural control problems, the results of the frequency weighted $\mathcal{H}_2$ controller show that it should be possible to design controllers that are capable of achieving a useful improvement in the open loop performance, are robust to the high frequency unmodeled dynamics, and are most likely, but not guaranteed, robust to the mismodeled dynamics in the design model.

Chapter 6

Conclusions and Suggestions for Future Work

6.1 Conclusions

The primary focus of this thesis has been to understand how to deal with the realistic types of modeling errors that will be present in models of complex structural systems like the Interferometer testbed in order to design robust, high authority, multivariable controllers. By pursuing a holistic approach in a simple sample problem framework, many of the crucial issues involved in designing such controllers were flushed out and investigated.

In the process of modeling the sample problem, a model reduction scheme was used that lead to a feed–forward D term in the outputs of the model to account for the truncated dynamics and mimic the fact that the actual system did not roll off beyond the frequency of the last mode kept in the reduced model. Even though the presence of such a term is not standard and often neglected in optimal controller synthesis, the development of the frequency weighted $\mathcal{H}_2$ controllers showed that the D term simply adds a few extra terms to the standard equations needed to find the optimal controller and poses no problem in meeting the roll off specification employed by the unmodeled dynamics robustness criterion.

As far as the assessment of the uncertainty is concerned, the exact framework of

the sample problem provided a simple way to check the realistic ways of assessing the fidelity of a structural model. In doing so, a fundamental understanding of how typical structural modeling errors manifest themselves in the common analysis tools of controller synthesis was obtained. Basically, all of the modeling uncertainty was broken up into two categories, mismodeled and unmodeled dynamics, that could be dealt with by respectively considering structured and unstructured robustness methods.

Acknowledging that there were nominally two classes of modeling errors that needed to be dealt with to design robustly stable controllers, a Nyquist domain visualization of stability robustness was used to investigate to what extent it was possible to guarantee robustness in the presence of unmodeled and mismodeled dynamics. It was concluded that the well known relative error stability robustness conditions are appropriate for dealing with the high frequency unmodeled dynamics since they consider the uncertainty to be a represented by a disk. Further, the simplicity of using a disk to describe the uncertainty allows for a simple and useful way of checking a given control system's robustness to the unmodeled dynamics. On the other hand, it was shown why there is no similarly appropriate and useful method for analyzing a control system's robustness to the highly structured mismodeled dynamics. This was done by creating the analogous uncertainty region to the disk for the mismodeled dynamics and showing that it is a complex shape whose distance to the critical point can not be easily computed.

To confirm the extent to which it is possible to design robustly stable controllers based on an uncertain model, frequency weighted $\mathcal{H}_2$ compensators were developed based on the uncertain beam model and applied to the actual truss model. These designs showed that it is necessary and possible to use frequency dependent weights to achieve a decent level of performance while satisfying the unmodeled dynamics stability robustness constraint. Further, by creating specific regions of mismodeled dynamics about the nominal Nyquist contour for an $\mathcal{H}_2$ design that met the unmodeled dynamics robustness constraint and achieved a decent level of performance, it was shown that slight errors in the model of a lightly damped multivariable system

may not be that drastic in terms of stability. This conclusion was based on the fact that for the sample problem the mismodeled dynamics uncertain regions point in favorable directions and do not encompass the critical point.

The bottom line here is that our approach within the mathematically exact sample problem framework was very useful in understanding the crucial issues involved in designing robust, high authority, multivariable controllers for complex structural systems like the Interferometer testbed. However, in the course of the investigation not all of the issues that surfaced could be sufficiently addressed. In the following section, some of the more important issues that still need to be investigated will be briefly mentioned.

6.2 Future Work

As was discussed in Chapter 5 no matter how well the uncertainty in a model is understood, it is only feasible to expect a useful performance improvement where the system is well modeled. Throughout the work, the accuracy of the initial beam finite element model was assumed to be the best possible model of the truss available. Even after all of the uncertainty was analyzed and dealt with, the $\mathcal{H}_2$ controllers could only improve the performance over the low frequency range of well modeled dynamics. Hence, the ability to obtain models of structural systems that are accurate over a large frequency range needs to be further researched. With a model of a system that is accurate over a larger frequency range and the stability robustness insights arrived at here, a greater improvement in performance can be achieved without sacrificing the robustness of the control system.

Unfortunately, as the bandwidth of accurately modeled dynamics in a structural system increases, the order of the model increases. Further since it is necessary to use frequency weights to achieve a decent level of performance while meeting the unstructured error robustness bound, the order of controllers based on a more accurate and thus higher order model will become quite large. For these reasons, model reduction and compensator implementation are two topics that will need further research if

high authority, robustly stable controllers are to be implemented on actual structural systems.

It goes without saying that the search for simple and useful stability robustness results for the highly structured mismodeled dynamics should continue. Even though the $\mathcal{H}_2$ frequency weighted design showed that the closed loop system was not that sensitive to slight mismodeled dynamics, the results did not provide any guarantees. In order to make multivariable, high authority control a viable method of improving or enabling performance in flexible spacecraft, stability guarantees for all classes of modeling errors must be available.

In the course of assessing the uncertainty, an interesting question arose that was not resolved. Does classifying the modeling errors as either structured or unstructured introduce conservatism into the design process? In actuality, their is most likely a transition region for the modeling errors from the highly structured mismodeled dynamics to the completely unstructured unmodeled dynamics. Whether or not it is worth it to consider how to model and deal with this transition region needs to be explored.

Finally, the results of this work are based on a mathematically contrived, two dimensional sample problem. As a result, it is necessary to verify if the methodology that lead to the robust, high authority, multivariable controllers for the sample problem can be successfully applied to a realistic system like the Interferometer. That is, the methodology and results presented in this thesis need to be experimentally verified if they are to hold water.

Appendix A

Sample Problem Data

This appendix contains the values of the state space matrices for the beam and truss models developed in Chapter 2. Using b subscripts to denote a model of the beam, recall from (2.52) that

$$\begin{aligned} \dot{x}(t) &= A_b x(t) + B_{2_b} u(t) + B_{1_b} d(t) \\ y(t) &= C_b x(t) + D_{2_b} u(t) \end{aligned} \tag{A.1}$$

is the state space representation of the beam that captures the input, output, and disturbance attributes of the truss, has scaled outputs, and contains 18 states with a static correction in the control loop. The specific values of the state space matrices, in which the missing elements represent zeros, are as follows.

$$A_b = \begin{bmatrix} 0^{9\times 9} & I^{9\times 9} \\ \Lambda_b & \Gamma_b \end{bmatrix} \tag{A.2}$$

$$\Lambda_b = \begin{bmatrix} -2.128 \times 10^3 & & & & & & & & \\ & -8.274 \times 10^4 & & & & & & & \\ & & -6.398 \times 10^5 & & & & & & \\ & & & -1.178 \times 10^6 & & & & & \\ & & & & -2.412 \times 10^6 & & & & \\ & & & & & -6.453 \times 10^6 & & & \\ & & & & & & -1.068 \times 10^7 & & \\ & & & & & & & -1.405 \times 10^7 & \\ & & & & & & & & -2.664 \times 10^7 \end{bmatrix} \tag{A.3}$$

$$\Gamma_b = \begin{bmatrix} -0.923 & & & & & & & \\ & -5.753 & & & & & & \\ & & -15.997 & & & & & \\ & & & -21.702 & & & & \\ & & & & -31.064 & & & \\ & & & & & -50.806 & & \\ & & & & & & -65.358 & \\ & & & & & & & -74.971 \\ & & & & & & & & -103.233 \end{bmatrix} \tag{A.4}$$

$$B_{1_b} = \begin{bmatrix} 0^{9\times1} & 0^{9\times1} \\ 0.0373 & 0.173 \\ -0.163 & -0.429 \\ 0.291 & -0.0316 \\ -0.215 & 0.0 \\ 0.290 & -1.273 \\ -0.135 & 1.987 \\ -0.572 & 0.0 \\ 0.115 & 0.997 \\ 0.345 & -1.337 \end{bmatrix} \qquad B_{2_b} = \begin{bmatrix} 0^{9\times1} & 0^{9\times1} \\ -2.644 \times 10^{-3} & 2.644 \times 10^{-3} \\ -0.0403 & 0.0403 \\ -0.0377 & 0.0377 \\ 0.0764 & 0.0764 \\ -0.184 & 0.184 \\ -0.173 & 0.173 \\ -0.292 & -0.292 \\ -0.352 & 0.352 \\ 0.423 & -0.423 \end{bmatrix} \tag{A.5}$$

$$C_b = \begin{bmatrix} C_{\alpha_b} & 0^{1\times9} \\ C_{\beta_b} & 0^{1\times9} \end{bmatrix} \tag{A.6}$$

$$C_{\alpha_b}^T = \begin{bmatrix} -2.962 \times 10^5 \\ -2.808 \times 10^5 \\ -2.653 \times 10^5 \\ 3.741 \times 10^{-4} \\ 2.476 \times 10^5 \\ 2.286 \times 10^5 \\ 3.096 \times 10^{-4} \\ -2.083 \times 10^5 \\ 1.865 \times 10^5 \end{bmatrix} \qquad C_{\beta_b}^T = \begin{bmatrix} 1.844 \times 10^5 \\ -6.391 \times 10^5 \\ -1.046 \times 10^6 \\ 3.845 \times 10^6 \\ 1.456 \times 10^6 \\ 1.850 \times 10^6 \\ -3.884 \times 10^6 \\ -2.216 \times 10^6 \\ 2.535 \times 10^6 \end{bmatrix} \tag{A.7}$$

$$D_{2_b} = \begin{bmatrix} -2.169 \times 10^{-3} & 2.169 \times 10^{-3} \\ -9.391 \times 10^{-2} & -2.211 \times 10^{-2} \end{bmatrix} \tag{A.8}$$

A similar state space model for the truss was also developed and represented by

$$\dot{x}(t) = A_t x(t) + B_{2_t} u(t) + B_{1_t} d(t) \tag{A.9}$$

$$y(t) = C_t x(t) + D_{2_t} u(t)$$

in which the t subscript is used to differentiate the truss model from the beam model in (A.1). The outputs of the truss are scaled, the model contains 60 states, and the following are the values of the state space matrices in (A.9).

$$A_t = \begin{bmatrix} 0^{30\text{x}30} & I^{30\text{x}30} \\ \Lambda_t & \Gamma_t \end{bmatrix} \tag{A.10}$$

Here $\Lambda_t = \text{diag}\{\lambda_t\}$ and $\Gamma_t = \text{diag}\{\gamma_t\}$ in which λ_t and γ_t are vectors whose i^{th} element is the $(i,i)^{th}$ element of Λ_t and Γ_t respectively.

$$C_t = \begin{bmatrix} C_{\alpha_t} & 0^{1\text{x}30} \\ C_{\beta_t} & 0^{1\text{x}30} \end{bmatrix} \tag{A.11}$$

$$D_{2_t} = \begin{bmatrix} -5.930 \times 10^{-4} & 5.323 \times 10^{-4} \\ -6.836 \times 10^{-2} & -5.202 \times 10^{-2} \end{bmatrix} \tag{A.12}$$

$$\lambda_t = \begin{bmatrix} -2.218 \times 10^{3} \\ -7.994 \times 10^{4} \\ -5.386 \times 10^{5} \\ -8.232 \times 10^{5} \\ -9.037 \times 10^{5} \\ -9.448 \times 10^{5} \\ -1.054 \times 10^{6} \\ -1.176 \times 10^{6} \\ -1.201 \times 10^{6} \\ -1.230 \times 10^{6} \\ -1.262 \times 10^{6} \\ -1.265 \times 10^{6} \\ -1.298 \times 10^{6} \\ -1.334 \times 10^{6} \\ -1.366 \times 10^{6} \\ -1.389 \times 10^{6} \\ -1.430 \times 10^{6} \\ -1.545 \times 10^{6} \\ -1.625 \times 10^{6} \\ -1.682 \times 10^{6} \\ -2.923 \times 10^{6} \\ -3.348 \times 10^{6} \\ -5.088 \times 10^{6} \\ -5.956 \times 10^{6} \\ -6.630 \times 10^{6} \\ -7.793 \times 10^{6} \\ -1.004 \times 10^{7} \\ -1.172 \times 10^{7} \\ -1.563 \times 10^{7} \\ -2.199 \times 10^{7} \end{bmatrix} \qquad \gamma_t = \begin{bmatrix} -0.942 \\ -5.655 \\ -14.678 \\ -18.146 \\ -19.013 \\ -19.440 \\ -20.533 \\ -21.690 \\ -21.916 \\ -22.180 \\ -22.469 \\ -22.494 \\ -22.783 \\ -23.097 \\ -23.373 \\ -23.575 \\ -23.914 \\ -24.856 \\ -25.497 \\ -25.937 \\ -34.193 \\ -36.593 \\ -45.113 \\ -48.808 \\ -51.497 \\ -55.832 \\ -63.372 \\ -68.474 \\ -79.068 \\ -93.783 \end{bmatrix} \tag{A.13}$$

$$C_{\alpha_t}^T = \begin{bmatrix} 3.030 \times 10^5 \\ 2.756 \times 10^5 \\ 2.275 \times 10^5 \\ -2.426 \times 10^4 \\ 3.610 \times 10^4 \\ 2.933 \times 10^2 \\ 4.311 \times 10^4 \\ 1.866 \times 10^2 \\ -2.327 \times 10^2 \\ -2.856 \times 10^2 \\ -3.285 \times 10^2 \\ -7.381 \times 10^3 \\ 3.580 \times 10^2 \\ -3.688 \times 10^2 \\ 3.448 \times 10^2 \\ 2.423 \times 10^2 \\ 1.284 \times 10^3 \\ -8.042 \times 10^4 \\ 5.807 \times 10^2 \\ 1.095 \times 10^5 \\ 3.623 \times 10^5 \\ -1.622 \times 10^5 \\ -1.424 \times 10^4 \\ -1.757 \times 10^5 \\ -4.280 \times 10^4 \\ -1.070 \times 10^5 \\ 1.849 \times 10^5 \\ -8.276 \times 10^2 \\ 1.452 \times 10^5 \\ 1.075 \times 10^5 \end{bmatrix} \qquad C_{\beta_t}^T = \begin{bmatrix} 1.873 \times 10^5 \\ 6.223 \times 10^5 \\ 8.959 \times 10^5 \\ -4.679 \times 10^4 \\ 4.289 \times 10^4 \\ 2.438 \times 10^5 \\ 2.776 \times 10^4 \\ 1.657 \times 10^5 \\ -1.304 \times 10^5 \\ -1.314 \times 10^5 \\ -1.363 \times 10^5 \\ 1.755 \times 10^5 \\ 1.443 \times 10^5 \\ -1.497 \times 10^5 \\ 1.464 \times 10^5 \\ 1.077 \times 10^5 \\ 6.457 \times 10^5 \\ -5.445 \times 10^5 \\ -3.237 \times 10^6 \\ 4.239 \times 10^5 \\ 1.524 \times 10^6 \\ -6.174 \times 10^5 \\ -7.358 \times 10^5 \\ -1.219 \times 10^6 \\ 2.130 \times 10^5 \\ -3.280 \times 10^5 \\ 1.670 \times 10^6 \\ -4.131 \times 10^6 \\ 1.658 \times 10^6 \\ 1.484 \times 10^6 \end{bmatrix} \tag{A.14}$$

$$B_{1_t} = \begin{bmatrix} 0^{30\times1} & 0^{30\times1} \\ -3.859 \times 10^{-2} & -1.754 \times 10^{-1} \\ 1.675 \times 10^{-1} & 3.875 \times 10^{-1} \\ -2.793 \times 10^{-1} & 9.970 \times 10^{-2} \\ 2.171 \times 10^{-2} & -3.136 \times 10^{-2} \\ -3.082 \times 10^{-2} & 5.159 \times 10^{-2} \\ -1.385 \times 10^{-1} & 0 \\ -5.021 \times 10^{-2} & 9.962 \times 10^{-2} \\ 1.555 \times 10^{-2} & 0 \\ 8.063 \times 10^{-3} & 0 \\ 1.802 \times 10^{-3} & 0 \\ 4.976 \times 10^{-3} & 0 \\ 8.442 \times 10^{-2} & -2.897 \times 10^{-1} \\ -6.418 \times 10^{-3} & 0 \\ 5.899 \times 10^{-3} & 0 \\ -7.233 \times 10^{-3} & 0 \\ -4.890 \times 10^{-3} & 0 \\ -3.208 \times 10^{-2} & 0 \\ -1.544 \times 10^{-1} & 5.011 \times 10^{-1} \\ 1.844 \times 10^{-1} & 0 \\ 1.284 \times 10^{-1} & -6.871 \times 10^{-1} \\ 1.199 \times 10^{-1} & -5.431 \times 10^{-1} \\ 1.458 \times 10^{-1} & -6.678 \times 10^{-1} \\ -3.474 \times 10^{-2} & 3.364 \times 10^{-2} \\ 6.297 \times 10^{-2} & -1.241 \\ -1.016 \times 10^{-1} & 4.454 \times 10^{-1} \\ 3.570 \times 10^{-2} & -2.238 \times 10^{-1} \\ -1.276 \times 10^{-1} & -2.465 \times 10^{-1} \\ -6.143 \times 10^{-1} & 0 \\ 3.025 \times 10^{-1} & -1.093 \\ -3.526 \times 10^{-1} & 1.263 \end{bmatrix}$$

$$B_{2_t} = \begin{bmatrix} 0^{30\times1} & 0^{30\times1} \\ 2.697 \times 10^{-3} & -2.697 \times 10^{-3} \\ 3.802 \times 10^{-2} & -3.802 \times 10^{-2} \\ 3.325 \times 10^{-2} & -3.325 \times 10^{-2} \\ -8.189 \times 10^{-3} & 8.189 \times 10^{-3} \\ 1.227 \times 10^{-2} & -1.227 \times 10^{-2} \\ 4.869 \times 10^{-2} & 4.869 \times 10^{-2} \\ 1.237 \times 10^{-2} & -1.237 \times 10^{-2} \\ 1.099 \times 10^{-2} & 1.099 \times 10^{-2} \\ -2.044 \times 10^{-3} & -2.044 \times 10^{-3} \\ 1.189 \times 10^{-3} & 1.189 \times 10^{-3} \\ -1.723 \times 10^{-3} & -1.723 \times 10^{-3} \\ -3.829 \times 10^{-2} & 3.829 \times 10^{-2} \\ 4.325 \times 10^{-3} & 4.325 \times 10^{-3} \\ -3.697 \times 10^{-3} & -3.697 \times 10^{-3} \\ 2.252 \times 10^{-3} & 2.252 \times 10^{-3} \\ 1.425 \times 10^{-3} & 1.425 \times 10^{-3} \\ 1.281 \times 10^{-2} & 1.281 \times 10^{-2} \\ 9.837 \times 10^{-2} & -9.837 \times 10^{-2} \\ -6.472 \times 10^{-2} & -6.472 \times 10^{-2} \\ -2.510 \times 10^{-2} & 2.510 \times 10^{-2} \\ -6.987 \times 10^{-2} & 6.987 \times 10^{-2} \\ 8.336 \times 10^{-3} & -8.336 \times 10^{-3} \\ 1.042 \times 10^{-1} & -1.042 \times 10^{-1} \\ 1.100 \times 10^{-1} & -1.100 \times 10^{-1} \\ 2.004 \times 10^{-2} & -2.004 \times 10^{-2} \\ 4.020 \times 10^{-2} & -4.020 \times 10^{-2} \\ 1.942 \times 10^{-1} & -1.942 \times 10^{-1} \\ -3.066 \times 10^{-1} & -3.065 \times 10^{-1} \\ 2.530 \times 10^{-1} & -2.531 \times 10^{-1} \\ -1.287 \times 10^{-1} & 1.287 \times 10^{-1} \end{bmatrix} \quad \text{(A.15)}$$

Appendix B

A Matlab Function to Evaluate Singular Value Phase Information

This is the Matlab function that was used to evaluate the multivariable phase information described in Section 3.3.1 and used in Section 3.3.2 to assess the fidelity of the beam model. The following table describes the connection between the notation used in Chapter 3 to develop the singular value phase information and the variables used in the function.

Table B.1: Legend between the notation of the singular value phase information developed in Chapter 3 and the variables used in the function to evaluate the phase information.

Notation from Chapter 3	Equation #	Variable name in function
$\lvert\nu_{ij}\rvert$	(3.17)	mag_u
γ_{ij}	(3.17)	phase_u
$\sigma_j\lvert\mu_{ij}\rvert$	(3.18)	mag_y
ψ_{ij}	(3.18)	phase_y

```
function [mag_u,phase_u,mag_y,phase_y]=mimo_phase(A,B,C,D,w,j)
%
%  function      [mag_u,phase_u,mag_y,phase_y]=mimo_phase(A,B,C,D,w,j)
%
%  Purpose:      For a multivariable system y(s)=G(s)u(s) with
```

```
%               transfer function matrix G(s)=C*inv(sI-A)*B+D,
%               mimo_phase evaluates the specific, sinusoidal inputs
%               and associated sinusoidal outputs that provide a
%               measure of phase for multivariable systems.  The
%               specific values of the magnitude and phase of the
%               inputs and outputs are provided by a singular value
%               decomposition of G(jw) for the frequencies specified
%               in w.
%
% Notation:     A,B,C,D   -  State space description of the system.
%
%                    w    -  Frequency vector used to evaluate the
%                            quantities.
%
%                    j    -  Integer denoting the number of the right
%                            singular vector of G to use in defining
%                            the inputs that provide the multivariable
%                            phase.
%
%                 mag_u   -  Matrix containing the magnitudes of the
%                            j'th right singular vector of G.  Each
%                            row of mag_u corresponds to the magnitude
%                            of a particular input at the frequencies
%                            specified  in w.
%
%               phase_u   -  Matrix containing the phases of the
%                            j'th right singular vector of G.  Each
%                            row of phase_u corresponds to the phase
%                            of a particular input at the frequencies
%                            specified in w.
%
%                 mag_y   -  Matrix containing the magnitudes of the
%                            outputs associated with an input along
%                            the direction of the j'th right singular
%                            vector of G.  Each row of mag_y
%                            corresponds to the magnitude of a
%                            particular output at the frequencies
%                            specified in w.
%
%               phase_y   -  Matrix containing the phases of the
%                            outputs associated with an input along
%                            the direction of the j'th right singular
%                            vector of G.  Each row of phase_y
%                            corresponds to the phase of a particular
%                            output at the frequencies specified in w.
```

```
%
% Author:       Leonard Lublin
% Date:         January 8, 1992
%-------------------------------------------------------------------


%  Find sizes of Variables, initialize variables
%  ---------------------------------------------

  npts = length(w);
 [l,n] = size(C);
 [m,n] = size(B);
     k = min([l m]);

 if j > k
    disp(' ');
    disp('   Sorry, the singular value associated with the right');
    disp('   singular vector chosen is zero.');
    disp('   ');
   error('   Try another input direction');
 end

      ji = sqrt(-1);
      In = eye(A);
   mag_u = [];
 phase_u = [];
   mag_y = [];
 phase_y = [];


%  Evaluate Singular value decomposition
%  -------------------------------------


  for i=1:npts,

           G = C*inv(ji*w(i)*In-A)*B+D;
     [U,S,V] = svd(G);

     % Extracting data associated with the j'th right singular vector
     % --------------------------------------------------------------

             sj = S(j,j);       % j'th singular value
```

```
            vj = V(:,j);        % j'th right singular vector
            uj = U(:,j);        % j'th left singular vector


    % Fixing the phase of vj(1,1) to be the phase of vj(1,1) at the
    % first frequency in w.
    % ------------------------------------------------------------

            if i == 1
                  v_fix = angle(vj(1,1));
            end

    if angle(vj(1,1)) ~= v_fix
                  theta = v_fix-angle(vj(1,1));
                     vj = vj*exp(ji*theta);
                     uj = uj*exp(-ji*theta);
            end

    % Storing data at the current frequency in the appropriate
    % matrices
    % ------------------------------------------------------

             mag_u(:,i) = abs(vj);
           phase_u(:,i) = angle(vj);

             mag_y(:,i) = sj*abs(uj);
           phase_y(:,i) = angle(uj);

  end


%  Unwrapping the phases and converting to degrees
%  -----------------------------------------------

for i = 1:l
      phase_u(i,:) = unwrap(phase_u(i,:),3.14)*180/pi;
      phase_y(i,:) = unwrap(phase_y(i,:),3.14)*180/pi;
end
```

Appendix C

Specific $\mathcal{H}_2$ Design Models for the Sample Problem

In this section, the specific values of the state space matrices for the general feedback description shown in Figure C.1 with the state space representation

$$\left(\begin{array}{c} \dot{x}_p \\ \hline e \\ y \end{array}\right) = \left[\begin{array}{c|cc} A_P & B_{P_1} & B_{P_2} \\ \hline C_{P_1} & D_{P_{11}} & D_{P_{12}} \\ C_{P_2} & D_{P_{21}} & D_{P_{22}} \end{array}\right] \left(\begin{array}{c} x_p \\ \hline w \\ u \end{array}\right) \tag{C.1}$$

in which

$$w = \begin{pmatrix} d \\ \theta \end{pmatrix} \qquad \text{and} \qquad e = \begin{pmatrix} e_1 \\ e_2 \end{pmatrix} \tag{C.2}$$

that were used to synthesize the $\mathcal{H}_2$ controllers for the sample problem will be presented. In doing so, Figure C.2, which is copy of Figure 5.3 with some additional

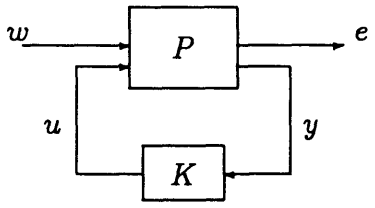

Figure C.1: The general feedback system description.

names given to a few of the signals, will be exploited to figure out the proper signal interconnection structure needed to form the state space description of (C.1). Realize

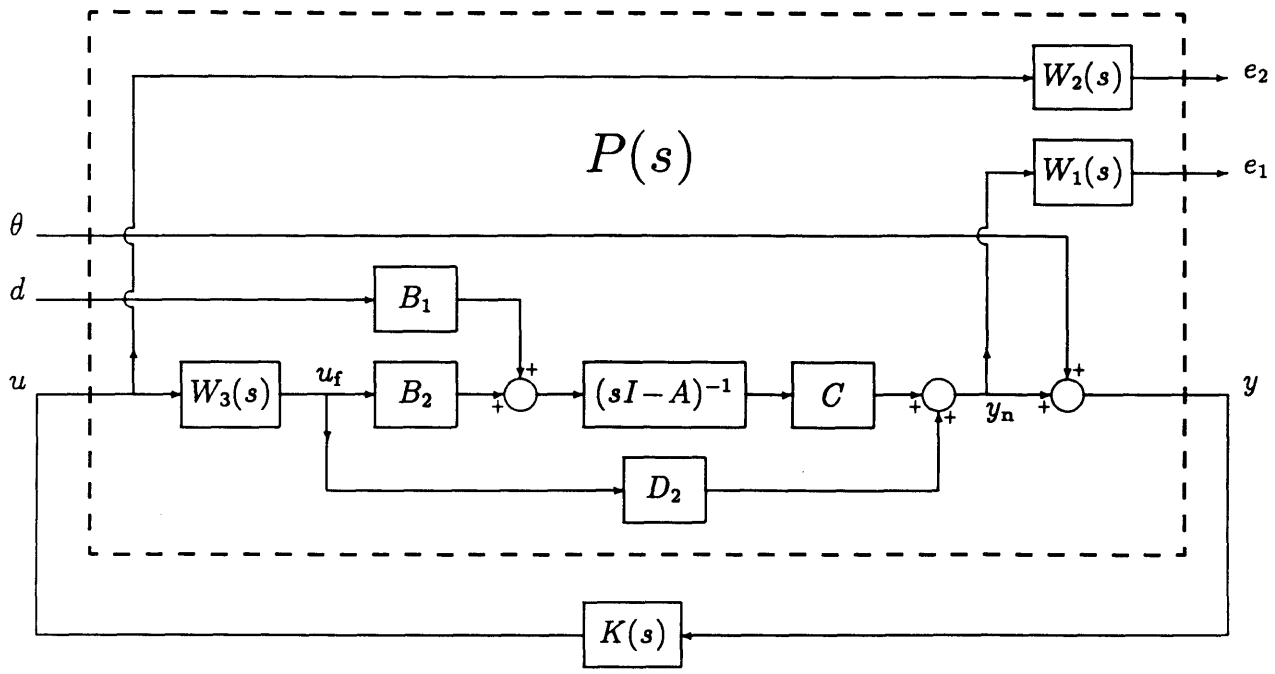

Figure C.2: Block diagram of the beam model with frequency weights.

that with the definition of the signals in Figure C.1, the dynamics of the beam model derived in Chapter 2, from (5.1,5.2), are now represented by

$$\dot{x}(t) = Ax(t) + B_2 u_f(t) + B_1 d(t) \tag{C.3}$$

$$y(t) = Cx(t) + D_2 u_f(t) + \theta(t). \tag{C.4}$$

Given these dynamics, once the dynamics of the weights are expressed in terms of the inputs and outputs in (C.1), it is simply a matter of state augmentation to evaluate the values of the matrices in (C.1).

C.1 Standard LQG Design

Recall from Section 5.4.1 that the standard LQG design uses

$$W_1(s) = W_3(s) = I \qquad \text{and} \qquad W_2(s) = \rho^{\frac{1}{2}} \cdot I, \tag{C.5}$$

as the values of the weights to synthesize the controllers. With these values of the weights

$$u_f(t) = u(t), \tag{C.6}$$

$$e_1(t) = y_n(t) = Cx(t) + D_2u(t), \tag{C.7}$$

$$e_2(t) = \rho^{\frac{1}{2}} \cdot Iu(t), \tag{C.8}$$

and all the signals are now in terms of the inputs and outputs of (C.1). No state augmentation is needed here since no extra dynamics are added to the system, and thus $x_p(t) = x(t)$. From (C.3,C.4,C.6,C.7,C.8) the state space description of (C.1) in terms of the known quantities can be directly written down.

$$A_P = A \qquad B_{P_1} = \begin{bmatrix} B_1 & 0 \end{bmatrix} \qquad B_{P_2} = B_2 \qquad C_{P_2} = C \tag{C.9}$$

$$C_{P_1} = \begin{bmatrix} C \\ 0 \end{bmatrix} \qquad D_{P_{12}} = \begin{bmatrix} D_2 \\ \rho^{\frac{1}{2}} \cdot I \end{bmatrix} \qquad D_{P_{21}} = \begin{bmatrix} 0 & I \end{bmatrix} \qquad D_{P_{11}} = 0 \qquad D_{P_{22}} = D_2 \tag{C.10}$$

C.2 Frequency Weighted $\mathcal{H}_2$ Design

In the frequency weighted $\mathcal{H}_2$ design, all three weights were used to synthesize the controller. While a transfer function representation of the weights was used in Section 5.4.2, state space representations of the weights are needed to form the general state space system of (C.1). From Figure C.2 it is obvious what the inputs and outputs of the state space representations of each weight, $W_i(s)$, should be. Exploiting this knowledge, the state space representation of $W_1(s)$, the transfer function matrix between $e_1(s)$ and $y_n(s)$, will be written as

$$\dot{x}_{w_1}(t) = A_{W_1}x_{w_1}(t) + B_{W_1}y_n(t) \tag{C.11}$$

$$e_1(t) = C_{W_1}x_{w_1}(t). \tag{C.12}$$

Similarly, the state space representation of $W_2(s)$, the transfer function matrix between $e_2(s)$ and $u(s)$, will be written as

$$\dot{x}_{w_2}(t) = A_{W_2}x_{w_2}(t) + B_{W_2}u(t) \tag{C.13}$$

$$e_2(t) = C_{W_2}x_{w_2}(t) + D_{W_2}u(t), \tag{C.14}$$

and the state space representation of $W_3(s)$, the transfer function matrix between $u_f(s)$ and $u(s)$, will be written as

$$\dot{x}_{w_3}(t) = A_{W_3}x_{w_3}(t) + B_{W_3}u(t) \tag{C.15}$$

$$u_f(t) = C_{W_3}x_{w_3}(t). \tag{C.16}$$

The presence of the D_{W_2} term in the dynamics of $W_2(s)$ is necessary given that a proper weight, (5.50), was used in the controller synthesis of the frequency weighted $\mathcal{H}_2$ design.

To arrive at the correct signal interconnection structure, the noiseless output, which is now given by

$$y_n(t) = Cx(t) + D_2u_f(t), \tag{C.17}$$

was substituted into (C.11), and the filtered control signal, $u_f(t)$ from (C.16) was substituted into (C.3), (C.4), and (C.17). In doing this, the derivative of the augmented state,

$$x_p(t) = \begin{pmatrix} x(t) \\ x_{w_1}(t) \\ x_{w_2}(t) \\ x_{w_3}(t) \end{pmatrix}, \tag{C.18}$$

will be expressed solely in terms of the the state, $x_p(t)$, and the inputs of the general system (C.1). Further realize that with the above substitutions, the outputs of (C.1) from (C.4), (C.12), and (C.14) are also expressed solely in terms of the state, $x_p(t)$, and the inputs of the general system (C.1). As a result, after performing the mentioned substitutions, it is a simple manner to simply collect all of the above dynamics and outputs to arrive at the values of the state space matrices in (C.1).

$$A_P = \begin{bmatrix} A & 0 & 0 & B_2C_{W_3} \\ B_{W_1}C & A_{W_1} & 0 & B_{W_1}D_2C_{W_3} \\ 0 & 0 & A_{W_2} & 0 \\ 0 & 0 & 0 & A_{W_3} \end{bmatrix} \tag{C.19}$$

$$B_{P_1} = \begin{bmatrix} B_1 & 0 \\ 0 & 0 \\ 0 & 0 \\ 0 & 0 \end{bmatrix} \qquad B_{P_2} = \begin{bmatrix} 0 \\ 0 \\ B_{W_2} \\ B_{W_3} \end{bmatrix} \qquad D_{P_{11}} = \begin{bmatrix} 0 & 0 \\ 0 & 0 \end{bmatrix} \quad D_{P_{12}} = \begin{bmatrix} 0 \\ D_{W_2} \end{bmatrix}$$

$$D_{P_{21}} = \begin{bmatrix} 0 & I \end{bmatrix} \quad D_{P_{22}} = 0 \tag{C.20}$$

$$C_{P_1} = \begin{bmatrix} 0 & C_{W_1} & 0 & 0 \\ 0 & 0 & C_{W_2} & 0 \end{bmatrix} \qquad C_{P_2} = \begin{bmatrix} C & 0 & 0 & D_2 C_{W_3} \end{bmatrix} \tag{C.21}$$

References

[1] Wada, B., Fanson, J., and Crawley, E., "Adaptive Structures," in *Adaptive Structures*, pp. 1–8, American Society of Mechanical Engineers, New York, NY, 1989. AD–Vol. 15.

[2] Wada, B., Fanson, J., and Chen, G., "Using Adaptive Structures to Enable Future Missions by Relaxing Ground Test Requirements," *AIAA Journal of Spacecraft and Rockets*, Vol. 28, No. 6, November-December 1991, pp. 663–669.

[3] Blackwood, G. H., Jacques, R. N., and Miller, D. W., "The MIT multipoint alignment testbed: Technology development for optical interferometry," in *Proceedings of the SPIE Conference on Active and Adaptive Optical Systems*, (San Diego, CA), July 1991.

[4] Anderson, E., Moore, D., and Fanson, J., "Development of an Active Member Using Piezoelectric and Electrostrictive Actuators for Control of Precision Structures," in *Proceedings of the* 31^{st} *AIAA/ASME/ASCE/AHS Structures, Structural Dynamics, and Materials Conference*, (Long Beach, CA), 1990.

[5] Bathe, K.-J., *Finite Element Procedures in Engineering Analysis*, Prentice-Hall, Inc., New Jersey, 1982.

[6] Meirovitch, L., *Elements of Vibration Analysis*, McGraw–Hill Book Co., New York, NY, second ed., 1986.

[7] Collins, E., Phillips, D., and Hyland, D., "Design and Implementation of Robust Decentralized Control Laws for the ACES Structure at Marshall Space Flight Center," in *Proceedings of the American Control Conference*, (San Diego, CA), May 1990, pp. 1449–1454.

[8] Fanson, J., Brigs, H., Chu, C., Lurie, B., Smith, R., Eldred, D., and Liu, D., "JPL CSI Phase-0 Experiment Results and Real Time Control Computer," in *Proceedings of the* 4^{th} *NASA/DoD Control/Structures Interaction Technology conference*, (Orlando, FL), 1990, pp. 614–628.

[9] Gilpin, K., *Identification of a Lightly Damped Structure for Control/Structure Interaction*, Master's thesis, Massachusetts Institute of Technology, Aug. 1991. SERC report #11-91.

[10] Smith, R., "Procedures for the Identification of the Precision Truss," tech. rep., Jet Propulsion Laboratory, 1990. report JPL D-7791.

[11] Ljung, L., *System Identification: Theory for the User*, Prentice–Hall, Inc., 1987.

[12] Lew, J.-S., Juang, J.-N., and Longman, R., "Comparison of Several System Identification Methods for Flexible Structures," in *Proceedings of the 32nd Structures, Structural Dynamics and Materials Conference*, (Baltimore, MD), Apr. 1991, pp. 2304–2318.

[13] Blackwood, G., Chu, C., Fanson, J., and Sirlin, S., "Uncertainty Modeling for the Control of an Active Structure," in *Proceedings of the ASME Winter Annual Meeting*, (San Francisco, CA), 1989.

[14] Skelton, R., "Model Error Concepts in Control Design," *International Journal of Control*, Vol. 49, No. 5, May 1989, pp. 1725–1753.

[15] Lehtomaki, N., *Practical Robustness Measures in Multivariable Control System Analysis*, Ph.D. thesis, Massachusetts Institute of Technology, May 1981.

[16] Lehtomaki, N., Castanon, D., Levy, B., Stein, G., Sandell, Jr., N., and Athans, M., "Robustness and Modeling Error Characterization," *IEEE Transactions on Automatic Control*, Vol. AC–29, No. 3, Mar. 1984, pp. 212–220.

[17] Doyle, J., Wall, J., and Stein, G., "Performance and Robustness Analysis for Structured Uncertainty," in *Proceedings of the* 21^{st} *IEEE Conference on Decision and Control*, (Orlando, FL), Dec. 1982, pp. 629–636.

[18] Doyle, J., "Structured Uncertainty in Control System Design," in *Proceedings of the* 24^{th} *IEEE Conference on Decision and Control*, (Ft. Lauderdale, FL), 1985, pp. 260–265.

[19] Fan, M., Tits, A., and Doyle, J., "Robustness in the Presence of Mixed Parametric Uncertainty and Unmodeled Dynamics," *IEEE Transactions on Automatic Control*, Vol. 36, No. 1, Jan. 1991, pp. 25–38.

[20] Hagood, N., *Cost Averaging Techniques for Robust Control of Parametrically Uncertain Systems*, Ph.D. thesis, Massachusetts Institute of Technology, June 1991. SERC report #9-91.

[21] Kwakernaak, R. and Sivan, R., *Linear Optimal Control Systems*, John Wiley and Sons, Inc., 1972.

[22] Doyle, J., Glover, K., Khargonekar, P., and Francis, B., "State Space Solutions to Standard $\mathcal{H}_2$ /$\mathcal{H}_\infty$ Control Problems," *IEEE Transactions on Automatic Control*, Vol. 34, No. 8, Aug. 1989, pp. 831–847.

[23] Lim, K., Maghami, P., and Joshi, S., "A Comparison of Controller Designs for an Experimental Flexible Structure," in *Proceedings of the American Control Conference*, (Boston, MA), June 1991.

[24] Fanson, J., C.C.Chu, Smith, R., and Anderson, E., "Active-Member Control of a Precision Structure with an $\mathcal{H}_\infty$ Performance Objective," in *Proceedings of the AIAA Dynamics Specialists Conference*, (Long Beach, CA), 1990.

[25] Carrier, A., Bryson, A., Aubrun, J.-N., and Lorell, K., "$\mathcal{H}_\infty$ Control Design for the ASCIE Segmented Optics Testbed: Analysis, Synthesis, and Experiment," in *Proceedings of the 4^{th} NASA/DoD Control/Structures Interaction Technology conference*, (Orlando, FL), 1990, pp. 172–201.

[26] Wie, B. and Bernstein, D., "Benchmark Problems for Robust Control Design," in *Proceedings of the American Control Conference*, June 1991.

[27] Miller, D., Jacques, R., and de Luis, J., "Typical Section Problems for Structural Control Applications," in *Dynamics Specialist Conference*, (Long Beach, CA), Apr. 1990. Paper # AIAA-90-1225.

[28] Spanos, J., "Control-Structure Interaction in Precision Pointing Servo Loops," *Journal of Guidance, Control, and Dynamics*, Vol. 12, March-April 1989, pp. 256–263.

[29] Eyerman, C., *A Systems Engineering Approach to Disturbance Minimization for Spacecraft Utilizing Controlled Structures Technology*, Master's thesis, Massachusetts Institute of Technology, 1990. MIT SERC report # 2-90.

[30] Fanson, J., Blackwood, G., and C.C.Chu, "Active-Member Control of a Precision Structure," in *Proceedings of the 30th AIAA/ASME/ASCE/AHS Structures, Structural Dynamics, and Materials Conference*, (Mobile, AL), Apr. 1989, pp. 1154–1163.

[31] Spector, V. and Flashner, H., "Modeling of Non–Collocated Structural Control Systems," in *Proceedings of the AIAA Guidance Navigation and Control Conference*, 1989, pp. 74–83. Paper No. 88-4060.

[32] Crawley, E. and Hall, S., "Dynamics of Controlled Structures," Tech. Rep. 10-91-I, MIT SERC, July 1991. course lecture notes.

[33] Anderson, E., Blackwood, G., and How, J., "Passive Damping in the MIT SERC Controlled Structures Testbed," in *Proceedings of the International Symposium on Active Materials and Adaptive Structures*, (Alexandria, VA), Nov. 1991.

[34] ADINA R&D, Inc., *Automatic Dynamic Incremental Nonlinear Analysis (ADINA)*, Dec. 1987.

[35] Noor, A., Anderson, M., and Greene, W., "Continuum Models for Beam and Platelike Lattice Structures," *AIAA Journal*, Vol. 16, No. 12, Dec. 1978, pp. 1219–1228.

[36] Sun, C., Kim, B., and Bogdanoff, J., "Derivation of Equivalent Simple Models for Beam and Plate–Like Structures in Dynamic Analysis," in *Proceedings of the 22nd AIAA/ASME/ASCE/AHS Structures, Structural Dynamics, and Materials Conference*, 1981, pp. 523–532. Paper No. 81-0624.

[37] Doyle, J. C. and Stein, G., "Multivariable System Design: Concepts for a Classical/Modern Synthesis," *IEEE Transactions on Automatic Control*, Vol. AC–26, No. 1, Feb. 1981, pp. 4–6.

[38] Doyle, J., Francis, B., and Tannenbaum, A., *Feedback Control Theory*, Macmillan Publishing Company, New York, 1992.

[39] Freudenberg, J. and Looze, D., *Frequency Domain Properties of Scalar and Multivariable Feedback Systems*, Springer-Verlag, Berlin, 1988.

[40] Athans, M., Kapasouris, P., Kappos, E., and Spang, H., "Linear–Quadratic Gaussian with Loop–Transfer Recovery Methodology for the F–100 Engine," *Journal of Guidance, Control, and Dynamics*, Vol. 9, No. 1, Jan-Feb 1986, pp. 45–52.

[41] Fleming, F., *The Effect of Structure, Actuator, and Sensor on the Zeros of Controlled Structures*, Master's thesis, Massachusetts Institute of Technology, 1991. MIT SERC report # 18-90.

[42] Ewins, D., *Modal Testing: Theory and Practice*, John Wiley and Sons Inc., New York, 1984.

[43] Postlethwaite, I., Edmunds, J. M., and MacFarlane, A. G., "Principal Gains and Principal Phases in the Analysis of Linear Multivariable Feedback Systems.," *IEEE Transactions on Automatic Control*, Vol. AC–26, No. 1, Feb. 1981, pp. 32–46.

[44] Douglas, J., *Linear Quadratic Control for Systems with Structured Uncertainty*, Master's thesis, Massachusetts Institute of Technology, 1991. MIT SERC report # 12-91.

[45] Byun, K.-W., Wie, B., .Geller, D., and Sunkel, J., "Robust $\mathcal{H}_\infty$ Control Design for the Space Station with Structured Parameter Uncertainty," *Journal of Guidance, Control, and Dynamics*, Vol. 14, No. 6, November-December 1991, pp. 1115–1122.

[46] Ogata, K., *Modern Control Engineering*, Prentice-Hall, Inc., 1990.

[47] Crawley, E., Barlow, M., van Schoor, M., and Bicos, A., "Variation in the Modal Parameters of Space Structures," in *Proceedings of the 33rd AIAA/ASME/ASCE/AHS Structures, Structural Dynamics, and Materials Conference*, (Dallas, TX), Apr. 1992.

[48] Doyle, J., "Analysis of Feedback Systems with Structured Uncertainties," *IEE Proceedings*, Vol. 129, No. 6, Nov. 1982, pp. 242–250. Part D.

[49] Stein, G. and Doyle, J., "Beyond Singular Values and Loop Shapes," *Journal of Guidance, Control, and Dynamics*, Vol. 14, No. 1, jan-feb 1991, pp. 5–16.

[50] Morton, B. and McAfoos, R., "A Mu-Test for Robustness Analysis of a Real Parameter Variation Problem," in *Proceedings of the American Control Conference*, (Boston, MA), June 1985, pp. 135–138.

[51] Gupta, N., "Frequency–Shaped Cost Functionals: Extension of Linear–Quadratic–Gaussian Methods," *Journal of Guidance, Control, and Dynamics*, Vol. 3, No. 6, Nov.–Dec. 1980, pp. 529–535.